Geoid Monitoring Techniques for the National Spatial Reference System

Course No: L07-004
Credit: 7 PDH

Gilbert Gedeon, P.E.

Continuing Education and Development, Inc.

P: (877) 322-5800
info@cedengineering.com

This course was adapted from the U.S. Department of Commerce, Technical Report NOS NGS 69, "A Preliminary Investigation of the NGS's Geoid Monitoring Service (GeMS)", which is in the public domain.

Table of Contents

Reference in this document to any specific commercial product, process, or service, or the use of any trade, firm or corporation name is for the information and convenience of the public, and does not constitute endorsement, recommendation, or favoring by the U.S. Department of Commerce.

1 Background

1.1 Introduction

The NGS definition of the Earth's geoid is "the equipotential surface of the Earth's gravity field which best fits, in a least squares sense, global mean sea level." A geoid model is a mathematical approximation of this surface at some point in time, as constructed from multiple observational techniques. One current method of realizing a vertical datum is to use a geoid model as the zero-level for orthometric elevations, which are surface heights above or below the geoid measured along the local plumb line. However, the Earth is not static; various geophysical processes that redistribute mass on or within the Earth can cause changes to the geoid that will affect the movement of water (such as in runoff, floods, or ground water). When this occurs, orthometric elevations also change, and a static geoid model becomes outdated; an updated geoid model that reflects local changes in gravity potential is therefore required to maintain vertical datum relative accuracy over all distances. There are a variety of geodetic instrumentation and techniques that can be used to monitor the geoid for shape changes, including gravity-observing satellites like GRACE, terrestrial gravity surveys, GNSS, InSAR, and geodetic leveling. The intent of this document is to summarize our state of knowledge about how the shape of the geoid changes in time and space, and to provide an inventory of the geodetic instrumentation and techniques presently available to monitor these changes.

The mission of the National Geodetic Survey (NGS) is to define, maintain and provide access to the National Spatial Reference System (NSRS), to meet our nation's economic, social, and environmental needs. The need for a time-dependent vertical datum within the NSRS is laid out within NGS' most recent Strategic Plan (NGS, 2019a), which specifies "Objective 2-2: Define and provide access to a geocentric, time-dependent, geopotential datum by year 2022." The modernized vertical datum, the North American-Pacific Geopotential Datum of 2022 (NAPGD2022), includes multiple time-dependent components to be defined and maintained by a Geoid Monitoring Service (GeMS) as specified in Blueprint for 2022, Part 2: Geopotential Coordinates (NGS, 2017b).

GeMS is the second component of the Gravity for the Re-definition of the American Vertical Datum (GRAV-D) project, and is described in the GRAV-D Project Plan as a "low-resolution movie to track the temporal changes to the gravity field on a broad scale—a re-occurring survey with very coarse spatial coverage and a long temporal span" (NGS, 2007).

1.2 Goals of the Geoid Monitoring Service (GeMS)

In a 1967 discussion of the requirements for a precise geoid, Heiskanen and Moritz wrote that "… an error of probably less than 1 meter in [geoid height] . . . can be neglected for most practical purposes" (p. 94) The geodetic infrastructure and observing systems of today can easily meet meter-level accuracies, and are now approaching the 1 cm-level. In the next 10-20 years, 1 mm-level accuracies will be targeted. At cm-level and mm-level accuracies, geodetic sensors are sensitive to a number of different geophysical phenomena that were previously considered to be within the noise level of the measurements. Nowadays and into the future, the effects of these phenomena on the geoid surface will need to be considered in NGS's modeling and geodetic infrastructure.

The goal of GeMS is to build a robust NGS service that will provide the highest possible accuracy of the

dynamic components of the NAPGD2022 geopotential datum into the future. The primary purpose of GeMS is therefore to **define** and **maintain** the time-dependent variables necessary for a Dynamic Geopotential Model of 2022 (DGM2022), and for derivative products such as a Dynamic Geoid model of 2022(DGEOID2022) (see Section 5.1 for definitions and additional variables). GeMS has the goal of maintaining 1 cm geoid undulations over a decade, which implies a 1 mm/yr target accuracy. The magnitude of gravity change and geographic extent of concern to ongoing NSRS definition and maintenance is illustrated in Figure 1, where everything to the above-right of the (blue) curve yields a 1 cm geoid change (S. Holmes, personal communication, 2016). The resolution of satellite observations (GRACE/GRACE-FO) is shown as a vertical line at 200 km. Additionally, special consideration must be taken to capture changes to the left of this line using techniques other than GRACE (shaded region shown in Figure 1).

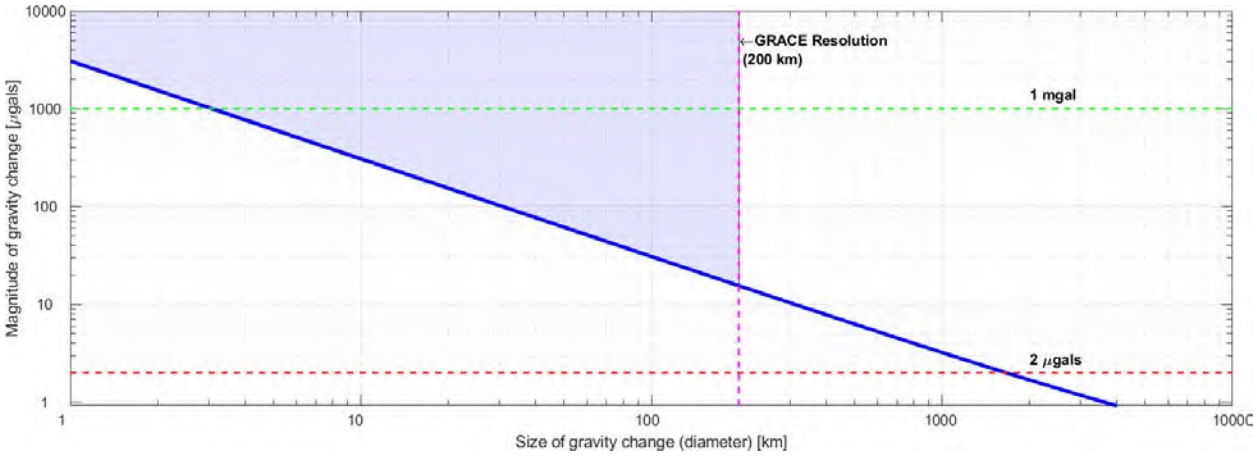

Figure 1: Gravity Change with Geographic Size of Feature (at logarithmic scales). Combinations to the right of the (blue) curve will produce a 1 cm geoid change. (S. Holmes, personal communication, 2016). Shaded region represents combinations that are not captured by GRACE and require special consideration in GeMS.

To design GeMS, NGS must consider the following topics:

A. What signals to monitor
    a. Magnitudes of geoid change
    b. Characteristics of geoid change (secular, episodic, regional, isolated)
B. Where those signals are important
    a. Spatial variability
    b. Uncertainties
C. How to monitor the important signals in the near-term (next 10 years)
    a. Available methods
    b. Performance metrics
D. How to implement for maintenance of a time-dependent NSRS
    a. Feasibility of GeMS approaches
    b. Integration of dynamic products with static products
    c. Communication with constituents (not addressed in this document)
    d. Assessment and program modification
E. How to adapt the service for long-term changes in methods/needs (next 10-30 years)

a. Future techniques that could be used for GeMS
b. Updates to GeMS products, models, and structure.

The remainder of section 1 addresses which signals are generally important to monitor (considerations A and B) for North America, and includes a review of how other countries around the world have approached these topics. Sections 2 and 3 address this with greater specificity for the entire United States, noting available techniques that could be used for geoid monitoring and evaluating them based on five shared metrics (consideration C; see below). Section 2 covers techniques with which NGS has long-standing expertise and section 3 covers techniques that are outside NGS's existing expertise, but which could be developed in-house or utilized through partnerships. Section 4 explores monitoring methods in the basic research phase that may yet become useful, but are not ready for inclusion in an operational GeMS model (in line with consideration E). Section 5 focuses on general implementation (consideration D) of GeMS into the NSRS. Finally, Section 6 combines techniques described in Sections 2 and 3 to create three recommended GeMS designs with associated development plans. This section also proposes assessment or validation options for ensuring that the selected GeMS is able to perform with the accuracy needed to support NSRS maintenance.

Evaluating techniques for geoid monitoring is extremely challenging because of the complexity of different geophysical phenomena that cause geoid change, how the geoid responds to these phenomena, and limitations/capabilities of available techniques. Additionally, no operational technique measures geoid change directly; some indirect measurement or combination must be used to estimate the geoid change. Therefore, we have employed a set of metrics, adapted from a system used to evaluate performance of the U.S.' Global Positioning System (GPS; see Grimes, 2008), to more consistently compare the known techniques as follows.

a) Availability - Spatial and temporal coverage and resolution currently available to NGS. The techniques supporting GeMS must have appropriate coverage coincident with NAPGD2022.
b) Operability – The capacity of NGS to feasibly sustain the technique into the future, and how well the technique fits into NGS's mission. The operating status of GeMS techniques must be known.
c) Feasibility – Ease of incorporating a given method into a time-dependent geoid model – Assuming availability of data, how difficult is it for NGS to ingest that data for use by GeMS.
d) Affordability – The relative cost to NGS for data collection/acquisition, storage, and incorporation into GeMS products; this includes any equipment acquisition or additional staffing requirements.
e) Accuracy - Spatial and temporal accuracy of the technique. Need to ensure that the DGEOID2022 uncertainty provided to 95% of users does not exceed 50% of the achieved accuracy of the SGEOID2022 definition over a decade.

Each technique has been evaluated according to these metrics using a 5-point relative scale of Low, Medium, High, Very High, and Extremely High.

1.3 The importance of a static geoid model

Orthometric heights are important because they functionally represent heights that are predictive of the

direction that water will flow[1]. Prior to satellite technology, orthometric heights were determined by specifying some value as a starting point (e.g. local Mean Sea Level at a tide gauge), measuring the height differences from location to location with a geodetic level, and transferring the height as one progresses geographically (with appropriate corrections). For heights that are more fully representative of water flow, co-located gravity measurements should be made at each leveled locations, but in practice this is only done when absolutely necessary. This network of orthometric heights provides a very accurate differential height; however, there are numerous problems with this situation for defining a continent-wide vertical datum.

The vertical datum portion of the NSRS—the North American Vertical Datum of 1988 (NAVD 88) for CONUS and Alaska along with other defined datums for other US states and territories—was defined and accessed through nationwide leveling measurements at passive control marks. The following is from NGS, 2017b:

> Around 2005 or thereabouts, it finally became possible to independently evaluate the absolute accuracy of NAVD 88 heights. By that time GNSS-derived ellipsoid heights were accurate to centimeters, and the Gravity Recovery and Climate Experiment (GRACE) mission yielded a continental scale geoid model accurate to 1 centimeter over wavelengths longer than approximately 200 kilometers
>
> This revealed that NAVD 88 heights were, on average, biased by 50 centimeters in CONUS and were tilted about 1 meter from the Pacific Northwest to the Southeast of CONUS.
>
> Knowledge of the bias and tilt problem in NAVD 88, as well as uncertainty about the viability and stability of the passive control network, led NGS to study the problem in preparation of the 2008-2018 NGS Ten-Year Plan (NGS, 2008). Estimates of the resources required to re-level the entire network were extrapolated from existing labor and contracting costs. The estimate to completely re-level NAVD 88 ranged between $200 Million and $2 Billion dollars. It was concluded that—even if NGS could secure funding at that level—re-leveling would not solve the underlying problems that (a) leveling builds up large systematic errors over a continent, (b) passive control can move, unchecked, and (c) passive control can easily be destroyed.

As a result of these severe difficulties with perpetuating NAVD 88, NGS and its federal and international partners proposed a modernized vertical datum (NAPGD2022) accessed through a user submitted GNSS positions and a NGS-supplied gravimetric geoid model.

1.4 GeMS and the National Spatial Reference System

In 2022, the modernized NSRS will provide orthometric heights and other gravity-based quantities through the North American-Pacific Geopotential Datum of 2022 (NAPGD2022). This geopotential

[1] Actually, geopotential differences (capable of overcoming friction) determine water flow, but orthometric heights provide the same information in almost all cases.

datum will be primarily defined by a geopotential model (GM2022) and a geoid model (GEOID2022)[2]. The dynamic component will be defined by a dynamic geopotential model (DGM2022) and a dynamic geoid model (DGEOID2022). A benefit of using a geopotential model is that it provides consistency between various geopotential quantities (orthometric heights, deflections of the vertical, surface gravity, etc.). For more information about the NAPGD2022 definition, as well as a history of NGS vertical datums and geoid models, see NOAA Technical Report NOS NGS 64 "Blueprint for 2022, Part 2: Geopotential Coordinates" (NGS, 2017b).

GEOID2022 will consist of a static geoid model (SGEOID2022) and a dynamic component (DGEOID2022), so that from a user's GNSS-derived geodetic coordinates (ϕ, λ, h, t), NGS models will provide the following three components, where N is the geoid undulation:

$$N(t - t_0) = N_{SGEOID2022}(t_0) + N_{DGEOID2022}(t - t_0) \quad (1)$$

Upon release of NAPGD2022, the t_0 will be equal to 2020.00. For the purposes of NAPGD2022, the geoid is defined by convention rather than by a physical surface. Although the NGS definition of the geoid is "the equipotential surface of the Earth's gravity field which best fits, in the least-squares sense, mean sea level," the realization of that surface is problematic. Instead, the geoid for NAPGD2022 is defined by a reference geopotential value (W_0 = 62,636,856.00 m^2/s^2).

Additionally, there are two categories of geoid change that must be considered in DGEOID2022: 1) changes in the geoid's relationship to mean sea level and 2) changes in the shape of the geoid surface due to mass redistribution. The first category results in a change to the definitional W_0 constant that aligns the geoid with mean sea level; this is addressed in Section 8 of NGS Blueprint Part 2. The second category is the focus of GeMS, and all discussion of DGEOID2022, the secular geoid change rate ($\dot{N}$), and other dynamic geoid considerations in this document are limited to the deformation of the geoid shape due to mass re-distribution.

The National Geodetic Survey (NGS) has nearly four decades of experience creating and refining regional static geoid models; the first such static geoid model was GEOID90 (Milbert, 1991). NGS now creates static experimental geoid models (xGEOID) annually (https://beta.ngs.noaa.gov/GEOID/xGEOID/). Future xGEOID models will include both the static and dynamic component of the geoid model in preparation for NSRS modernization in 2022.

1.5 Spatial and Temporal Changes to the Geoid in North America and the U.S. Territories

This geoid monitoring effort is ambitious, and the DGEOID2022 model will be the first of its kind, globally. Until now, NGS has not needed to continuously monitor geoid change everywhere in the United States because the uncertainty in past static geoid models has always been large relative to the accumulated geoid change between releases. Net uncertainty in the geoid modeling has been reduced

[2] There will also be mutually consistent additional components of NAPGD2022, namely DEFLEC2022, GRAV2022, and DEM2022. However, most of this document concerns the geoid model and discussion will focus on that.

by the Gravity of the Redefinition of the American Vertical Datum (GRAV-D) campaign (see Section 2.1.3). The target accuracy of the 2022 geoid is set at 1 cm over all distances, wherever possible. Based on recent Geoid Slope Validation Surveys conducted by NGS (Smith, *et al*., 2013; Wang, *et al*., 2017), the 1 cm geoid slope accuracy is an achievable goal in nearly all places. Note that the accuracy goal is differential over all distances. As stated in Smith, *et al*., 2013, attempts to quantify absolute geoid height accuracy yield only "problematic definitional, and relatively unproductive concerns."

New, high-accuracy geoid models are known to require monitoring for geoid change over time. Two existing studies summarize the state of knowledge for spatial and temporal changes to the geoid in North America: Rangelova, *et al.,* (2009) entitled "A Dynamic Reference Surface for Heights in Canada" and Jacob, *et al.,* (2012) entitled "Estimating geoid height change in North America: past, present, and future".

Rangelova, *et al.,* (2009) provides a detailed discussion of dynamic geoid model adoption in the context of Canada's vertical datum modernization. To determine feasibility and accuracy, they created a dynamic geoid model and assessed it. The dynamic geoid model was created from available GRACE time-dependent gravity data (see Section 3.1), continuous GNSS data (see Sections 2.2 and 3.5) and terrestrial gravity data (see Section 2.1.1). The methods of model creation were discussed in a previous paper (Rangelova and Sideris, 2008).

They present a useful function to represent the variations of geoid undulation (N) over time (t) and space (latitude φ, longitude λ):

$$N(\varphi, \lambda, t) = N_{static}(\varphi, \lambda, t) + \dot{N}(\varphi, \lambda, t) + \widetilde{N}(\varphi, \lambda, t) \quad (2)$$

In this function, the dynamic geoid (N) is the sum of a static geoid (which will be produced by NGS as SGEOID2022) plus two time-dependent components. Here, we call these pieces: 1) the "trend" or secular, linear rate of geoid change ($\dot{N}$) and 2) the "variable", non-linear geoid changes ($\widetilde{N}$). The variable geoid change is the sum of many signals, including annual cycles, seasonal cycles (caused by processes like snow melt or monsoon), temporary changes (like drought or relaxation after an earthquake), and permanent episodic geoid change (such as volcanic eruptions and tectonic deformation). Variable geoid changes are the least well understood, and so Rangelova, *et al.,* (2009) did not consider them in their study. Each quantity on the right hand side of (2) has its own uncertainty values and the sum of those would be the uncertainty assigned to the dynamic geoid model.

Considering only the trend of geoid change, their first major conclusion was that the study "... again demonstrates the importance of more and densely distributed terrestrial measurements in the areas with the largest secular signal" (Rangelova, *et al*., 2009). This is because the terrestrial gravity and GNSS data provide new information and error statistics that the GRACE satellite gravity data cannot provide. Their second major conclusion was that accounting for geoid change would ultimately not matter for orthometric heights in Canada within a decade, primarily because orthometric height errors were too large (~3.2 cm). When Canada modernized their vertical reference system in 2013, they adopted only a static geoid and not a dynamic geoid.

Of interest to the United States, Figure 4 in Rangelova, *et al.,* (2009) (reproduced here as Figure 2) shows that the high geoid change rates in Canada would significantly affect heights within 9 years for 2 cm of

orthometric height error, and within ~4.25 years for 1 cm of orthometric height error. Although the geoid change rates in Canada are generally higher than those for the continental United States, the Canadian rates are similar to those observed by GRACE in Alaska (see Jacob, *et al.,* (2012) discussion below). At these rates, the U.S. would indeed require adoption of a dynamic geoid model to maintain modernized 2 cm-accurate orthometric heights in Alaska. Otherwise, the geoid error would accumulate to unacceptable levels within 5-10 years after the adoption of a static geoid model.

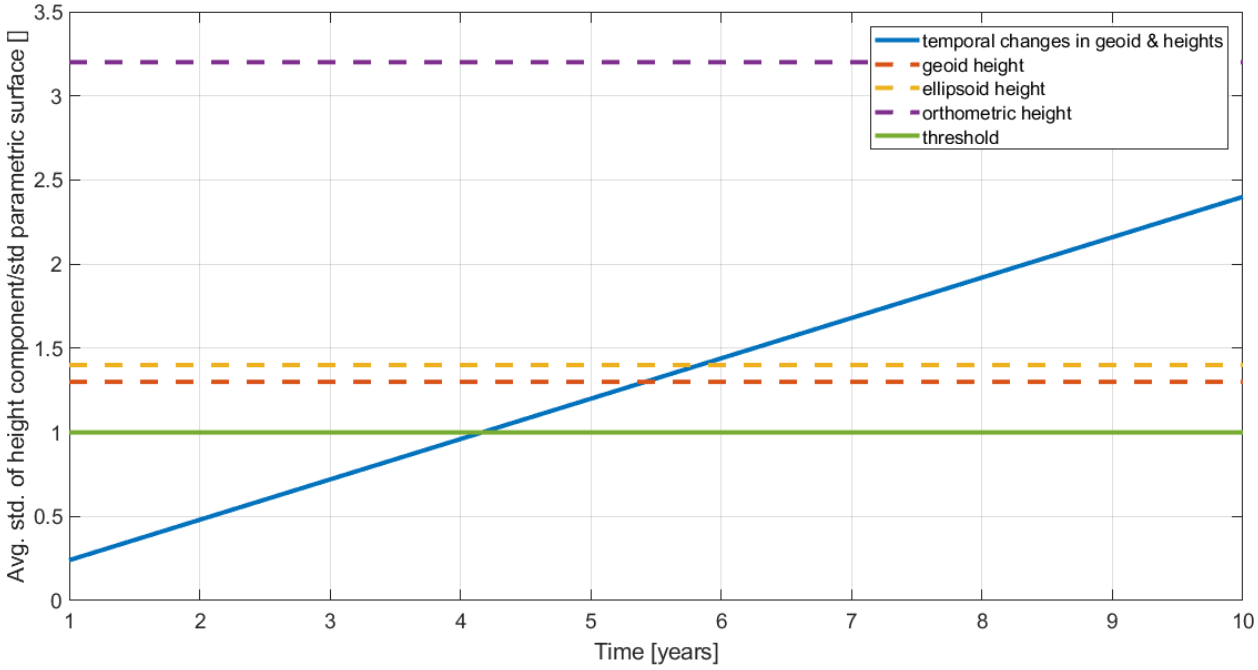

Figure 2: Accumulated effect of the secular change in physical height surfaces in Canada (from Figure 4, Rangelova, et al., 2009)

A second study, Jacob, *et al.,* (2012), examined both the trend and variability of geoid change for all of North America. The work was done in direct response to NGS's 2009 Workshop on North American Geoid Change, held in Boulder, CO. This analysis relies primarily on GRACE time-varying gravity data derived from spherical harmonic models. Jacob, *et al.* conclude that the variability of geoid change ($\widetilde{N}$) is important to include in monitoring because it can cause well over the 1 cm threshold of change within a decade. Their results for the $\dot{N}$ and $\widetilde{N}$ signals they considered are presented in Table 1 (based on Table 7, Jacob, *et al*., 2012).

Table 1: Geophysical phenomena effecting the shape of the geoid

	Frequency	Time span for a 1 cm geoid change	Observations/models needed (incomplete list)	Comments
Continental hydrology and climate variability	Secular / Periodic / Episodic	~50-100 years	Meteorological forcings, GRACE-like missions, LSMs, GCMs	Predicted geoid changes from LSMs and GCMs vary greatly
Groundwater withdrawal	Secular / Periodic /	~30-60 years	Hydrological/meteorological measurements, 3D aquifer-	Will depend on pumping rates and

	Episodic		scale models	future climate
Glacial isostatic adjustment	Secular	<10 years	Ice history, mantle rheology, ground-based geodesy, GRACE-like missions	Use of current model leads to a 1-cm error after 20 years
Ice mass loss	Secular / Periodic	<10 years	Ground-based geodesy, ice sheet elevations, GRACE-like missions, ice sheet mass balance	Rates are not linear, depends on future climate
Earthquakes	Episodic	Coseismic: instant; Post-seismic: 1-10 years	Seismic networks, ground-based geodesy, mantle rheology	Important for only the largest megathrust subduction earthquakes
Volcanic eruptions	Episodic	Instant	Ground-based geodesy, seismic networks	Significant only for cataclysmic events, flank collapse

The geoid change sources identified in Table 1 can be considered in three distinct groups: episodic cataclysms (earthquakes and volcanic activity), continuous sub-decadal sources (ice mass loss and glacial isostatic adjustment), and complex multi-decadal sources (hydrology and climate).

1.6 Methodology and Geodetic Constraints

Monitoring changes to the geoid shape is not a new idea in the geodetic community, but until recently, the magnitudes of these changes (a few mm/yr) were simply not operationally necessary due to other error sources swamping out this signal, lack of precision in geodetic surveying techniques and equipment, and because very precise, repeat observations over many years or decades were impractical. NGS has defined the NAPGD2022 orthometric height to be the following (NGS, 2017b), which is illustrated in Figure 3 at a hypothetical point P:

$$H_P = h_P - N_P \tag{3}$$

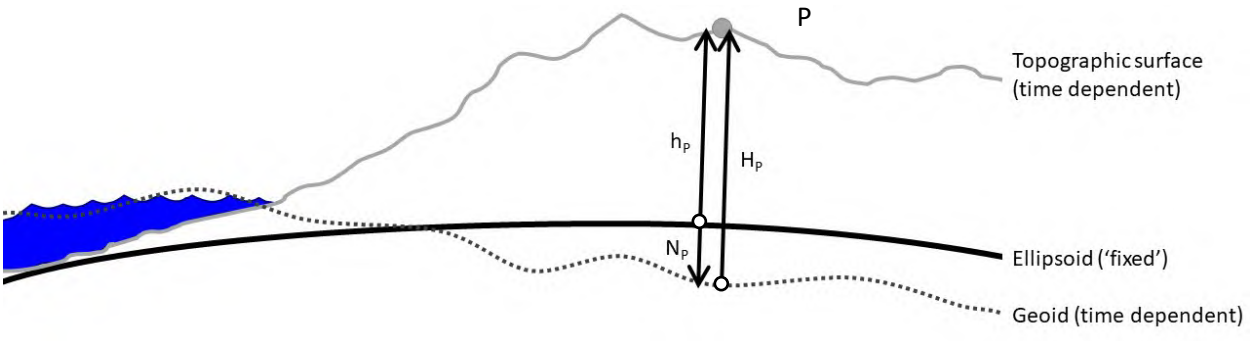

Figure 3: Physical surfaces and height components at a hypothetical point P. The topographic surface and the geoid are both considered to be time-dependent.

In addition to the classical elements of Figure 3, in a time-dependent geodetic world, both the topographic surface and the geoid are allowed to change with respect to time, while the ellipsoid is

considered static. Equation (3) can be written in terms of the time rates of change for each height term (where the time derivatives are written with dot notation throughout this section). While this is written to consider the secular rates, the $\widetilde{N}$ terms, as described in the previous section, could also be included in the time rate of change.

$$\dot{H}_P = \dot{h_P} - \dot{N}_P \tag{4}$$

It is apparent from (4) and Figure 3 that changes in the ellipsoid height reflect changes in the topographic surface only, whereas changes in the orthometric height reflect topographic surface changes together with changes in the shape of the geoid surface.

The historical NGS approach to computing the geoid undulation uses Stokes' integral (Stokes, 1849):

$$N_P = \frac{R}{4\pi\gamma}\iint_\sigma \Delta g\, S(\psi)\, d\sigma \tag{5}$$

where: *R* = radius of the earth, γ = normal gravity (average and assumed constant), Δg = gravity anomaly, $S(\psi)$ = Stokes' function. However, in order to avoid assumptions about how the gravity anomaly is determined with respect to the now changing geoid, we make use of gravity disturbances and Hotine's integral to compute the geoid undulation:

$$N_P = \frac{R}{4\pi\gamma}\iint_\sigma \delta g\, K(\psi)\, d\sigma \tag{6}$$

where: δg = gravity disturbance and $K(\psi)$ is Hotine's kernel (Hotine, 1969):

$$K(\psi) = \csc\left(\frac{\psi}{2}\right) - \ln\left(1 + \csc\left(\frac{\psi}{2}\right)\right) \tag{7}$$

Taking the derivative with respect to time results in:

$$\dot{N}_P = \frac{R}{4\pi\gamma}\iint_\sigma \dot{\delta g}\; K(\psi)\, d\sigma \tag{8}$$

The change in the gravity disturbance ($\dot{\delta g}$) term is comprised of two components: the change in gravity due to the vertical displacement of the surface and the change in gravity due to the redistributed masses, which is evident when expanding the free-air time rate of change:

$$\dot{\delta g} = \dot{g} - \dot{\gamma} = \dot{g} + \frac{2\gamma}{R}\dot{h} \tag{9}$$

Both of the components on the right hand side of (9) are sensed by a gravimeter on the surface, i.e. the change in gravity from mass redistribution and the change in gravity due to surface deformation (closer or further from the center of mass of the earth). However, only the mass redistribution component is present in the satellite gravity signal since the satellite is not connected to the ground surface. The crustal deformation rate ($\dot{h}$) can be estimated by common geodetic techniques, including the use of GNSS. Combining (8) and (9) and substituting $\dot{h}$, results in the following for the geoid rate of change with respect to time:

$$\dot{N}_P = \frac{R}{4\pi\gamma}\iint_\sigma \left(\dot{g} + \frac{2\gamma}{R}\dot{h}\right) H(\psi)\, d\sigma \tag{10}$$

Equation 8, like Stokes' original equation, relies on a number of assumptions in combination with observational data to solve. The greatest difficulty comes from the need for data be well-distributed over the entire Earth. However, it is apparent that a time-dependent geoid surface can be determined

by a combination of both the rate of change in terrestrial gravity and the rate of change in the topographic surface.

An alternative method to model rates of geoid change exists in a theoretical sense using geopotential surfaces. This method observes the rate directly by measuring the change in the gravity potential at a point P ($\dot{W}_P$). The method is illustrated in Figure 4 where W_P is the gravity potential at point *P* defined by the level (equipotential) surface through point *P*. Also illustrated in Figure 4 is the orthometric height at point *P* (H_P) that is measured along the plumb line from P_0 to *P*.

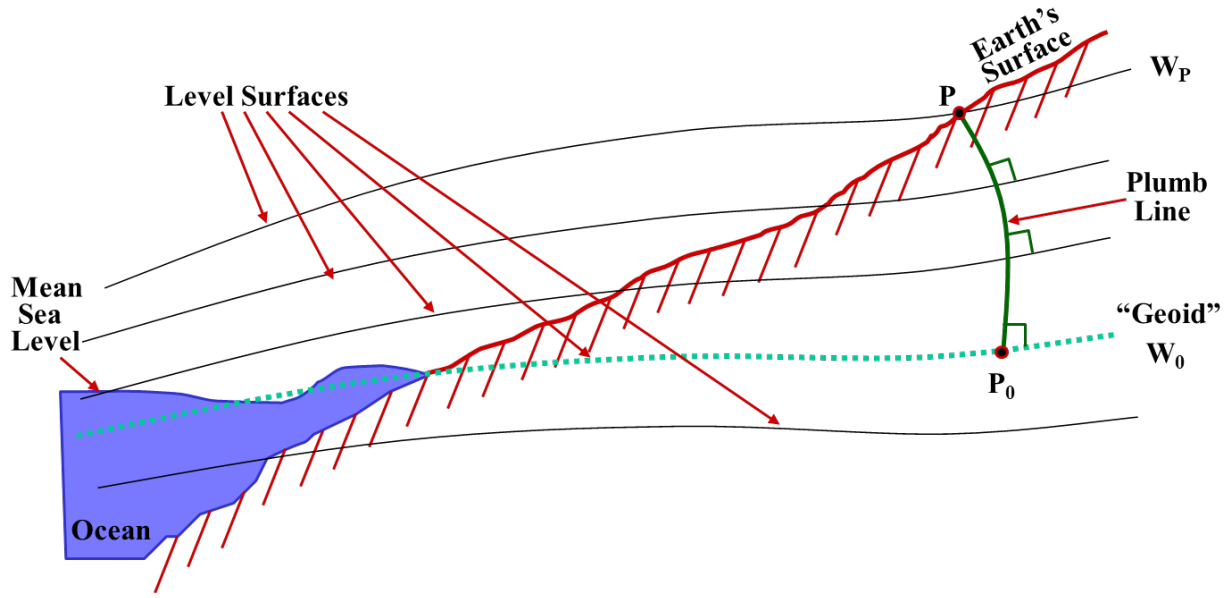

Figure 4: Level (geopotential) surfaces with constant W values. One geopotential surface with a specified W_0 that aligns with mean sea level is chosen to represent the geoid (dotted cyan surface). For an arbitrary location P on the earth's surface, the geopotential value of W_P represents the geopotential surface that intersects P.

The potential energy difference between two points, also known as the geopotential number C_P can be computed from the following:

$$C_P = W_0 - W_P \tag{11}$$

To determine the height of P using C_P, the mean gravity along the plumb line is required. There are a number of different approximations to estimate mean gravity leading to a slightly different height definition (i.e. orthometric, dynamic, normal). All of these height definitions effectively scale C_P into a height-like quantity. NGS uses the Helmert orthometric height definition (Helmert, 1890; see also Heiskanen and Moritz, 1967) which defines the mean gravity along the plumb line as shown in the denominator in the following equation:

$$H_P = \frac{C_P}{g_P + 0.0424H_P} \tag{12}$$

Changes in W_P (and C_P) cause changes in H_P, but it is also possible that changes to the two terms in the denominator of (12) also effect H_P. The influence of changes in the denominator (either in g_P or H_P) are illustrated in Figure 5 where a rate of 100 μGals/yr is used to simulate the maximum secular surface

gravity rate that is present on Earth. Changes to the H_P term in the denominator are insignificant as that term is scaled to effectively zero. Changes to g_P are not entirely insignificant, but at this simulated rate, it would take 40 years for a 1 mm effect in H_P to build up. Therefore, only changes to C_P over many decades will have a significant influence on the orthometric height, assuming C_P is directly measurable. The $\dot{H}_P$ term obtained here can be combined with the $\dot{h}$ component obtained with GNSS or InSAR to yield the geoid rate of change with respect to time.

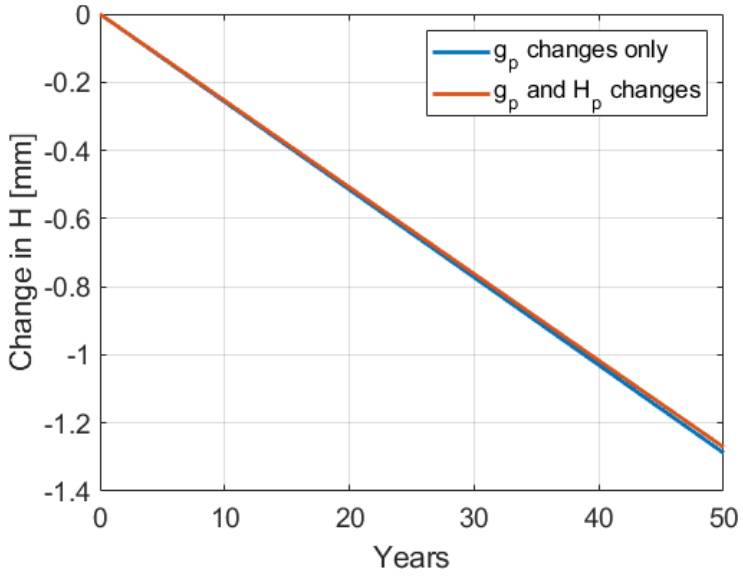

Figure 5: Changes in Orthometric Height due to surface gravity changes (g_P) and H_P. The geopotential number (C_P) is held constant. A rate of 100 μGals/yr is used for g_p, which represents the maximum surface gravity rate on Earth. The blue curve illustrates the g_p rate only, whereas the red curve illustrates the combined effect of changes in the denominator of (12).

One method to obtain W_P, and therefore C_P, is currently achievable with atomic clock networks (see Section 4.4), which permit the *relative* change in *W* to be measured between two clock locations (Bjerhammer, 1985). For example, a clock at hypothetical point *Q* and another clock at point *P* would measure the gravity potential difference (ΔW) between *P* and *Q* (assuming W_0 is constant) as shown in (13).

$$\Delta W_{PQ}(t) = W_P(t) - W_Q(t) = C_Q(t) - C_P(t) \quad (13)$$

Using a completely terrestrial-based optical clock network, the slope (or relative) changes in the geoid surface are directly observable through time. It is less evident how changes with respect to a reference ellipsoid (i.e. absolute changes) are obtained. However, the specific location of a reference (i.e. definitional) clock might mitigate and potentially solve this absolute issue. For example, a space-based clock reference (placed on a satellite) or a datum definitional clock[3] would possibly satisfy GeMS need

[3] A datum definitional clock would be some 'stable' clock that defines the datum with a known W value. Like Father Point tide gauge defines the datum for NAVD 88, but a clock that all other clocks are connected to.

for absolute accuracy. The nuances of how an optical atomic clock network is optimally used for vertical datum maintenance is still under investigation by the global geodetic and metrological community.

In summary, NGS needs to observe, model, or otherwise define changes in surface gravity and ellipsoid height with respect to time throughout the NAPGD2022 area. Alternatively, NGS requires changes in the gravity potential and ellipsoid height with respect to time, which can then be converted to changes in the shape of the geoid surface at these locations. Both approaches require either continuously observing instrumentation or campaign-style repeat observations. Table 2 provides a general overview of which geodetic methods and/or types of models are suitable for determining these different rates, alongside their corresponding spatial and temporal resolutions, achievable accuracies, and related commentary.

Additionally, many authors in the geodetic and geophysical literature directly tie the crustal deformation ($\dot{h}$) with geopotential change in many localized situations with different assumptions regarding the loading situation (elastic loading only, constant and assumed $\dot{g}/\dot{h}$ ratio, etc) (Farrell, 1972; Wahr, *et al*., 1995; Argus, *et al*., 2014). We do not make that connection in this publication as assumptions in these specific cases cannot be generalized and applied on continental scales, but note that for specific regions, the crustal deformation can reflect geopotential change.

Table 2: Observables and Geodetic Methods/Geophysical Models

Observable	Geodetic Methods / Constraints				Geophysical Models
$\dot{g}$ (time rate of change of gravity)	Terrestrial Gravity • Precisions obtainable at 3-5 μGals • Over large areas, more expensive • Over limited areas, more cost effective than airborne • Variety of sensors available to meet signal requirements	Airborne Gravity • Precisions obtainable at 1000 μGal • Higher costs for small areas than terrestrial • More cost effective for large to very large geographic areas • Variety of sensors and platforms • Ability to alter altitudes and ground speeds	Satellite Gravity • Very accurate at long wavelengths • Poor spatial resolution • Near global spatial coverage • Cost-prohibitive to launch but very low cost for use • Dependent on a space mission and its continuity		Forward models of mass change • DEM • Ice-Mass Balance • Hydrologic • Co-seismic • Volcanic
$\dot{h}$[4] (time rate of change of ellipsoid height)	GPS/GNSS • Very precise (CORS have 1-sigma ~0.1 mm/yr) • Needs to be repeated at different epochs • CORSs and cGNSS are continuously operating • Spatial resolution is only as good as the station spacing	InSAR • Detailed, relative height changes over contiguous areas • Needs to be repeated at different epochs • Significant costs for detailed surveys • Inexpensive for satellite data	Altimetry • Poor spatial resolution between tracks • Absolute accuracy at 3-5 cm (sea surface relative to ellipsoid). (Fu & Cheney, 1995) • Dependent on a satellite mission and its continuity • Various missions for measuring solid earth, ice sheets, and water bodies. • Over ocean, gravity/geoid slopes can be derived. • Example: ICESat(-2) / CryoSat for ice-sheets	LiDAR • Needs to be repeated in time • Precision at cm-level • Multiple platforms available • Frequent collaborative funding opportunities	GIA models
$\dot{H}$ (time rate of change of orthometric height)	Geodetic Leveling • Needs to be repeated at different epochs • Very precise for relative height change (sub cm-level) • Difficult to obtain absolute rates of H • Combine with $\dot{h}$ technique to get $\dot{N}$				NA

[4] This observable is also the major focus for the NGS's Intraframe Velocity Model (IFVM) (NGS, 2017a), and GeMS will likely leverage the IFVM for this observable once operational.

$\dot{W}$ (time rate of change of geopotential)	Optical Clock Network • Relative change in gravity potential (ΔW) between two locations • Direct way of obtaining geoid rates • Current precisions at dm-level. Precisions expected to be cm-level in a few years. • Not quite operationally ready at this time • Difficult to link clocks resulting in low spatial resolution. Need line of sight or fiber optic connection.	NA

1.7 Geoid Monitoring around the world

No other country or agency is known to be actively monitoring geoid change in an operationally continuous manner. A limited survey of efforts at international geodetic agencies include "doing nothing," employing accurate vertical velocity models of vertical heights, and ad hoc reassessment of the geoid model after cataclysmic events.

Areas like Fennoscandia and Canada are experiencing a large-scale—but predictable—change in the geoid shape due to Glacial Isostatic Adjustment (GIA). In Fennoscandian countries, highly detailed land uplift models (that include localized ice mass changes) are used to describe and predict geoid change. Canada's spatial reference system has a static gravimetric geoid model only, but there are plans to reassess users' needs for a dynamic geoid model by 2022. Natural Resources Canada Geodetic Survey expects that the most stringent users of geoid models (e.g. scientific community) will be interested in a geoid velocity correction (Veronneau, personal communication, 6/19/2018). In both of these regions, geodetic networks are being actively maintained (see Section 3.4.1 for Canada's current CGSN program), but there is no coordinated or explicit "monitoring" of the geoid beyond that.

Other countries are engaged in what can best be described as "ad hoc reassessment." Tectonically active countries like New Zealand and Japan can expect to experience geoid changes that are large in magnitude, but localized in extent. Areas near earthquakes or volcanic eruptions can be re-observed with GNSS, gravity, etc. as needed after such an event. Jack McCubbine of Geoscience Australia says of the Kaikoura (M7.8) earthquake in New Zealand: "We are looking at ~1 cm changes in the quasigeoid due to this single event. These appear to have been too small to be seen in GRACE data though." Continuous monitoring is not a priority for these countries because the changes can be captured with post-event observations on an as-needed basis.

Most countries are "doing nothing" in the sense that the changes they expect to see in the next ~25 years are smaller than the uncertainty in their current static geoid models. Geodetic networks are maintained, but as Jack McCubbine says, "at the moment, the absolute gravity time series data is only really being used to validate the lack of change in the GNSS data." This approach applies in central and southern Europe, South America, Australia, and presumably Africa.

In summary, the efforts of NGS to continuously monitor the time rate of change in the geoid will be pioneering. Maintaining a geoid model that extends from a subsiding Mississippi River region in Louisiana to thawing and calving glacier changes in Alaska will require coordinated efforts and innovative techniques that must leverage existing expertise at NOAA and expand through the development of collaborative partnerships.

2 Available Geoid Monitoring Techniques

NGS has three existing program areas and associated technical expertise that could be utilized in an operational GeMS: NGS's Gravity Program, the NOAA CORS Network, and GPS/geodetic leveling campaigns. None of these techniques could individually provide 100% of what GeMS requires but various combinations would be sufficient.

Table 3: Summary of Geoid Monitoring Techniques within NGS's Current Expertise

Type of Data:	Subtypes:	Availability:	Operability:	Feasibility:	Affordability:	Accuracy:
NGS's Gravity Program	Terrestrial (Absolute)	**Medium** Limited observation and repeat observation across North America	**Very High** Expertise to continue to expand and develop network at NGS	**Very High** Easy to incorporate into GeMS for modeling and validation.	**Medium** Acquisition, Operational, Maintenance costs	**Very High** Absolute at 1-2 μGals
	Terrestrial (Relative)	**Medium** Limited repeat observations across North America with poor metadata.	**Very High** Expertise at NGS to develop techniques	**High** Can be incorporated but some questionability with regards to accuracy of old data	**Medium** Acquisition, Operational, and Maintenance costs	**High** Relative to a few μGals
	Airborne	**Low** Coverage over North America but all has been observed only a single time.	**Low** Need repeat campaigns	**Low** Need repeat campaigns with much better accuracy	**Low** Very expensive to fly over small and large areas	**Low** Approximately 1000 μGals. GeMS needs a few μGals/yr.
The NOAA CORS Network		**Very High** Good spatial coverage throughout U.S. Continuously operating for many years in most cases.	**Very High** Maintained by NGS's Spatial Reference System Division	**Very High** Easy to incorporate into vertical deformation model as data are processed daily	**Medium** Some cost for NGS to maintain this network.	**Very High** Vertical accuracies at the sub-mm / yr level
GPS / Geodetic Leveling Campaigns		**Low** Only available in a few places. Need repeat occupations to be useful.	**Very High** Within NGS's mission to maintain these sites.	**High** Can incorporate but only get the relative rate of the entire line rather than the absolute rate.	**Low to Medium** Expensive to repeat the leveling. Repeat GPS is rather inexpensive.	**Medium to High** GPS rates at 1 mm/yr. Leveling rates at sub mm/yr.

2.1 NGS' Gravity Program

The mission of NGS Gravity Program is to provide high quality gravity data to internal and external stakeholders; providing gravity data required for NGS's geoid modeling is the primary component of that mission. The Gravity Program has a long history of collecting and processing terrestrial gravity data as well as ingesting data from outside sources. The Gravity Program also operates the Table Mountain Geophysical Observatory (TMGO) outside of Boulder, Colorado. Started in 2008, the Gravity for the Redefinition of the American Vertical Datum (GRAV-D) project has built expertise in collecting and processing airborne gravity data and will provide a consistent gravity dataset for the entire U.S. and territories by 2022. The expertise and instrumentation of the Gravity Program, including some information on historical methods, is described in the sections below.

2.1.1 Terrestrial Gravity

2.1.1.1 FG5 Absolute Gravimeter

The FG5(X) absolute gravimeter (see Figure 6) is manufactured by Micro-g LaCoste Inc. in Lafayette, Colorado. It is currently the highest-accuracy, commercially-available absolute gravity meter, with an accuracy of about ±2 μGals (Niebauer, *et al.*, 1995). NGS owns and operates instrument number FG5X-102.

Figure 6: FG5 Absolute Gravimeter with supporting equipment (Photo used with permission: Micro-g LaCoste)

A frequency-stabilized laser (effectively a length standard) is used to track the free fall of an object in a vacuum. An atomic clock (tied to a cesium time standard which is typically a GNSS signal) is used to

timestamp the trajectory. The value of the Earth's acceleration due to gravity is determined by a least squares fit to the trajectory—g being a free parameter. Corrections for barometric pressure, polar motion, Earth tide, and ocean loading are applied to estimate gravity on an "average day". A local gravity gradient (change with height) is provided *a priori* a) as part of the least squares fit and b) in transferring the gravity value to a convenient height (such as a survey mark). This gradient is typically determined with a portable, relative gravity meter (see Section 2.1.1.3 or 2.1.1.4).

The FG5(X) is primarily operated in laboratory conditions (AC power, ambient temperature between 15 and 30°C), though it is possible to operate in the field (with tent, generator, temperature control, etc.). Set-up time is about one hour, depending on instrument temperature. Observations last a minimum of 12 hours (to minimize errors due to tide model uncertainties) and are more commonly 24 hours (with 100 observations, or "drops", per hour). In micro-seismically noisy areas or unstable ground conditions, 48 hours is typical.

Because the measurement is based on absolute (NIST-traceable) standards, there is no need to "calibrate" the FG5(X). However, periodic annual inter-comparisons with similar instruments are used to identify any instrument bias.

2.1.1.2 A10 Absolute Gravimeter

A field deployable version of the laboratory FG5 absolute gravimeter, was developed by Micro-g LaCoste in the early 2000's. This instrument, now known as the A10 (see Figure 7), operates on principals nearly identical to the FG5 free fall gravimeter (Niebauer, *et al.*, 1995). However, the laser used in the A10 system is not a primary standard due to the low power and fragile nature of the Iodine based laser, and does need to be calibrated routinely.

Figure 7: A10 Absolute Gravimeter deployed in the field

To increase utility in a wide variety of environments, the instrument was designed to be smaller, lighter, easier to set up and operate than the FG5, and several engineered sub-systems were added to allow the instrument to operate in non-laboratory conditions. An internal temperature control system allows the A10 to conduct measurements in ambient temperatures ranging from -40 to +40°C. Automatic instrument levelling provides for fast set up in the field and can be deployed on concrete, asphalt, and with a small tripod, can measure on dirt, ice, and/or snow. The A10 requires about 10 – 15 amps of continuous 12 Volt DC current, so it is usually operated within about 20m from a generator (e.g. vehicle) of some kind.

A typical A10 measurement takes about 20 – 30 minutes, and is usually repeated at least once for quality control purposes. The instrument yields an absolute gravity measurement with a ±10 μGal accuracy on stable sites. As with the FG5, vertical gravity gradient measurements are typically measured in conjunction with the absolute gravity measurement.

2.1.1.3 Scintrex CG-6 Relative Gravimeter

The Scintrex CG-6 relative gravimeter (Figure 8) is the newest generation of the CG line of quartz sensor relative gravity meters. The CG-6 (like its predecessors the CG-3 and CG-5) operates on the same fundamental theory as the LaCoste and Romberg G and D relative gravimeters (see 2.1.1.4), but uses a quartz sensor spring instead of a metal sensor. The primary advantage of a quartz sensor is its insensitivity to instrument shock or vibration that can cause offsets in the gravity measurements.

Figure 8: Scintrex CG-6 Relative Gravity

NGS acquired a CG-6 gravimeter in the summer of 2017. Initial surveys and tests have demonstrated an improved repeatability (typically 1 – 2 μGals) and quicker measurement setup (typically under 1 minute) when compared to the previous CG-5 model (van Westrum and Kanney, 2017). One of the main uses of this meter at NGS is to perform vertical gravity gradient measurements to transfer the gravity value from an A10 measurement, which reports gravity at 72.2 cm above ground level, to another height, such as the airborne gravimeter height on a specific aircraft or to a survey disk on the ground. This meter can also be used to transfer gravity values from known sites to unknown sites that may be difficult to measure with absolute gravimeters. NGS has experience operating all of these types of relative gravimeters in the CG series (CG-3, CG-5, and CG-6).

2.1.1.4 LaCoste and Romberg Relative Gravimeter

LaCoste and Romberg (L&R) relative land, air/sea, borehole, and tidal gravimeters have been manufactured by LaCoste and Romberg Gravity Meters, Inc. since 1959. The company later merged into Micro-g LaCoste, Inc., and the LaCoste land gravimeters were discontinued. Unlike the Scintrex gravimeters, these rely on metal zero-length-springs (LaCoste, 1934).

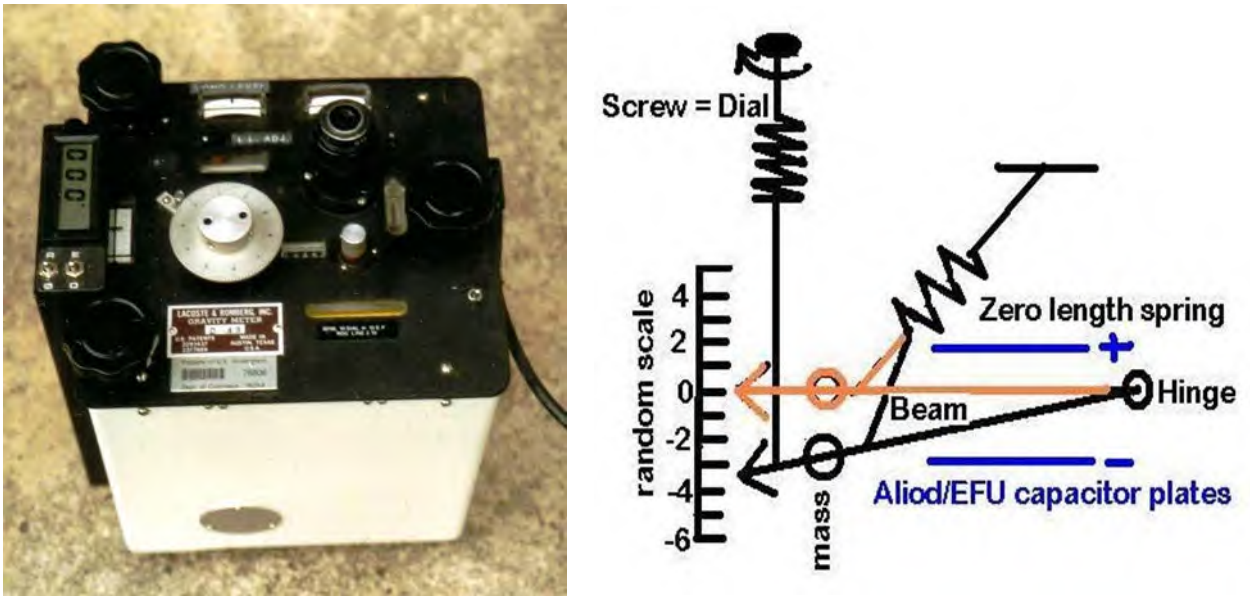

Figure 9: Lacoste and Romberg relative gravimeter (Model G) (left) and internal schematics of Model G gravimeter (right).

When a relative gravimeter is set up at a site, the instrument is leveled (see Figure 9B). Then the beam, which hangs by the hinge and the zero-length-spring, moves to its natural hanging point based on the gravity value (black arrow = Beam). Then the operator turns the screw to bring it up to a nulling position ("0" = orange arrow), with the number of turns being calibrated to gravity units. In modern forced feedback system enhancements, such as the EFU or Aliod, the screw is (optionally) replaced by moving the beam in an electromagnetic field between two capacitor plates.

The land and tidal gravimeters have a precision of 100 μGals and a survey repeatability of a few hundred μGals, depending on survey design. Land meters are designed to do station-to-station, terrestrial or gradient, relative surveys. Tidal gravimeters are designed to observe in one spot for months or years, measuring continuously (see Section 2.1.1.6). Air/sea gravimeters are designed to observe from moving platforms such as airplanes, helicopters, trucks, ships, and submarines. They have gimbals and other vibration dampening modifications. They have typical accuracies of a few hundred μGals (see Section 2.1.3). They can also be configured for boreholes. All are used for relative observations, observing the gravity difference from a known base station to a new station.

Since the 1960s, NGS has operated three model G and two model D L&R land gravity meters. All have been upgraded over the years and now have Aliod systems. They have been used on innumerable projects including the NGSGN, numerous calibration lines, and gradients for AG observations.

2.1.1.5 Superconducting Cryogenic Gravimeter

A superconducting cryogenic gravimeter (SG; see Figure 10) is designed to be continuously monitor

relative changes in the local gravity over time. Its main applications include precise tidal analysis, ground water monitoring, and geodynamics. The precision of an SG is still unmatched by any other instrument at better than 0.1 μGals at short time scales.

NGS owns SG CT-024, a superconducting relative gravimeter manufactured by GWR Instruments Inc. in San Diego, CA. This unit was deployed on 'Pier AK' at the TMGO facility outside of Boulder, CO where it operated from 1994 until its decommissioning in 2019.

Figure 10: NGS' SG CT-024 manufactured by GWR Instruments Inc.

The instrument uses the magnetic field produced by a permanent current in a superconducting coil to levitate a 1" niobium sphere (see Figure 11). As local gravity increases (due to tides, soil moisture, etc.), more force is required to support the sphere. Electrostatic feedback is used to hold the sphere in a fixed position, meaning the necessary electrical force is proportional to gravity. An absolute gravimeter is used to calibrate the instrument providing the necessary conversion from volts to μGals.

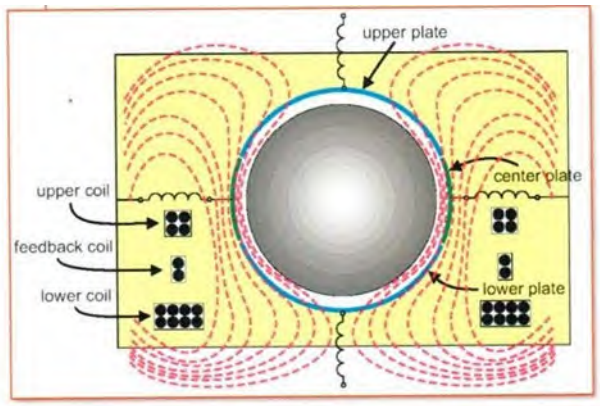

Figure 11: Conceptual drawing for GWR SG Instrument (used with permission from GWR, Inc.)

A database of worldwide SG observations is archived at the *International Geodynamics and Earth Tide Service (IGETS)*. NGS only provided intermittent SG data to IGETS in the past. Information about this international collaboration from the IGETS home page:

> "IGETS is the International Geodynamics and Earth Tide Service of the International Association of Geodesy (IAG). The main objective of IGETS is to monitor temporal variations of the Earth gravity field through long-term records from ground gravimeters, tiltmeters, strainmeters and other geodynamic sensors.
>
> IGETS continues the activities of the Global Geodynamics Project (GGP) to provide support to geodetic and geophysical research activities using superconducting gravimeter (SG) data within the context of an international network. Furthermore, IGETS continues the activities of the International Center for Earth Tides (ICET), in particular, in collecting, archiving and distributing Earth tide records from long series of gravimeters, tiltmeters, strainmeters and other geodynamic sensors."

2.1.1.6 gPhoneX Gravity Meter

The gPhoneX, manufactured by Micro-g LaCoste, is a low (linear) drift, metal spring-based gravimeter. Like the SG, it is designed to measure relative changes in gravity over time, at a fixed location. While not as precise as the SG at short time scales; at periods of longer than a few hours, the noise characteristics of the two instruments are quite similar. The advantages of a gPhoneX compared to a SG for long term monitoring include lower cost, lower power consumption, increased portability, and lack of a requirement for maintaining superconducting temperatures. At publication, NGS is in the process of acquiring a gPhoneX and plans to initially install it at 'Pier AK' at TMGO.

Figure 12: gPhoneX gravity meter (Photo used with permission from Micro-g LaCoste)

2.1.1.7 JILAg Absolute Gravimeter

The AFGL, JILA/IGPP and JILAg series of absolute gravimeters are the out-of-production predecessors to the FG5 gravity meter. These instruments were developed by James Faller and colleagues beginning in the mid-1970s, and were crucial for defining and providing the basis for the IGSN71, NGSGN, and other scientific projects. They were field-deployed by the Air Force Geophysical Laboratory, the Defense Mapping Agency (now NGA), the University of California at San Diego (IGPP), and NGS. NGS measured with JILAg-4 (Figure 13), which was acquired by NGS in 1986 and remained in use until 1993. Field data results are in the NSRS, but there are data and software limitations on reprocessing these surveys going into the future.

Figure 13: JILA gravity meter

2.1.2 U.S. Gravity Networks and Available Repeat Measurements

2.1.2.1 International Gravity Station Net of 1971 (IGSN71)

In the mid-1950s, a coordinated effort was initiated by the IAG to make relative pendulum and spring gravimeter ties throughout collaborating parts of the world to support establishment of a gravity datum.

The previous Potsdam datum, as realized, contained accumulated error in the network as it stretched away from Potsdam, and there was an offset in its absolute value (about 12 – 15 mGals too high). The new network was to be constrained by a network of ballistic absolute gravimeters. It incorporated intercontinental, north-south, calibration lines and long-distance ties established by airplane. Survey contributors in the USA included the USAF 1st Geodetic Survey Squadron (GSS), the US Coast and Geodetic Survey, and the University of Wisconsin. The majority of USA relative gravimeter work was done from 1965 – 1967, resulting in the network shown in Figure 14. Five of the eight absolute gravimeter sites were in CONUS. Major metropolitan areas were selected as sites, with the number of stations per city ranging from one to 26, with four being typical. There were 1854 stations worldwide; 453 of these stations were in the USA, including territories (plus more in US military bases on foreign soil). Many of these stations have been destroyed over the decades, in particular those at passenger airport terminals.

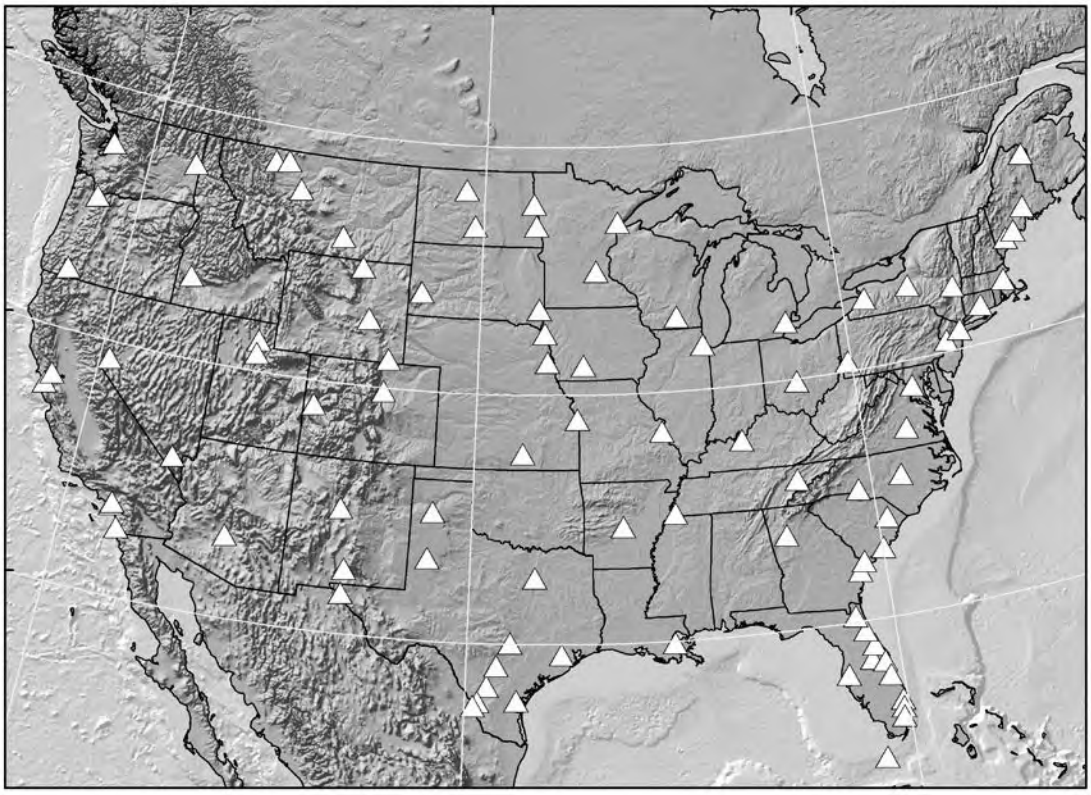

Figure 14: IGSN71 Gravity Stations

Calculations were completed by Urho A. Uotila of The Ohio State University around 1970. This was a world-wide, simultaneous adjustment, which eliminated the ladder of additive uncertainties away from Potsdam. This was published as The International Gravity Standardization Net 1971 (I.G.S.N. 71) by C. Morelli, *et al*, 1974, IAG Special Publication No. 4, 194 p. A latitude-dependent tidal effect, called the Honkasalo correction, had been included in the IGSN71. In 1979, the IAG-IUGG voted to remove this correction. The standard error for almost all sites was below ±0.060 mGals globally, and approximately ±0.030 mGals in CONUS. As of the publication of this document (2019), the IGSN71 remains the official international gravity datum, despite decades of geodynamics, not to mention increased accuracies in absolute gravity meters. In the USA, many state-wide gravity networks have designated one or more

IGSN71 sites as control hubs, with most of this work continuing by or for the US Air Force GSS or US Army Topographic Command.

2.1.2.2 National Geodetic Survey Gravity Network (NGSGN)

In the mid-1970s, most of the IGSN71 measurements were ten years old. Several countries ran relative gravimeter surveys to re-observe the IGSN71 sites either for validation or to detect change. The National Geodetic Survey Gravity Network (NGSGN) (Moose, 1986) was NGS's version of this. Between 1975 and 1979, L&R relative gravimeters were deployed around CONUS by NGS or DMA (now NGA). This network consists of 232 stations as shown in Figure 15, which were constrained by 8 absolute gravimeter observations. A total of 135 stations were also included in the IGSN71 (see Figure 16 for differences), with the remainder being newly established as gravity base stations. The NGSGN is a standalone network with an average standard error of 0.015 mGals. As of publication, about half of the stations (117) had been destroyed but the remaining stations are evenly distributed across CONUS. Figure 16 illustrates the first, high-precision, temporal gravity change map for the U.S.

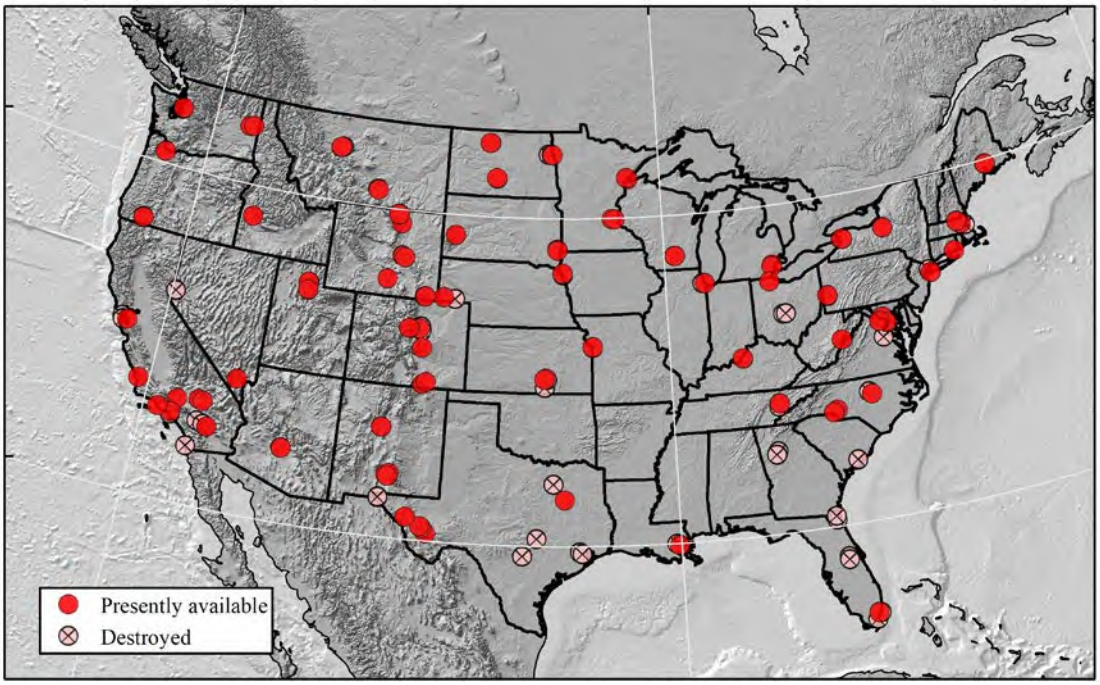

Figure 15: NGSGN Stations. Destroyed stations known as of July 2019.

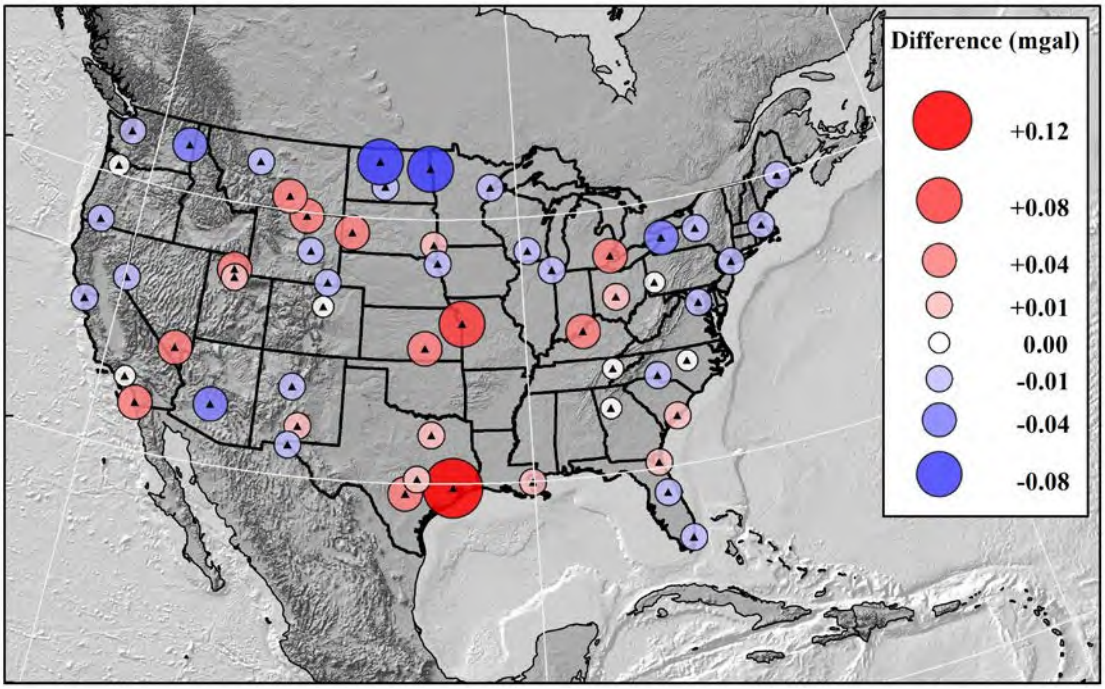

Figure 16: Difference between NGSGN and IGSN71 AG values [mgal]

2.1.2.3 United States Absolute Gravity Network (USAGN)

Following publication of the NGSGN, NGS took new steps towards monitoring gravity changes. NGS & DMA (now NGA) sponsored two JILAg absolute gravimeters. The plan was to observe a network of about 50 absolute sites annually (one per week). These stations would be spaced about 300 km apart in CONUS. The base plan was laid out in The National Geodetic Survey Absolute Gravity Program by G. Peter, *et al*, 1989, NOAA Technical Report NOS 130 NGS 43, 18 p. (see Figure 17), but this plan of annual absolute gravimeter measurements was never implemented. Stations were chosen to densify the IGSN71 and NGSGN Networks in the most stable locations.

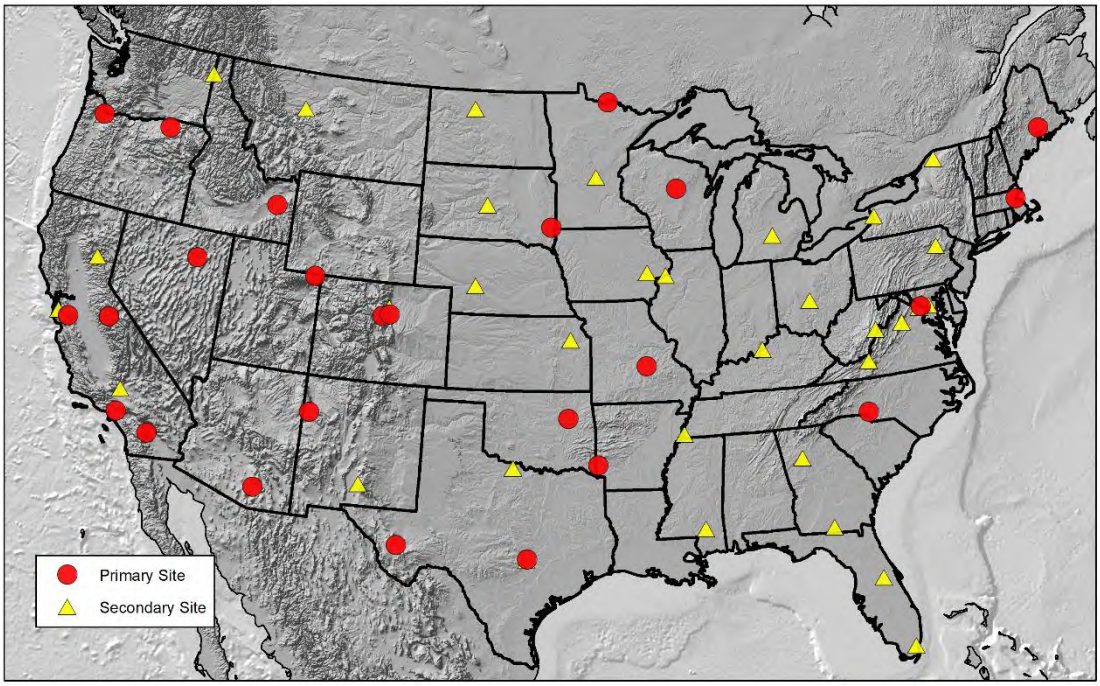

Figure 17: Proposed USAGN (from Peter, et al, 1989)

Instead, with changes in funding, special projects, and OCONUS work, many of the planned USAGN sites were never observed, however, gravity measurements continued steadily between 1987 and 2008. Projects included global sea level change, glacial isostatic adjustment, intercomparisons, local hydrology change, local elevation change, and other project-specific campaigns. Work of this nature slowed drastically after 2008. As a result, the USAGN has come to mean any USA site observed with a JILAg series or FG5 series absolute gravimeter along with their relative gravimeter excenters and intra-city ties. These stations are all part of the NSRS (or will be), and the realized network is shown in Figure 18 and Figure 19. In addition to the stations shown, surveys were also conducted in Hawaii, American Samoa, Puerto Rico and the US Virgin Islands over the last two decades

NGS has also made absolute gravity observations in foreign countries over the past decades. Surveys have been done in Bermuda, Canada, Mexico, Guatemala, El Salvador, Honduras and Nicaragua, and the Cayman Islands.

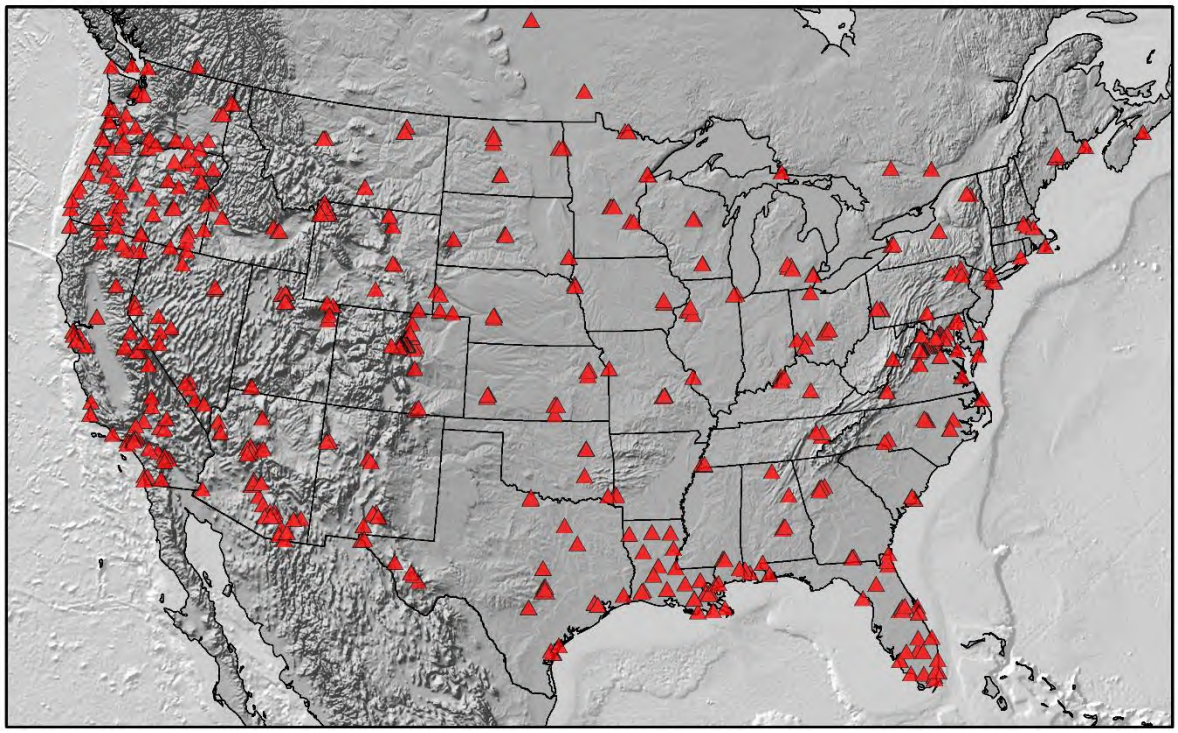

Figure 18: USAGN as realized in CONUS

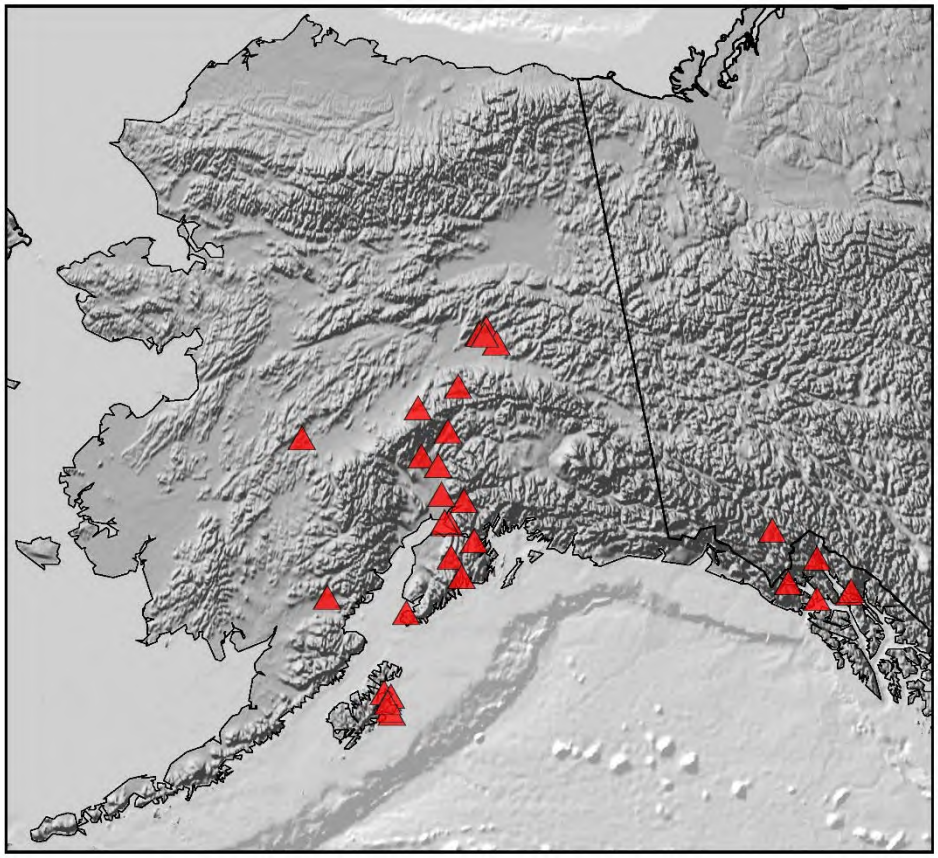

Figure 19: USAGN as realized in Alaska

2.1.2.4 International Comparisons of Absolute Gravimeters and Regional Comparisons

The International Association of Geodesy (IAG) established a new working group in 2015 with the stated goal of establishing a global absolute gravity reference system. This system will use periodic comparisons of absolute gravity instruments, conducted in cooperation with the International Committee for Weights and Measures (CIPM) and traced to metrological standards, to "define and harmonize" the measurements. International comparisons, held approximately every four years, are to be augmented by ad hoc "regional" comparisons held when and if it is convenient for participants (typically every two years). By overlapping attendance at these comparison events, a network of instrument consistency can be maintained. The comparison results and reference station gravity values will be collected in the AGrav database at the International Gravimetric Bureau (BGI) in France and mirrored at the Federal Agency for Cartography and Geodesy (BKG) in Germany.

NGS regularly participates in these international comparisons and often hosts the North American Regional Comparison (NACAG) at TMGO outside of Boulder, CO.

2.1.2.5 Mid-Continent Glacial Isostatic Adjustment Line (MCGL)

The Mid-Continent Glacial Isostatic Adjustment Line (MCGL) is a north-south transect of 10 absolute gravimeter stations in Canada and the USA established to observe temporal gravity change associated with glacial isostatic adjustment. It ranges from Churchill, Manitoba, at the southwest edge of Hudson

Bay to Rolla, Missouri, USA in central CONUS. The transect's first observation was in Churchill in late 1987 with first observations at other sites starting sporadically through 2005. There are also other 'off-line' stations that support this research. NOAA, the Geological Survey of Canada, and NRCan - Geomatics Canada have jointly accomplished this work. Approximately half of the sites have nearby continuous GNSS stations. For details on how this line fits with geoid rates that potential GeMS models would provide, see Section 6.3.2.

Maximum rebound is centered on Hudson Bay and decreases in magnitude radially (at least in southern semicircle). The data series at Churchill shows a trend of -1.9 μGals/year and a +10 mm/year height change. International Falls, MN, on US/Canada border has a trend of -0.45 μGal/year. Depending on the model, the hinge line (of 0 mm/yr) is either near the international border or in southern Minnesota. Southernmost stations in Rolla, MO and Iowa City, IA, show little or no gravity increase; however, the signal is near the uncertainty level.

2.1.3 Airborne Gravity

NGS's expertise and capability to collect and process airborne gravity data started with the GRAV-D project in 2008. GRAV-D is observing gravity data over the entire United States, Puerto Rico, Guam, and American Samoa (see Figure 20). As of July 2019, the project is approximately 75% completed with full completion planned for 2022. NGS will continue to be able to support airborne gravity surveying beyond the completion of the project's first phase in 2022. The instrumentation and experience acquired through this project will be available to GeMS for monitoring the gravity field changes, if necessary.

One might think that repeat GRAV-D airborne gravity data would be extremely useful for GeMS; however, the level of precision that is needed for GeMS is extremely high and beyond that of GRAV-D. For example, a 1 meter water equivalent (w.e.) mass change produces a gravity change of approximately 0.04 mGal. Maximum rates from GRACE are in the 10 cm w.e. / yr range or 0.004 mGal / yr. Most of the glaciers in Alaska have mass change rates of approximately 1 m w.e./yr or less. Even in extreme cases over individual glaciers, the maximum rates are approximately 4 m w.e / yr, which is 0.16 mGal / yr (Columbia and East Yakutat glaciers in Alaska – Larsen, *et al*., 2015). Even at these extreme rates, NGS's current GRAV-D survey would take at least 25 years to be able to resolve the gravity change assuming GRAV-D precision is 1 mGal.

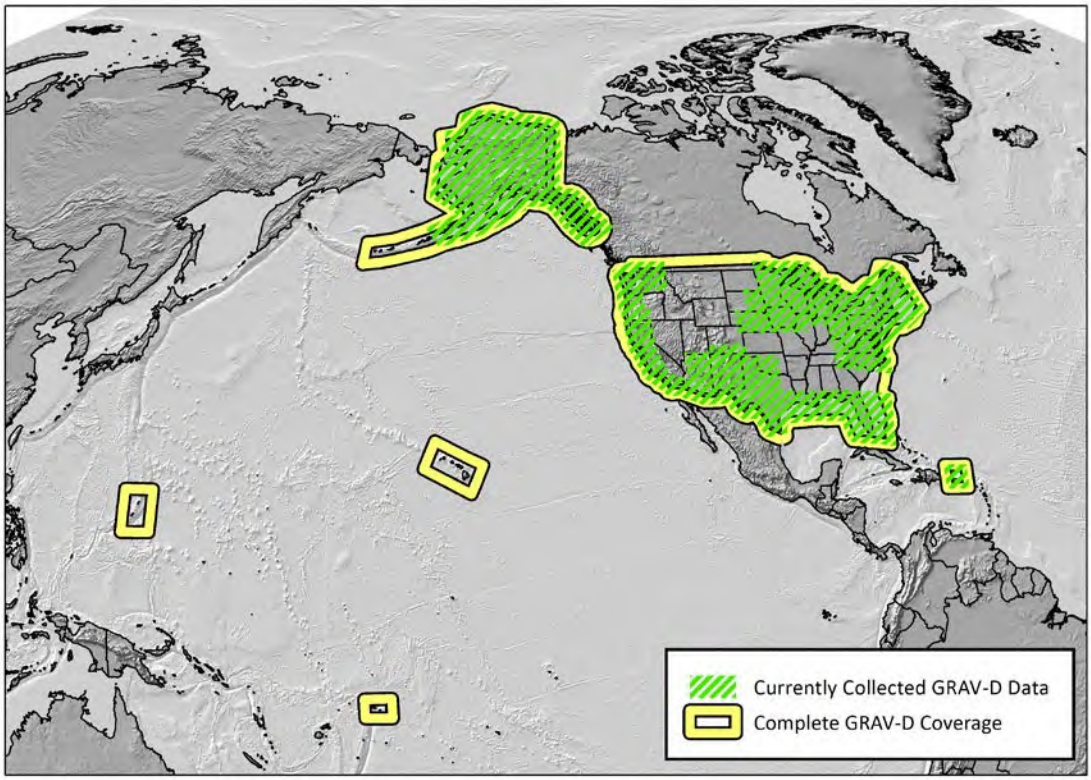

Figure 20: Current GRAV-D Status (as of 7/2019)

NGS currently owns three airborne gravimeters and two inertial measurement units (IMUs). These two instrument types are operated together to achieve more accurate gravity values compared to gravimeter-only measurements. The gravimeters are Micro-g Lacoste Turn-key Airborne Gravity Systems (TAGS). Two of the units are the Air/Sea III model (S-137 and S-161) and one unit is a model 7 (S-211). The Air/Sea III units have been operated almost continuously since early in the project and S-137 is nearing the end of its reliable lifespan. The major difference between the two Air/Sea III units is that S-137 uses an air damping system while S-161 uses magnetic damping. The gravimeters require a connection to a GPS or GNSS receiver on the aircraft, which should be a geodetic-grade antenna with at least L1/L2 capability for quality gravity measurements. The specifications of the models are provided in Table 4 below.

Table 4: NGS's Airborne Gravity Sensor Specifications

TAGS Air/Sea III	TAGS 7

- Sensor
  - Range: 20,000 milliGals (worldwide)
  - Drift: 3 milliGals per month or less
  - Temperature Setpoint: 45 to 65° C
- Stabilized Platform
  - Platform Pitch: ± 22°
  - Platform Roll: ± 25°
  - Platform Period: 4 to 4.5 minutes
  - Platform Damping: 0.71 of critical
- Control System
  - Recording Rate: 1 Hz
  - Serial Output: RS232
  - Additional I/O: Electronics, Sensor Temperature, Sensor Pressure
  - Resolution: 0.01 milliGals
- System Performance
  - Resolution: 0.01 milliGals
  - Static Repeatability: 0.05 milliGals
  - Accuracy: 1.0 milliGals, or better
    - 50,000 milliGal Horizontal Acceleration: 0.25 milliGals

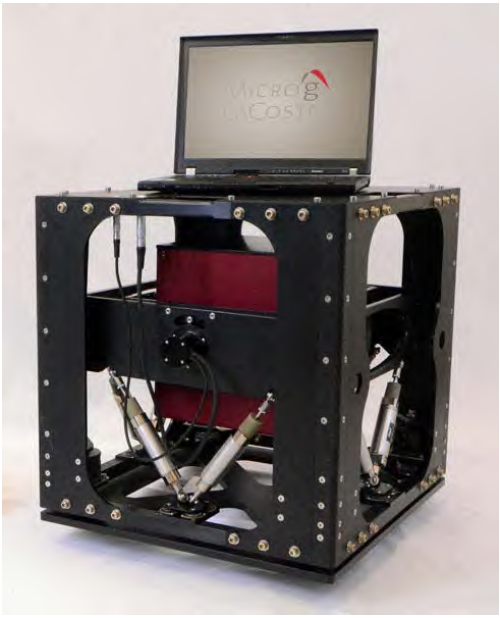

- Sensor
  - Range: ± 500,000 milliGals (worldwide)
  - Drift: 3 milliGals per month or less
  - Temperature Setpoint: 45 to 65° C
- Stabilized Platform
  - Platform Pitch: ± 25°
  - Platform Roll: ± 35°
  - Platform Period: 4 to 4.5 minutes
  - Platform Damping: 0.707 of critical
- Control System
  - Recording Rate: 20 Hz
  - Serial Output: RS232
  - Additional I/O: Electronics, Sensor Temperature, Sensor Pressure
- System Performance
  - Dynamic Range: 25,000,000
  - Static Repeatability: 0.02 milliGals in 2 minutes
  - Dynamic Repeatability: 0.75 milliGals in 2 minutes
- Misc.
  - Operating Temperature: 5 to 50° C

■ 100,000 milliGal Horizontal Acceleration: 0.50 milliGals ■ 100,000 milliGal Vertical Acceleration: 0.25 milliGals ● Misc. ○ Operating Temperature: 5 to 50° C ○ Storage Temperature: -10 to 50 ° C ○ Power Inputs (Into UPS) ■ 240 Watts average ■ 450 Watts maximum ■ 80-265 VAC, 47-63 Hz ○ Dimensions: ■ 71 x 56 x 84 cm ■ 28 x 22 x 33 inches ■ Weight: 140kg (310 lbs)	○ Storage Temperature: -10 to 50 ° C ○ Power Inputs (Into UPS) ■ 75 Watts average @ 27°C ■ 300 Watts maximum ○ Dimensions: ■ 58.4 x 53.3 x 55.9 cm ■ Weight: 73kg (161 lbs)

NGS owns two IMU kits which are comprised of a NovAtel SPAN system along with a Honeywell Laseref VI Micro IRS. The receivers in these systems were recently upgraded to the PwrPak 7 models. These are mounted as close to the gravimeter as possible. The specifications are summarized in Table 5 below.

Table 5: IMU Components and Specifications

NovAtel SPAN PwrPak 7	Honeywell Laseref VI Micro IRS
	
● Dimensions: 145 x 147 x 53 mm ● Weight: 500 g ● Power Consumption: 1.8 w ● Signal Tracking: ○ GPS (L1, L2, L2C, L5) ○ GLONASS (L1, L2, L2C) ○ BeiDou (B1, B2, B3) ○ Galileo (E1, E2a, E5b, E6, AltBOC) ○ SBAS, ○ QZSS ○ L-Band	● Dimensions: 6.5 x 6.4 x 6.4 inches ● Weight: 9.3 lbs ● Mounting Tray: 0.5 lbs ● Power Consumption: 20 w ● Accuracy (2-sigma) ○ Pitch Angle: 0.1 degrees ○ Roll Angle: 0.1 degrees ○ True Heading: 0.4 degrees ○ Ground Speed: 10 knots ○ Pitch Rate: 0.02 deg/sec ○ Roll Rate: 0.02 deg/sec

● Accuracy ○ Single Point L1: 1.5 m ○ Single Point L1/L2: 1.2 m ○ SBAS: 0.6 m ○ DGPS 0.4 m ● Communication Ports ○ RS-232 ○ RS-232/RS-422 Selectable ○ IMU ○ USB Device ○ USB Host ○ Ethernet ○ CAN Bus ○ Event Input and Output	○ Yaw Rate: 0.02 deg/sec ○ Longitudinal Acceleration: greater of 0.005 Gs or 0.5% of output ○ Lateral Acceleration: greater of 0.005 Gs or 0.5% of output ○ Vertical Acceleration: greater of 0.01 Gs or 1% of output ● Communication Ports ○ ARINC 429 Transmitters ○ ARINC 429 Receivers ○ Ethernet ○ Discrete Inputs (12)/Outputs (2)

Airborne gravity surveying also requires suitable aircraft to serve as a platform for the measurements. This is a critical component because any aircraft motion that overlaps with the frequency of the gravity signal will cause the data to be unusable. One of the lessons learned in the GRAV-D project is that each aircraft has slightly different flight characteristics, so even though an aircraft of one model collects quality gravity data that does not guarantee another aircraft of the same model will perform in the same way. The GRAV-D project has worked successfully with partners and contractors for aircraft services as summarized in Table 6.

Table 6: Aircraft used during GRAV-D (2008-2018)

Aircraft Operator	Aircraft Type	Engine Type	Number of Engines	Approx. Max. Duration (hrs)
NOAA	Cessna Citation II CE-550	Jet	Double	4.5
NOAA	Turbo Commander 1000 695A	Turboprop	Double	4
NOAA	Lockheed P-3 Orion	Turboprop	Four	9.5
NOAA	Gulfstream IV	Jet	Double	8.5
Naval Research Lab	Hawker Beechcraft King Air RC-12 (Non-military: 200)	Turboprop	Double	4
Bureau of Land Management	Pilatus PC-12	Turboprop	Single	5
Aurora Flight Sciences	Centaur	Turboprop	Double	4
Dynamic Aviation	King Air 200T	Turboprop	Double	4

Fugro Earth Data	Hawker Beechcraft King Air E90A	Turboprop	Double	5.5
Fugro Earth Data	Cessna 441 Conquest II	Turboprop	Double	6.5

Airborne gravity data can achieve different resolutions of data depending on the altitude and line spacing. Figure 21 illustrates the relationship between the flight altitude and the half wavelength, which would be the smallest feature that could be resolved at a given altitude. In addition, line spacing is important to consider. The line spacing should, at a minimum, be the width of the smallest feature that you want to resolve. The GRAV-D project has collected data between altitudes of 15,500 and 35,000 feet with a 10 kilometer data spacing, but the instrument systems are compatible with other flight plan configurations.

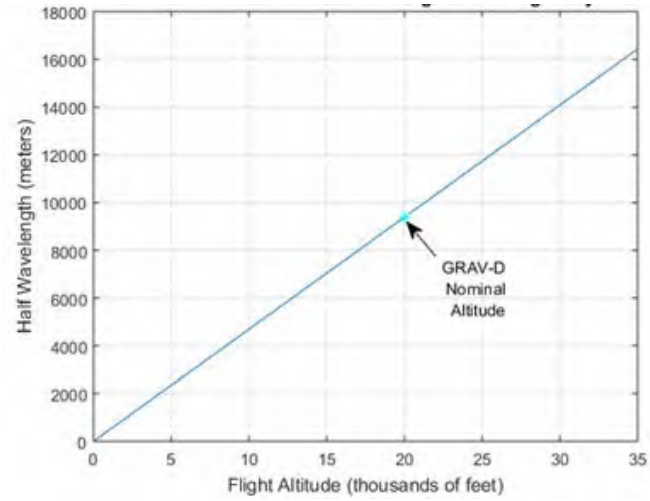

Figure 21: Airborne gravity half wavelength

The major constraint with airborne gravity surveying is the weather. Although gravimeter technology has and will continue to improve, turbulence and winds are the most common barriers to these surveys. Weather conditions will affect surveying differently depending on the geography, altitude, and wind direction. The anticipated effect of weather and mitigation measures must be considered for any airborne gravity survey.

2.2 The NOAA CORS Network (NCN)

The utility of the NOAA CORS Network (NCN) to support GeMS is 1) to observe and estimate $\dot{h}$ and 2) to provide existing infrastructure and sites to measure $\dot{g}$.

2.2.1 NOAA CORS Network Background and Current Status

NGS manages a network of Continuously Operating Reference Stations (CORSs) that collect GNSS data consisting of carrier phase and code range measurements in support of three dimensional positioning, meteorology, space weather, and geophysical applications throughout the United States, its territories, and a few foreign countries. The current NOAA CORS Network is shown in Figure 22 and Figure 23.

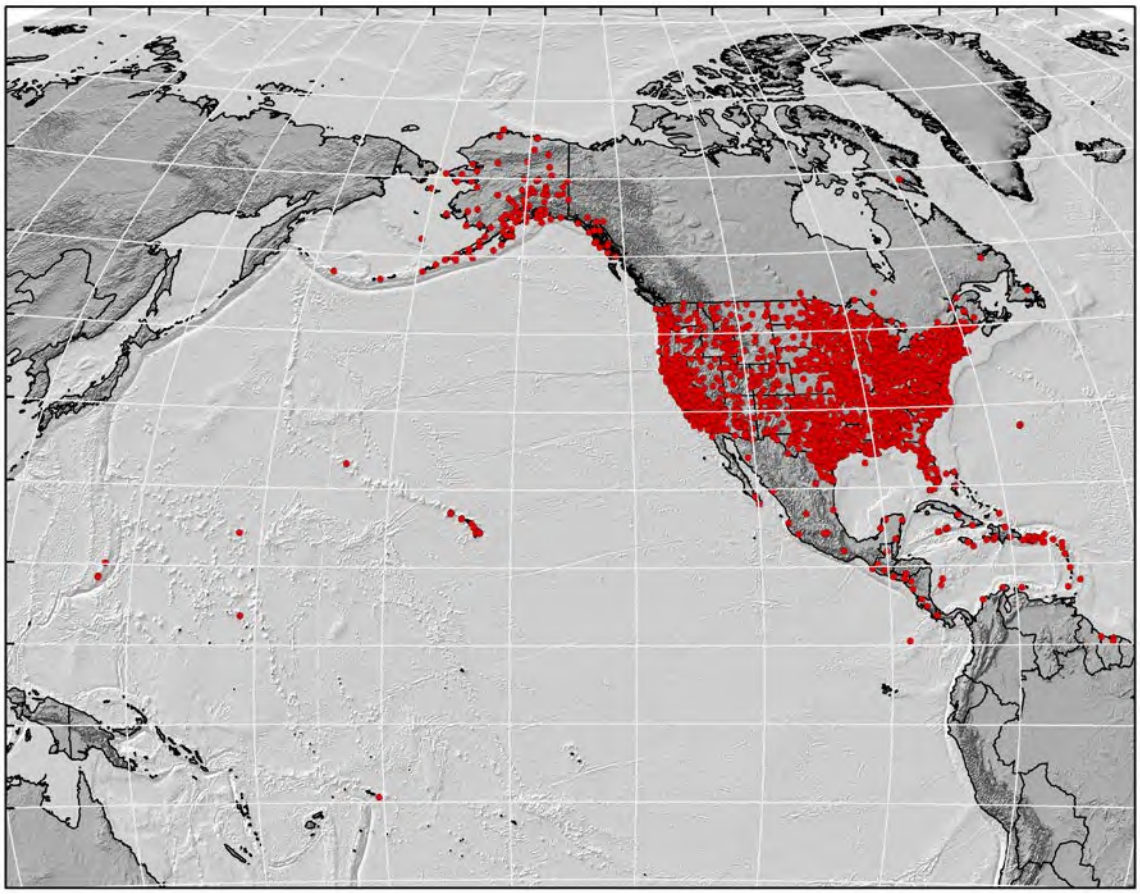

Figure 22: NOAA CORS Network geographic distribution across North America, Central America, and the Pacific

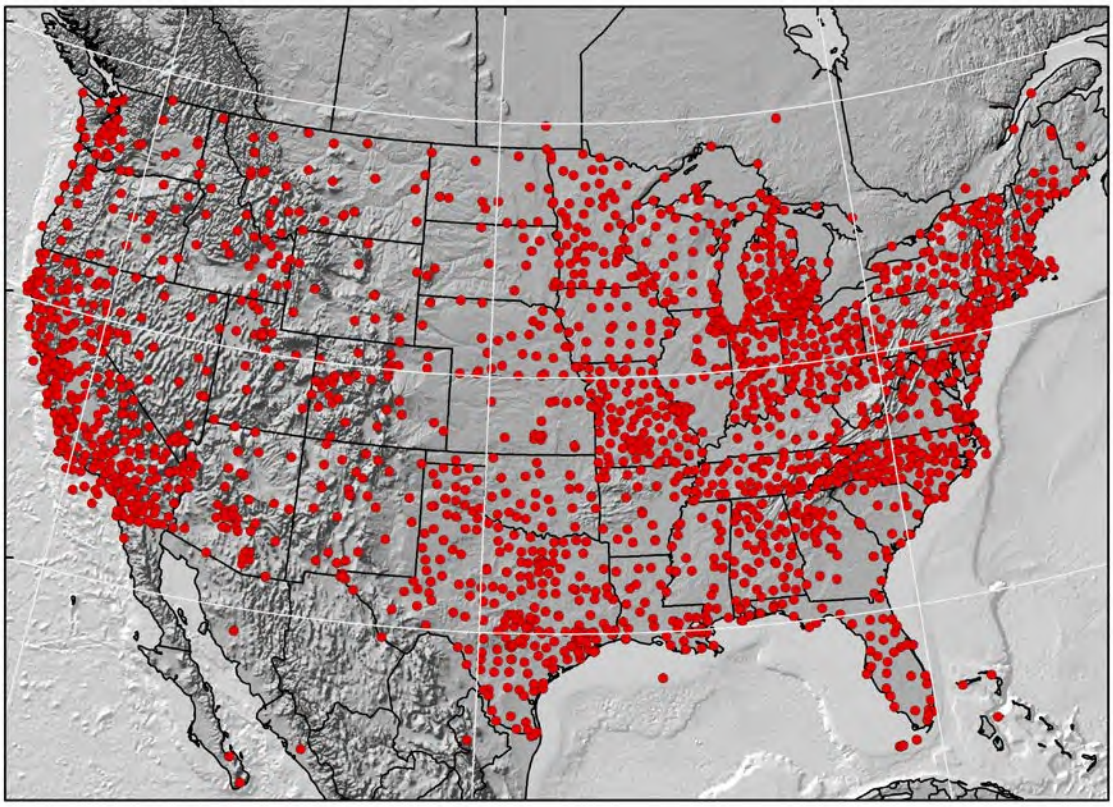

Figure 23: NGS CORS Network in CONUS

Surveyors, GIS users, engineers, scientists, and any member of the public that collects GNSS data can use CORS data to improve the precision of their positions. Accuracies of user-supplied coordinates are a few centimeters, horizontally and vertically, relative to the NSRS when post processed with the NOAA CORS Network for locations supported by the network.

The NCN is a multi-purpose cooperative endeavor involving government, academic, and private organizations. The sites are independently owned and operated. Each agency shares their data with NGS, and NGS in turn analyzes and distributes the data free of charge. As of August 2015, the NOAA CORS Network consists of almost 2,000 stations, contributed by over 200 different organizations, and the network continues to expand. The NOAA CORS Network provides the backbone control stations for NGS's OPUS solutions. Due to a variety of factors, NGS does not include every continuously operating GNSS (cGNSS) station in the NOAA CORS Network. Discussion of these additional cGNSS stations can be found in Section 3.5.

NGS recently established the NOAA Foundation CORS Network to ensure access to the NSRS. Because of the reliance on external entities to the NOAA CORS Network, NGS cannot control the quality of monumentation, data collection strategies, nor the spatial distribution of sites. The NOAA Foundation CORS Network is a subset of the NOAA CORS Network that NGS will maintain and build. The proposed configuration of the NOAA Foundation CORS Network (NFCN) is shown in Figure 24. Sites selection is based on quality metrics and characteristics that include distributed spacing, site stability, monumentation, multipath sources, power, and communications. The NOAA Foundation CORS Network also incorporates additional sensors like weather stations and soil moisture sensors, and many of these

CORSs will be colocated with instrumentation that provides other geodetic observing techniques like VLBI, DORIS, SLR, and absolute gravity.

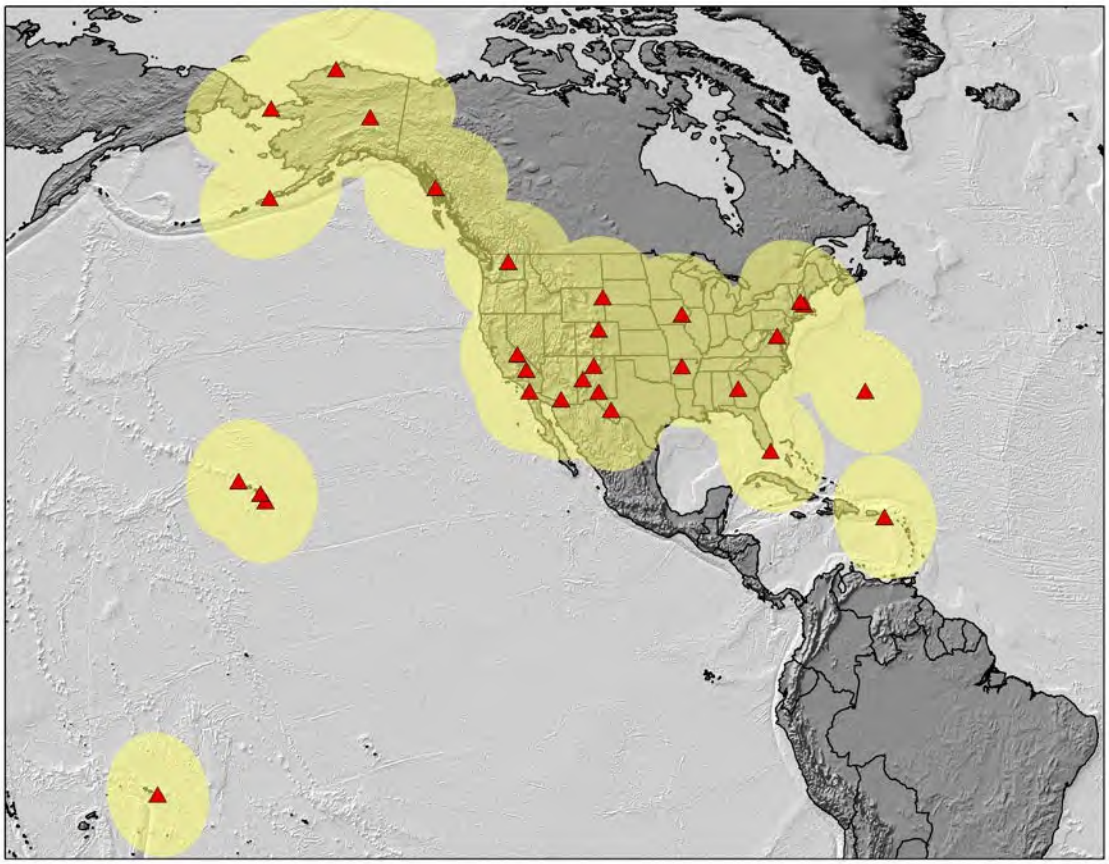

Figure 24: Proposed NGS Foundation CORS sites with 800 km buffer

There are a handful of NOAA CORSs that have been colocated with absolute gravity (see Figure 25). These USAGN stations have at least a single absolute gravity observation and are within 1 km of a continuous GNSS station (NOAA CORS Network, or other cGNSS stations as identified in the University of Nevada-Reno (UNR) database (Blewitt, *et al.*, 2018)).

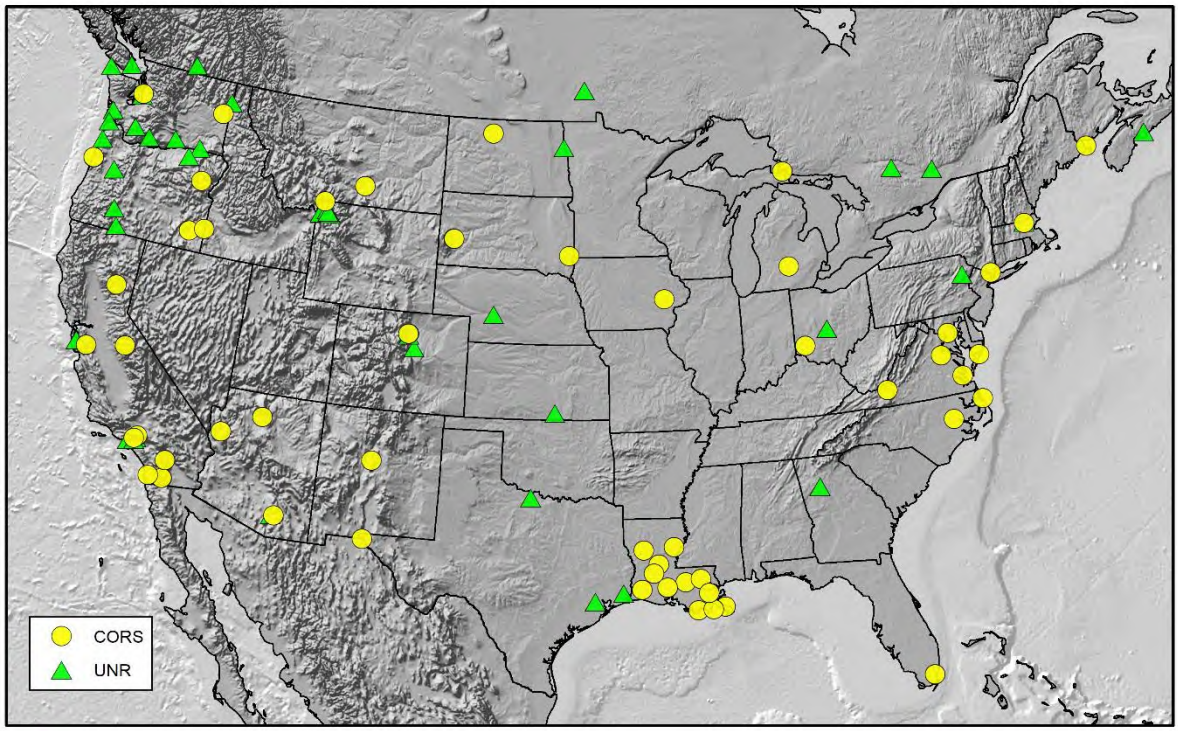

Figure 25: USAGN and NGSGN Gravity Stations colocated with Continuous GNSS (NOAA CORS Network or other cGNSS Networks). Locations are considered to be colocated if the separation distance is 1 km or less.

2.2.2 GGOS, IHRS, and IHRF

A number of international geodetic systems have been initiated over the previous 20 years under various IAG commissions, working groups, and other organizational structures. The Global Geodetic Observing System (GGOS) is the observing system of the IAG and established in 2003. GGOS is a broad system that is devoted to providing geodetic infrastructure to monitor the Earth, and it is organized under multiple Focus Areas. The Focus Area most relevant to GeMS is the 'Unified Height System'. This can be further divided into the International Height Reference System (IHRS) and International Height Reference Frame (IHRF), which aim to provide a global geopotential height system. A small subset of the NOAA CORS Network is included in the IHRF and inclusion of time-dependent geopotential height changes at these sites is a recommended NGS effort in the near future.

2.3 NGS's GPS and Leveling Campaign Capabilities

2.3.1 International Great Lakes Datum (IGLD)

The International Great Lakes Datum (IGLD) is a time-series of vertical datums for the Great Lakes and St. Lawrence Seaway. It is shared between Canada and the USA. Maintenance of IGLD supports vessel navigation, informs the management of water control structures and locks, and helps to establish changes over time due to the effects of GIA. It is tied to CGVD28 and NAVD 88 at lake level gauges via geodetic leveling. CGVD28 and NAVD 88 are the two vertical datums of Canada and the USA, respectively. There have been four GPS campaigns in 1997, 2005, 2010, and 2015 (conducted jointly by

the USA and Canada) at water gauges and associated benchmarks. A fifth campaign is planned for 2020.

2.3.2 Geoid Slope Validation Surveys (GSVS)

In the last decade, NGS has completed three terrestrial geodetic surveys: Texas, Iowa, and Colorado. Each of these surveys are similar in design and types of observations. The surveys are linear profiles along established roads with total lengths of approximately 300 km. Physical monuments at 1.6 km spacings are observed with high accuracy, high precision (sub-cm RMS) geodetic techniques including static GNSS, geodetic leveling (2^{nd} Order - Class I or better), absolute and/or relative gravity, and deflections of the vertical. These surveys are designed to validate the static portion of the geoid model (SGEOID2022 and its precursor xGEOID models).

NGS has the staff, knowledge, and equipment to complete additional GSVS-like surveys to validate the DGEOID2022 model in targeted areas of geoid change over time, if deemed necessary. Repeating a GSVS line with GNSS, geodetic leveling, deflections of the vertical (Repeat Geoid Slope Validation Surveys (RGSVS)) measurements in targeted areas of change, would be a viable way to validate the dynamic geoid model relatively (mark-to-mark) along the RGSVS line. Geographic areas that are strong candidates for this type of effort include the Great Lakes region, Alaska, Southern Louisiana, the Chesapeake Bay region, Yellowstone, or anywhere else with a significant rate of geoid change.

3 Geoid Monitoring Techniques External to NGS

The following section describes geodetic and geophysical techniques that are currently known to NGS and show promise for GeMS, but are outside of NGS's current expertise. All of these techniques rely on a non-NGS entity to create a product (model, dataset, etc.) that NGS could potentially utilize. NGS regularly leverages partnerships for other products such as the GOCO05S satellite gravity model produced by an ESA consortium led by the Technical University of Munich and used at NGS in static geoid modeling. Because NGS is not the primary developer, there is reduced control in the products' creation, accuracy, format, frequency of update, spatial resolution, and other parameters. Risks associated with any reliance on these outside products must therefore be mitigated, but the opportunity for a more comprehensive and efficient GeMS warrants exploration of these opportunities in more detail, and the interdisciplinary nature of the geophysical models in particular present an added opportunity to expand educational avenues and expose more early career researchers to reference frame elements of geodesy. These other techniques are supported by a wide range of entities like other parts of NOAA, federal agencies (NASA, USGS, JPL, NGA), universities and individual researchers (University of Texas at Austin Center for Space Research (UTCSR), University of Toronto, University of Nevada, Reno (UNR)), and international groups (GFZ, ESA). A summary of these techniques with GeMS related metrics is provided in the following table:

Table 7: Summary of Known Geoid Monitoring Techniques that are currently outside of NGS's Expertise

Type of Data:	Subtypes:	Availability:	Operability:	Feasibility:	Affordability:	Accuracy:
Satellite Gravity from GRACE / GRACE-FO		**Very High** – Global coverage with a resolution of ~200 km; available in monthly time periods from 2002-2017 with very few missing months	**Low** – Satellite missions are out of NGS's control, dependent on NASA for success.	**Very High** – Assuming available GRACE data, very easy to incorporate into GeMS	**Very High** – No cost to use global models created by others ***Low** – If funding is needed for new space mission*	**Medium to High** – Geoid rate accuracy at 0.25 mm/yr for 200 km spatial resolutions. Accuracy becomes questionable after 10 years of extrapolation.
Satellite InSAR		**High** – numerous satellite missions, processing software available.	**Low** - NGS currently does not have expertise in working with InSAR data	**Medium** – NGS currently does not have InSAR capability so rather difficult but could use models built by external groups.	**Medium** – Not in NGS's current staffing and would require additional resources	**Very High –** a few mm/yr for vertical surface rates.

Geophysical Models (Various)	**GIA**	**Very High** – Numerous external groups producing global models at adequate resolutions	**Low** – Out of NGS's mission to maintain GIA models	**Very High** – external models can easily be ingested into GeMS	**Very High** – Models are freely available.	**High** – long wavelength (100s of kms) accuracies are very well resolved (sub mm/yr)
	Ice-Mass	**Medium** – Annual models developed by cryosphere researchers, high spatial resolution but variable extent.	**Low** – Currently out of NGS's current expertise to maintain ice-mass models - dependent on external researchers.	**High** – Easy to incorporate into GeMS, depends on what models are used.	**Medium to High** – No cost for external models. Significant costs if NGS collects the data to build the model.	**Medium to High** – Dependent on models used
	Earth-quake	**Low** – limited models available over limited areas. NGS would likely need to survey.	**High** – rare events so not difficult to maintain	**Very High** – Incorporate large events after occurrence	**High** – Minimal costs to survey effected areas and build into model	**High** – can be controlled by NGS in survey specifications
	Volcanic	**Low** – limited models available over limited areas. NGS would likely need to survey.	**High** – Very rare events so not difficult to maintain	**Very High** – Incorporate large events after occurrence	**High** - Minimal costs to survey effected areas and build into model	**High** - can be controlled by NGS in survey specifications
	Hydro-logy	**High** – Numerous models available over global scales for many decades.	**Low** – difficulty to maintain due to constraints. Not in NGS mission.	**High** – Some work would be needed to build into GeMS but doable with current staff/ resources	**Very High** – freely available. ***Low*** *– if models are developed at NGS*	**Medium** – numerous background models and datasets incorporated into the models
Other Terrestrial Gravity Programs	**NRCan and Others**	**Medium** – Very sparse networks around North America	**Low** – not in NGS mission	**Very High** – Incorporate into GeMS models and validation	**Very High** – freely available	**Very High** – 1-2 μGals
Other GNSS Networks		**Very High**	**Low**	**Very High**	**Extremely High**	**Very High**
DoV		**Low**	**Medium**	**Very High**	**Low**	**High**
Satellite Altimetry		**Medium**	**Low**	**High**	**Very High**	**Low to Medium**

3.1 Temporal Geopotential Models from Satellite Gravimetry

3.1.1 Global Spherical Harmonic Models from GRACE

Temporal satellite gravity missions are a critical component of any geoid monitoring service. The U.S./German GRACE (Gravity and Climate Experiment) satellite mission was designed to provide the temporal gravity field variations throughout its mission duration which lasted from 2002 – 2017. The benefits in using this type of data product in GeMS include: 1) combination of all geophysical phenomena (e.g. land surface hydrology, cryosphere changes, episodic (earthquake) processes, glacial isostatic adjustment (GIA)) into a model of geoid change, 2) validation by international groups that provide independent models, 3) high accuracy at long wavelengths at monthly intervals, and 4) a global model provided as spherical harmonic coefficients for relative ease in computations anywhere on Earth.

A number of international GRACE groups are processing GRACE data and producing monthly global geopotential models. The three analysis centers are the University of Texas at Austin Center for Space Research (UTCSR), NASA Jet Propulsion Laboratory (JPLEM), and GFZ German Research Center for Geosciences (GFZOP). The most current GRACE data from these groups is Release 6 (RL06). These groups produce data at Level 1, Level 1B, Level 2, and Level 3 depending on the degree of processing. The global spherical harmonic geopotential models are considered Level 2. Typically, the geopotential models are produced to degree and order 60 (UTCSR also produces a model to degree and order 96). These models come in the form of monthly spherical harmonic coefficients ($C_{n,m}$, $S_{n,m}$). An example for the monthly $C_{4,0}$ term is shown in Figure 26 below. There is not a great deal of variability exhibited in the geoid rates coming from the different geopotential models (i.e. UTCSR, JPLEM, and GFZOP).

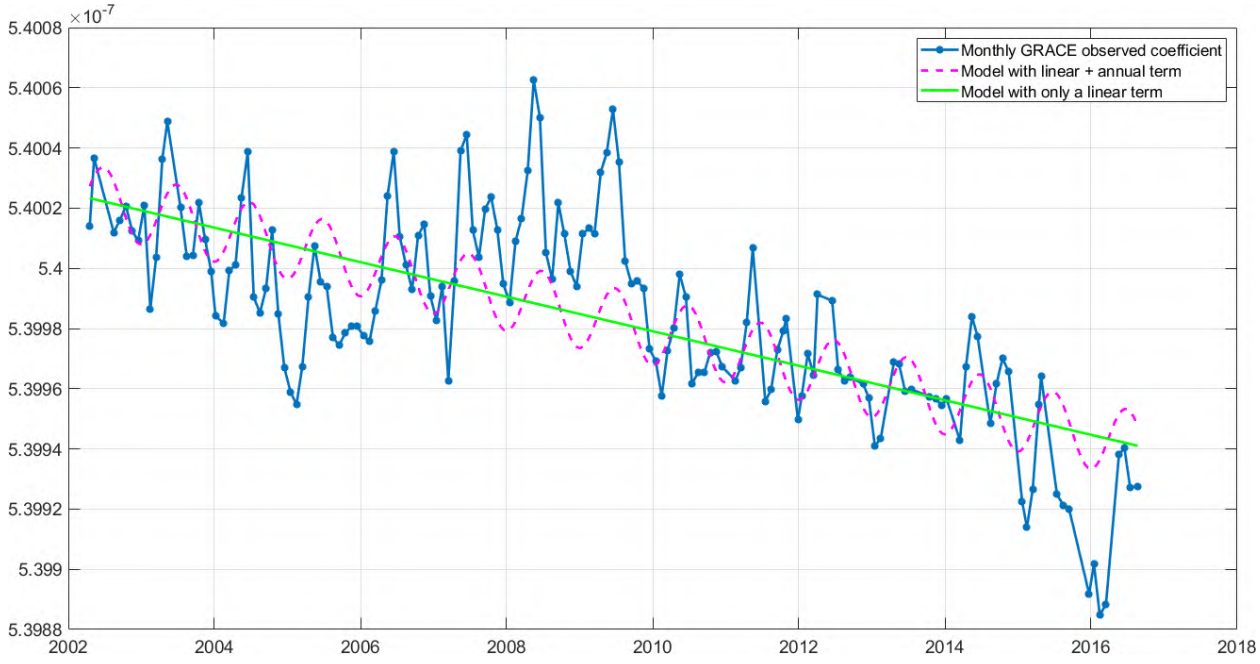

Figure 26: $C_{4,0}$ Time Series from UTCSR RL06 Spherical Harmonic Model

It is feasible at present to produce a time series for every $C_{n,m}$ and $S_{n,m}$, estimate the trend ($\dot{C}_{nm}$, $\dot{S}_{nm}$),

and then use all of the degree and order secular trends to compute the rate of change in N ($\dot{N}$) at every geographic location, globally. This is theoretically accomplished using (14) where the dot terms inside the double summation are the secular trends estimated from each individual time series.

$$\dot{N}(\theta,\lambda) = R_E \sum_{n=0}^{N}\sum_{m=0}^{n}\left(\dot{\bar{C}}_{n,m}cos(m\lambda) + \dot{\bar{S}}_{n,m}sin(m\lambda)\right)\bar{P}_{n,m}(cos\theta) \quad (14)$$

For all GRACE time series estimates presented in this document, the time series model takes the general form of Eq. (15) (after Bevis and Brown, 2014) where only the annual sinusoid is estimated (i.e. n_F = 1) and four parameters are estimated: an annual sine and cosine term (s_k and c_k), a linear rate (a_1), and a constant term (a_0). The unknown parameters are then estimated using robust least squares.

$$y(t) = a_0 + a_1 t + \sum_{k=1}^{n_F}[s_k \sin(\omega_k t) + c_k \cos(\omega_k t)] \quad (15)$$

where: $\omega_k = \frac{2\pi}{\tau_k}, where\ \tau_1 = 1\ year, \tau_2 = \frac{1}{2}year, \tau_3 = \frac{1}{3}year, \ldots$

Eq. (14) can be further expanded to estimate other geopotential-related secular trends like the time rate of change for gravity anomalies, gravity disturbances, DoV components, or heights. These equations are provided in Appendix A. Furthermore, any of the additional signal components estimated in the time series with Eq. (15) can be propagated to the corresponding geopotential field. For example, if we use the estimates of the annual cosine and sine terms (c_k and s_k), the two amplitudes can be combined into an estimate of the annual amplitude of geoid changes (see Figure 29).

To provide an illustration of the magnitudes and resolutions the GRACE models provide, the secular geoid rates for CONUS and Alaska are shown in Figure 27 and Figure 28. Both grids are in mm/yr. Additionally, the annual amplitude is shown in Figure 29. These models are at a fairly low spatial resolution where degree/order 60 or 96 implies ~333 km and ~208 km resolutions, respectively.

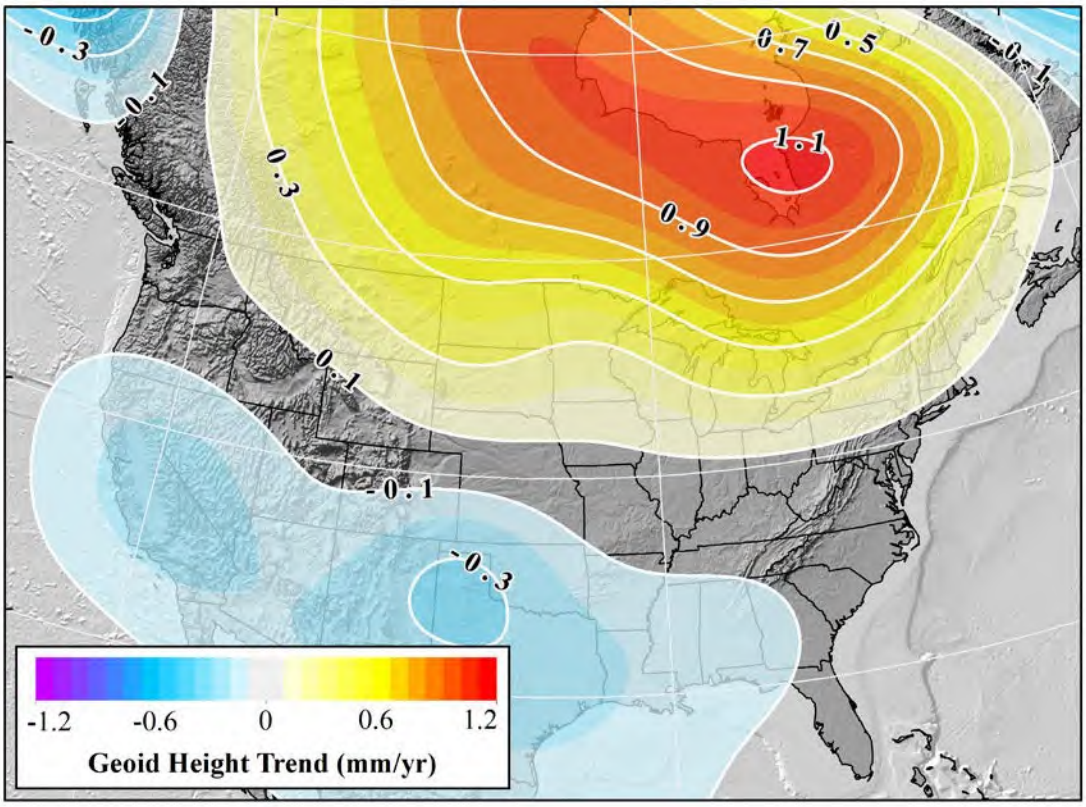

Figure 27: GRACE Trend over CONUS from UTCSR RL06 Model [mm/yr]

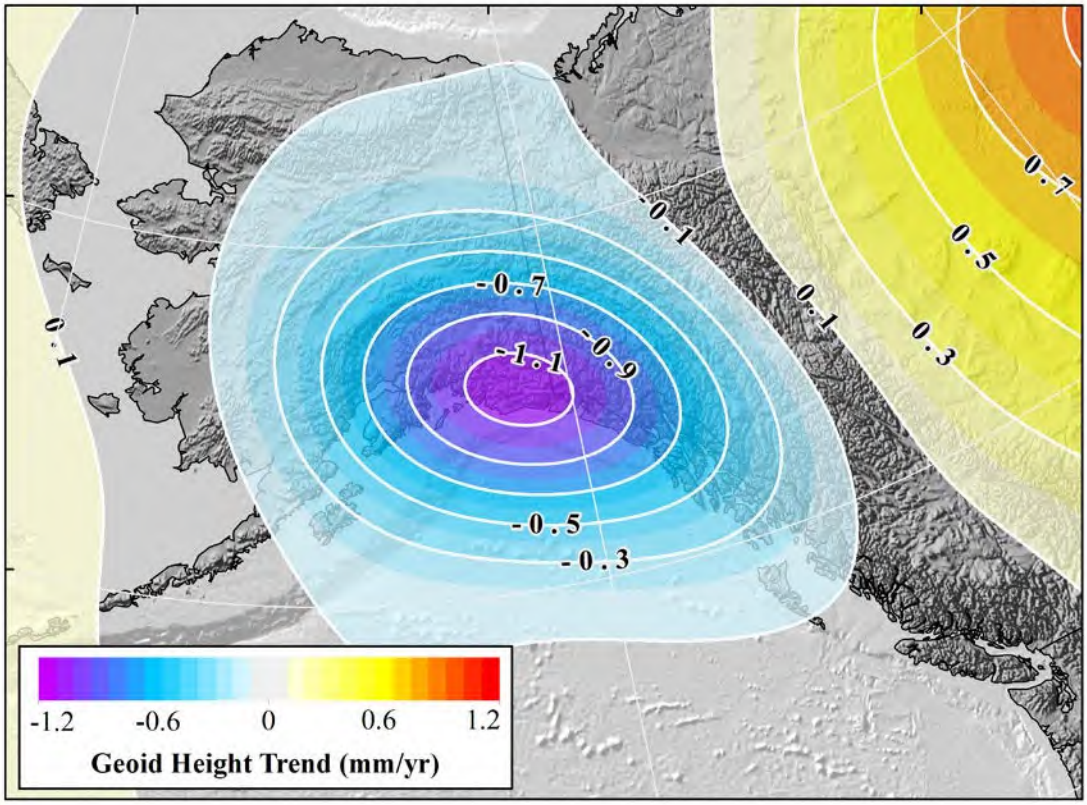

Figure 28: GRACE Trend over Alaska from UTCSR RL06 GRACE Model [mm/yr]

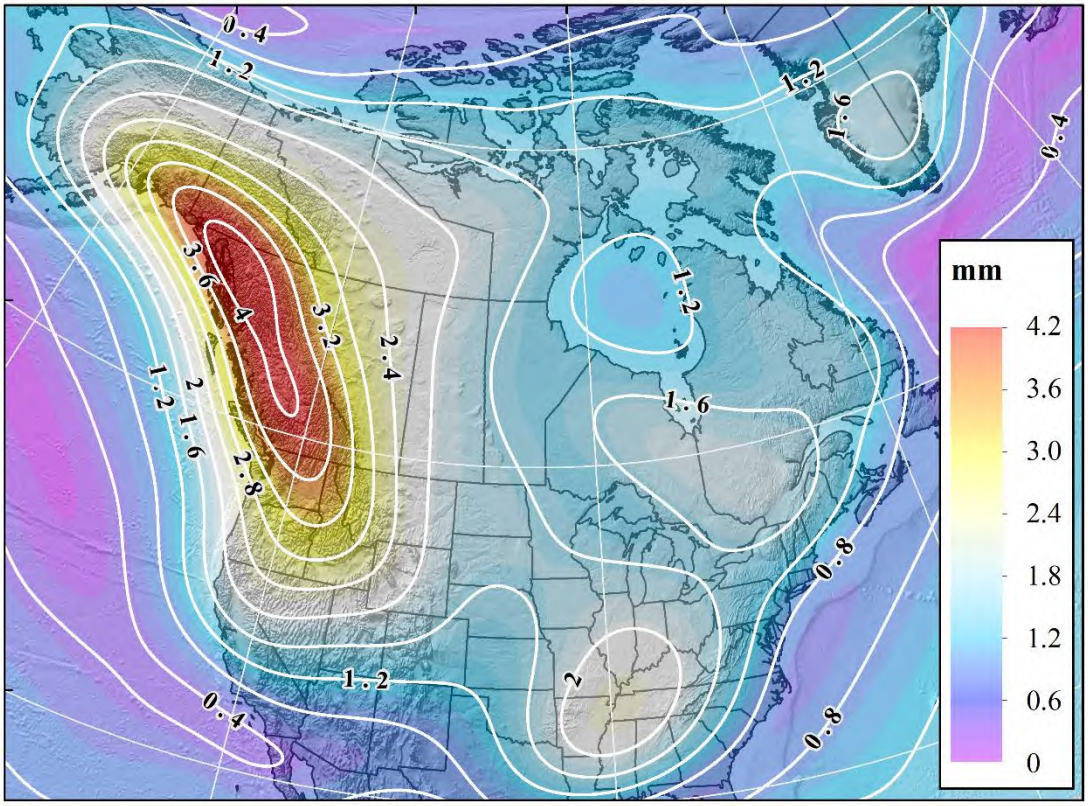

Figure 29: Geoid Annual Amplitude [mm] from UTCSR RL06 Model

One significant risk factor for GeMS is complete dependence on only one satellite system. GRACE had an original life-span of 5 years and operated over 15 years in orbit. GRACE-FO was launched on 22 May 2018 and has a mission duration of at least 5 years. Each of these satellite gravimetry missions has a finite lifespan, and NGS has almost no control over future missions, such as how long the missions will last. Additionally, the satellite gravity models have a low spatial resolution (approximately 200 km) relative to other techniques. While this resolution is adequate for large geophysical processes contributing to net geoid change (e.g. GIA), more localized processes are not well-captured at these satellite resolutions.

3.1.2 Global Mass Concentration (Mascon) Models from GRACE

Another product available from various processing centers including JPLEM, UTCSR, NASA Goddard Space Flight Center (GSFC), and GFZOP are surface mass concentrations (mascons) as observed by the GRACE satellites. These global solutions are tuned to produce similar results as the GRACE Level 2 products for scientific applications. In Figure 30, the 2002-2016 trend in water equivalent (w.e.) mass change is shown from NASA GSFC's current release (v02.4) (Luthcke, *et al.,* 2013). This product consists of monthly grids with a 1 degree spatial resolution and is estimated from the GRACE KBRR range-rate observations with their full noise covariance. The solution includes mascons over both continental areas and the oceans with 41,168 individual mascons in the global solution. There are a few flavors of these models produced using different background models, removing various GIA models, etc. We show the 'standard' mascon solution, which is most consistent with the GRACE Level 2 global spherical harmonic models and most suitable for GeMS since the GIA signal is intact.

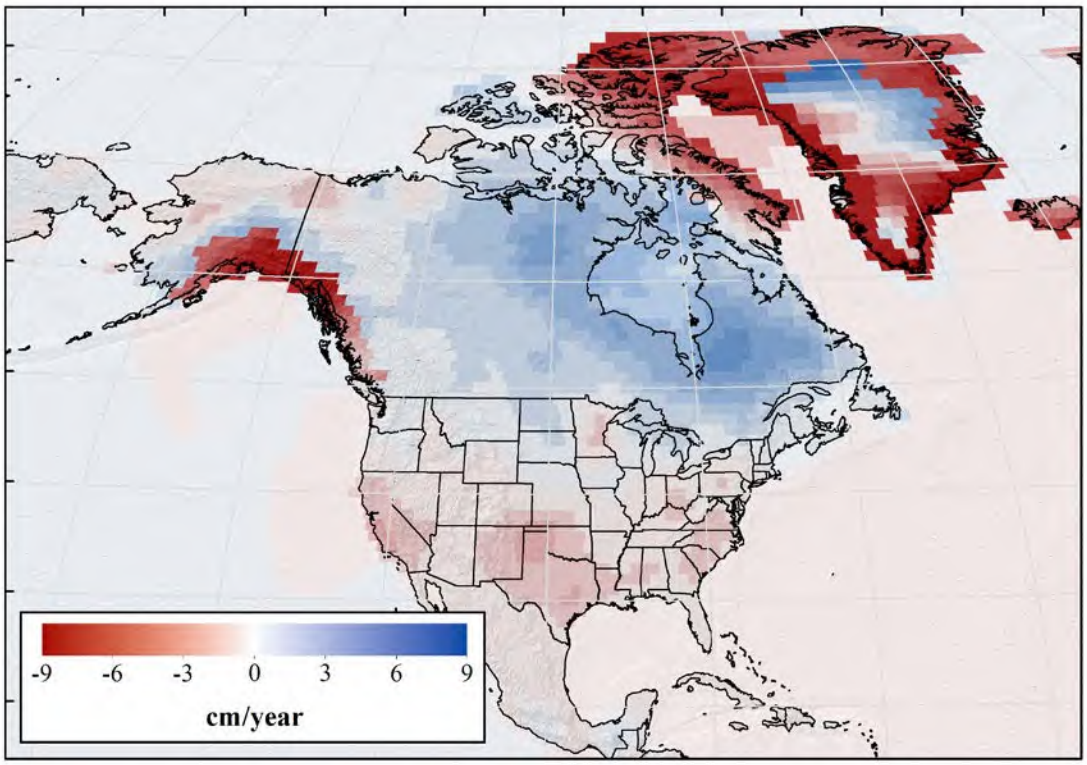

Figure 30: NASA GSFC Mascon trend in the surface mass anomalies as cm w.e. / yr from 2002-2016 based on v02.4 (Luthcke, et al., 2013).

To convert these monthly cm w.e. mass changes into geopotential quantities for GeMS (i.e. geoid change trends, or amplitudes) requires a process similar to the monthly GSM. First, we estimate a trend, annual sine component, and annual cosine component for each of the mascon blocks for the entire time period based on the model in Eq. (15) and robust least squares. An example of the time series and modeled components is shown in Figure 31 for a single mascon located in the Hudson Bay region of Canada.

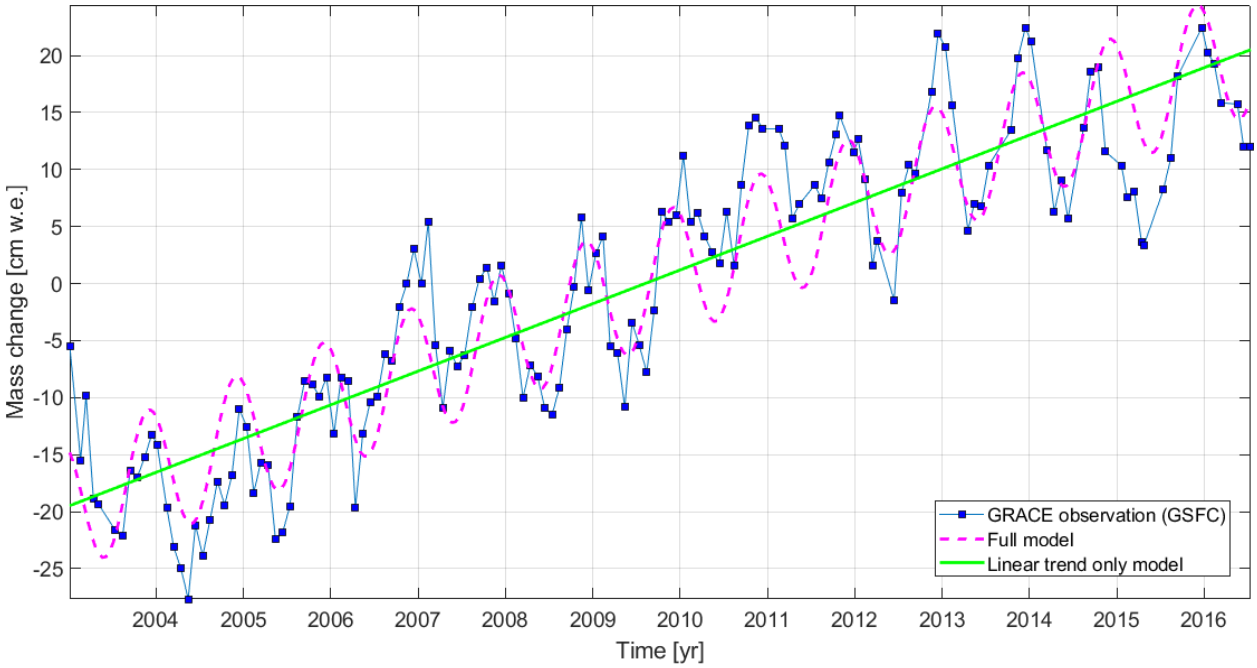

Figure 31: Mass change in cm w.e. from GSFC mascon solution v02.4 for a 1° x 1° block in the Hudson Bay region of Canada. GRACE derived mass change observations shown in blue. The full model and secular component are shown in pink and green, respectively.

These individual trends are then gridded, resulting in a global distribution of cm w.e. / year trends on an equally spaced 1 degree grid. This grid is then spherically analyzed resulting in coefficients for the trend in water equivalent height ($\dot{\tilde{C}}_{nm}$, $\dot{\tilde{S}}_{nm}$). The water equivalent coefficients still need to be converted into geopotential coefficients, which is done spectrally using Eq. (16) (Wahr, *et al.*, 1998), to obtain the geopotential coefficients that are desired and compatible with the GRACE Level 2 spherical harmonic models. The derived geopotential coefficients can be used in Eq. (14) to produce geoid rates and additional equations in Appendix A to obtain other geopotential related quantities.

$$\begin{Bmatrix} \dot{\tilde{C}}_{nm} \\ \dot{\tilde{S}}_{nm} \end{Bmatrix} = \frac{3\rho_w}{R_e \rho_e} \frac{1+k_n}{2n+1} \begin{Bmatrix} \dot{\tilde{C}}_{n,m} \\ \dot{\tilde{S}}_{n,m} \end{Bmatrix} \tag{16}$$

where:
$\rho_w = 1000\ kg/m^3$
$\rho_e = average\ Earth\ density = 5517\ kg/m^3$
$k_n = Love\ Load\ Number\ of\ degree\ n$ (see Farrell, 1972)

The secular geoid rate based on the NASA GSFC mascon model is shown in Figure 32 and Figure 33. These are comparable to the rates determined by the spherical harmonic model shown in Figure 27 and Figure 28 , respectively.

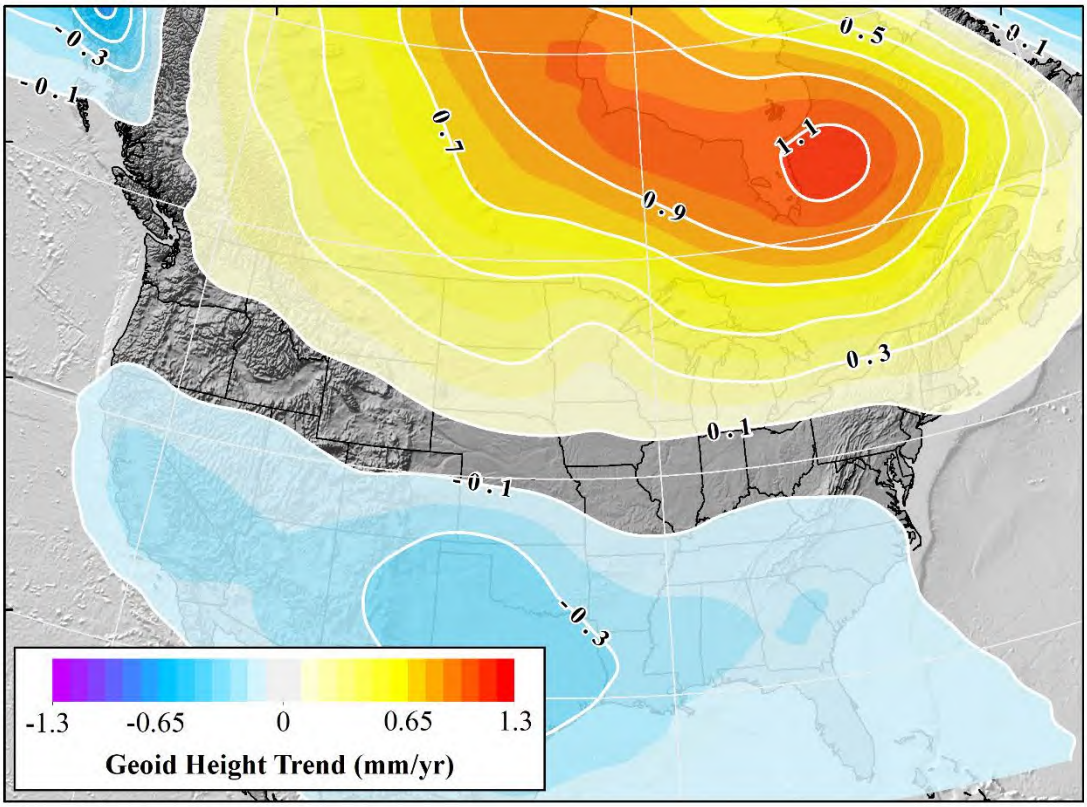

Figure 32: Geoid rate over CONUS based on the GSFC mascon model [mm/yr]

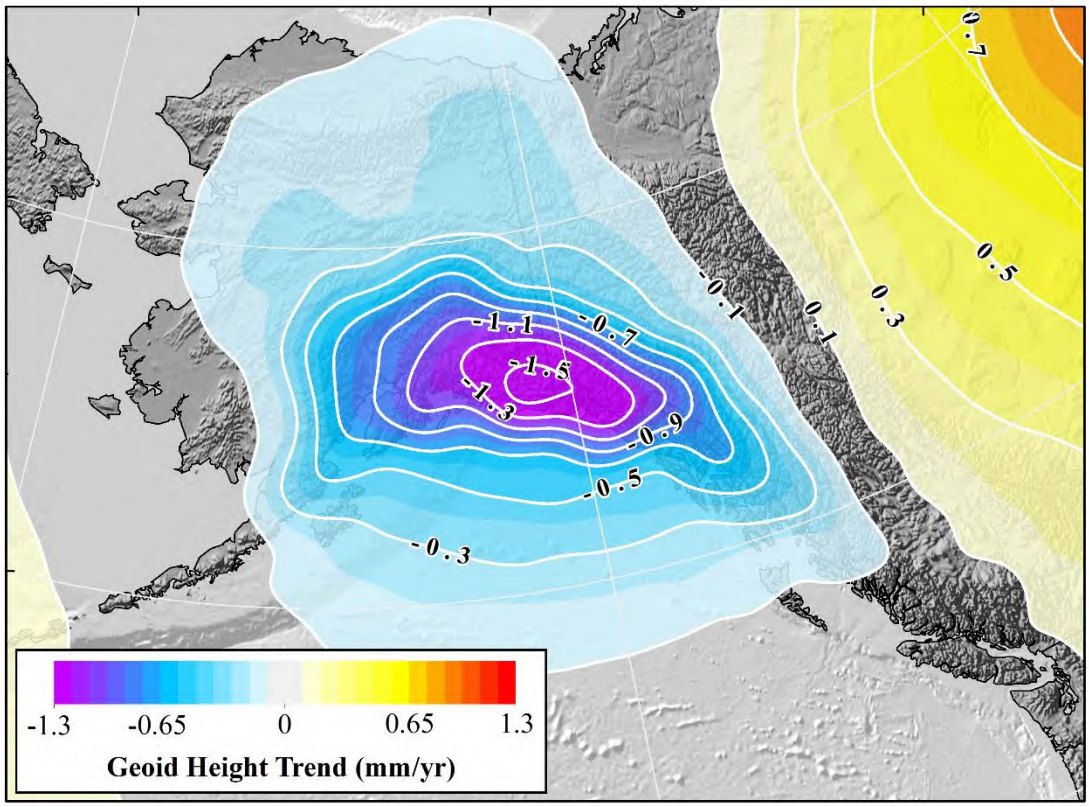

Figure 33: Geoid rate over Alaska from GSFC mascon model [mm/yr]

One can compare the models either in the spectral domain or the spatial domain. Comparing the spectral properties of the two models: the UTCSR RL06 spherical harmonic (SH) model and NASA GSFC's v02.4 mascon model, there are some significant spectral differences in the resulting geoid change as seen in the geoid rate degree variance illustrated in Figure 34. Below degree 40, both of the models produce almost identical spectra. The UTCSR model has a much lower degree cutoff with a maximum degree of 96 than the GSFC mascon solution with a maximum degree of 180. However, the mascon model doesn't contain additional spatial information but uses spatial constraints and leakage corrections to produce a more appropriate model. Additionally, a number of studies have discussed considerable error in the spherical harmonic solutions at the higher degrees. The increased power from about degree 60 up to degree 96 in the spherical harmonic model is evidence of this issue at the higher degrees. It is therefore recommended that a GeMS model should only use $n_{max} = 60$ from the spherical harmonic models currently in production. The mascon solution doesn't contain these power issues and could be used up to $n_{max} = 180$.

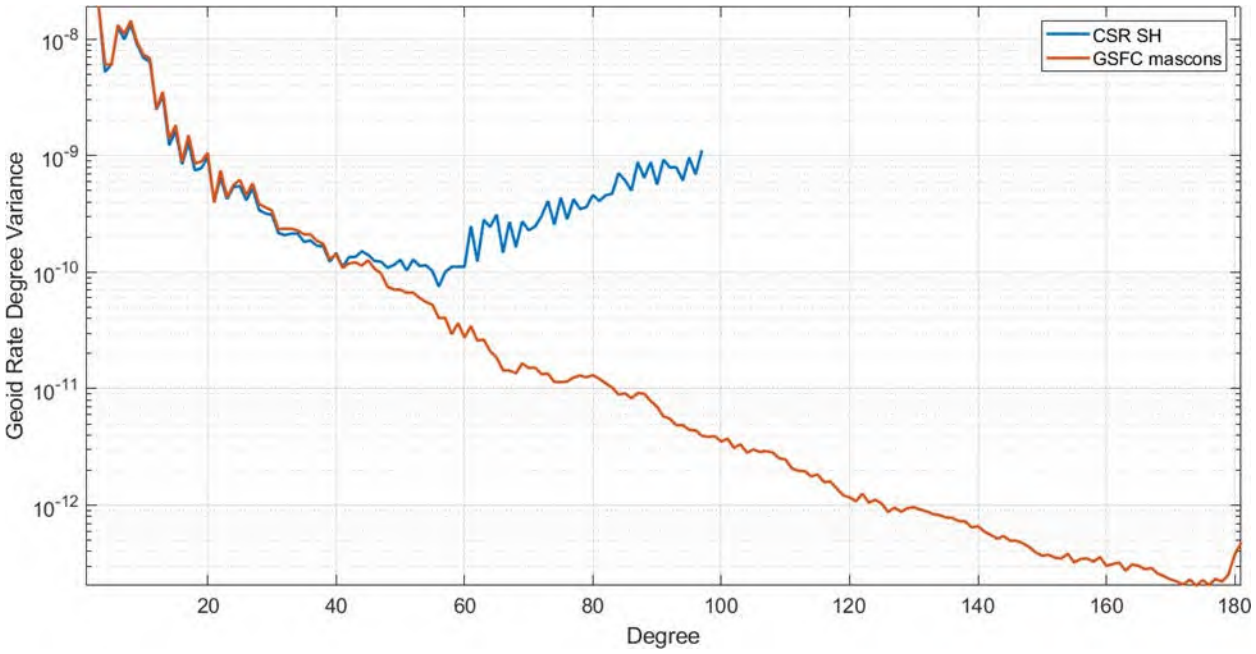

Figure 34: Geoid Rate Degree Variance for UTCSR RL06 Spherical Harmonics and GSFC (v02.4) Mascon models

From the spectral properties, the two types of GRACE models produce nearly identical results at the low degrees (below n = 40), have some disagreements from 40 to 100, and beyond that only the mascons are available.

The geographic differences between these two models are shown in the following figures with some GeMS-related perspectives with a summary of all results shown in Table 8. To compare these models, Figure 35 shows the difference in the geoid rate with both models evaluated up to degree 60 (the maximum 'high-quality' degree for the SH model). In CONUS where the geoid rates have a considerably smaller amplitude and the majority of the signal is caused by GIA, there is minimal difference in these models at n_{max} = 60. A few localized areas (like Florida and North/South Carolina) have differences greater than 0.1 mm/yr. However in Alaska, almost the entire southern portion of the state exhibits model disagreement at 0.1 mm/yr or more as illustrated in Figure 36.

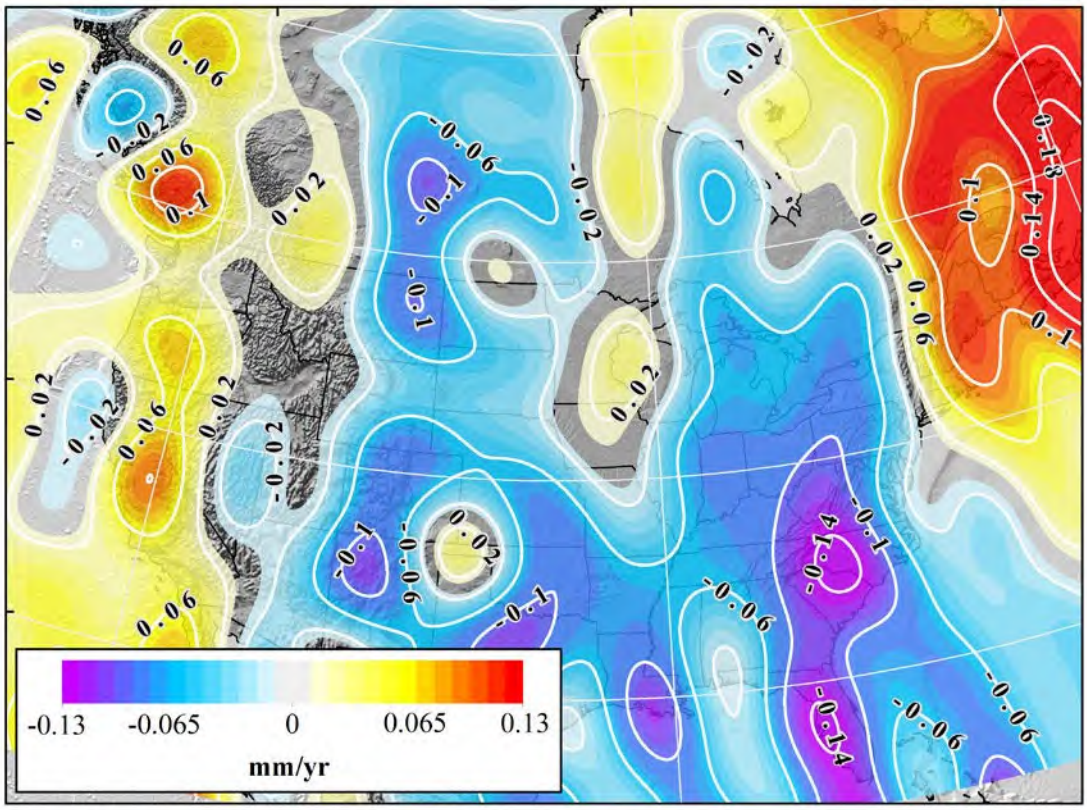

Figure 35: Difference in CONUS between GRACE derived UTCSR spherical harmonic model and NASA GSFC mascon model compared at n_{max} = 60

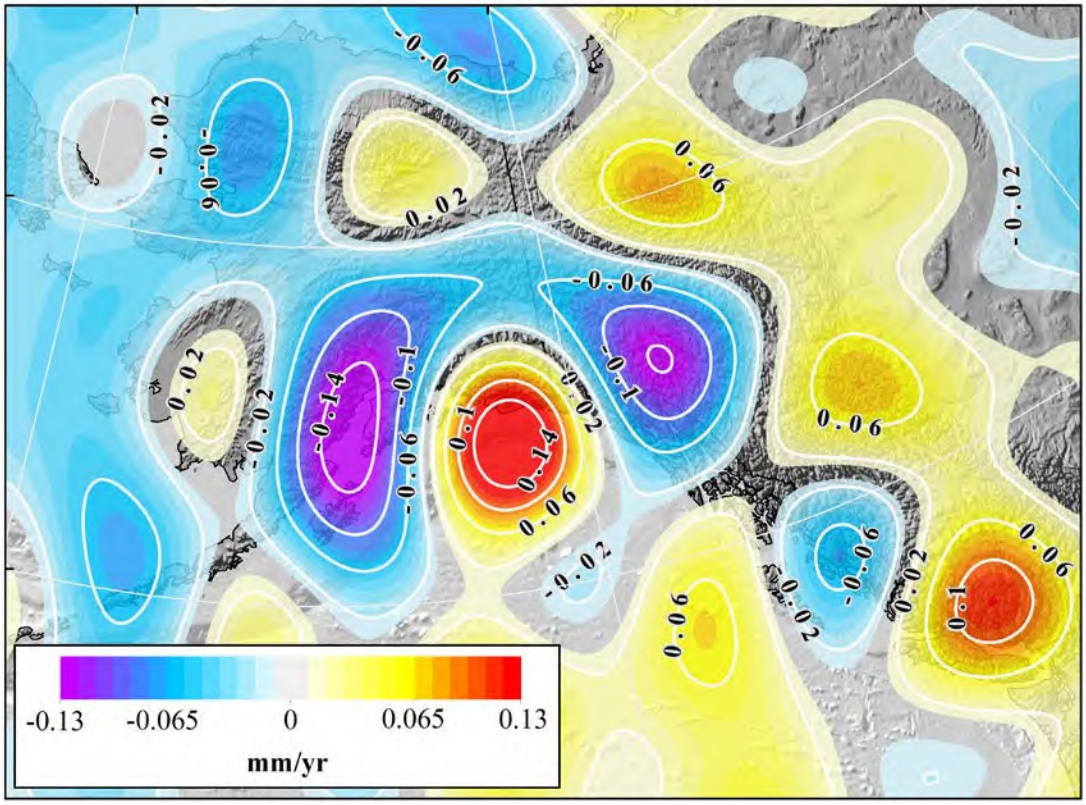

Figure 36: Difference in Alaska between GRACE derived UTCSR spherical harmonic model and NASA GSFC mascon model compared at n_{max} = 60

If both models are compared at the full resolution of the UTCSR SH model (n_{max} = 96), a slightly different pattern emerges. These differences are shown in Figure 37 and Figure 38 for CONUS and Alaska, respectively. Over CONUS, the models have very little disagreement at the 0.1 mm/yr level. However, the models show a significant difference over Alaska. These two models exhibit differences of up to 0.35 mm/yr and the large differences are over a fairly large geographic region that is correlated with the location of the ice field present in the region. As expected, the spherical harmonic model appears to smear out any localized signal present. This is similar to a low-pass filtering process. The mascon model is specifically designed to control this leakage and keep signals constrained to their respective geographic area (or block).

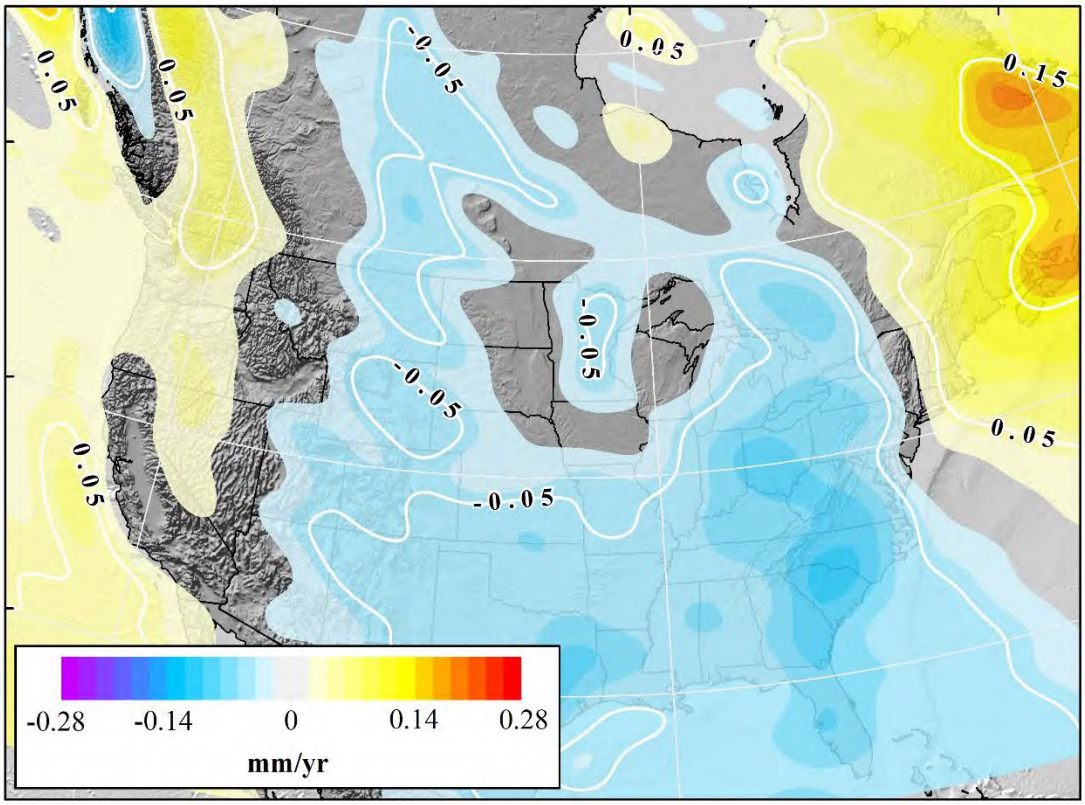

Figure 37: Difference between GRACE derived UTCSR spherical harmonic model and NASA GSFC mascon model compared at n_{max} = 96

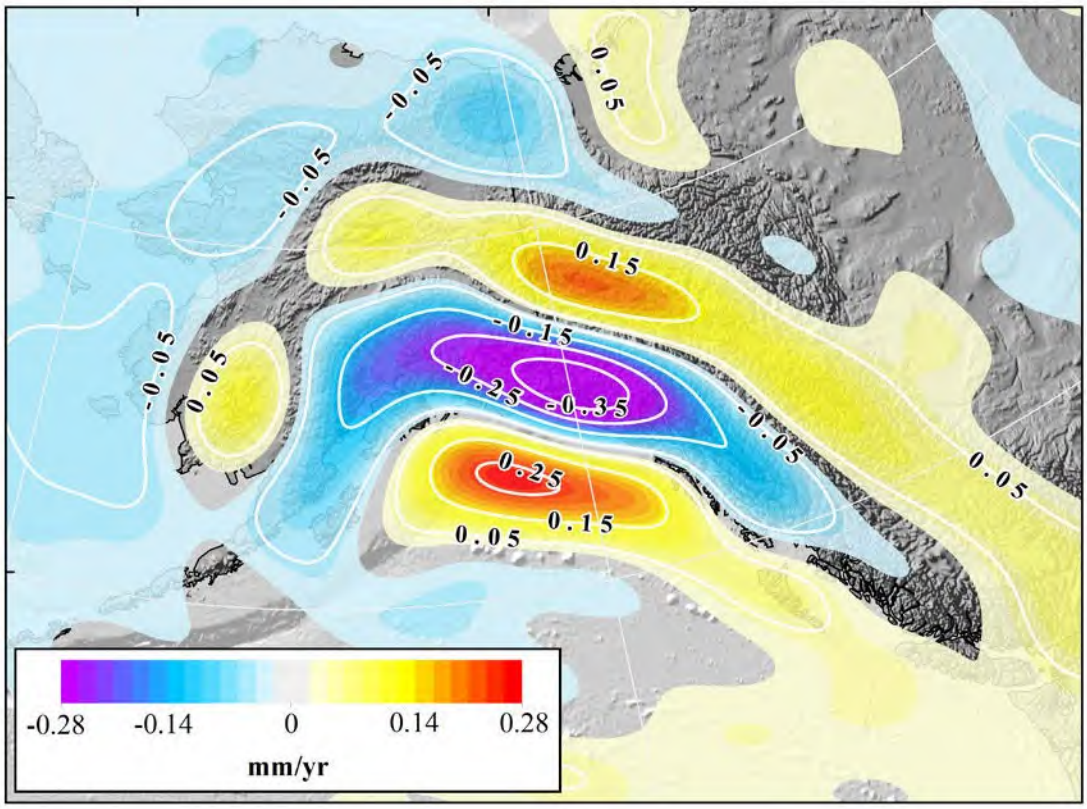

Figure 38: Difference in Alaska between GRACE derived UTCSR SH model and NASA GSFC mascon model compared at n_{max} = 96

Additionally, the omission error in the GRACE-derived UTCSR spherical harmonic model is shown in Figure 39 and Figure 40 where the CSR SH model is evaluated to its maximum degree/order (n_{max} = 96) and the NASA GSFC model is evaluated to its maximum degree/order (n_{max} = 180). This represents the difference in models at each models' highest resolution, further illustrating the similarity of the two models over CONUS and the diverging nature of the models over Alaska. The high frequency nature of the difference over Alaska is the primary justification for NGS use of the mascon model within GeMS.

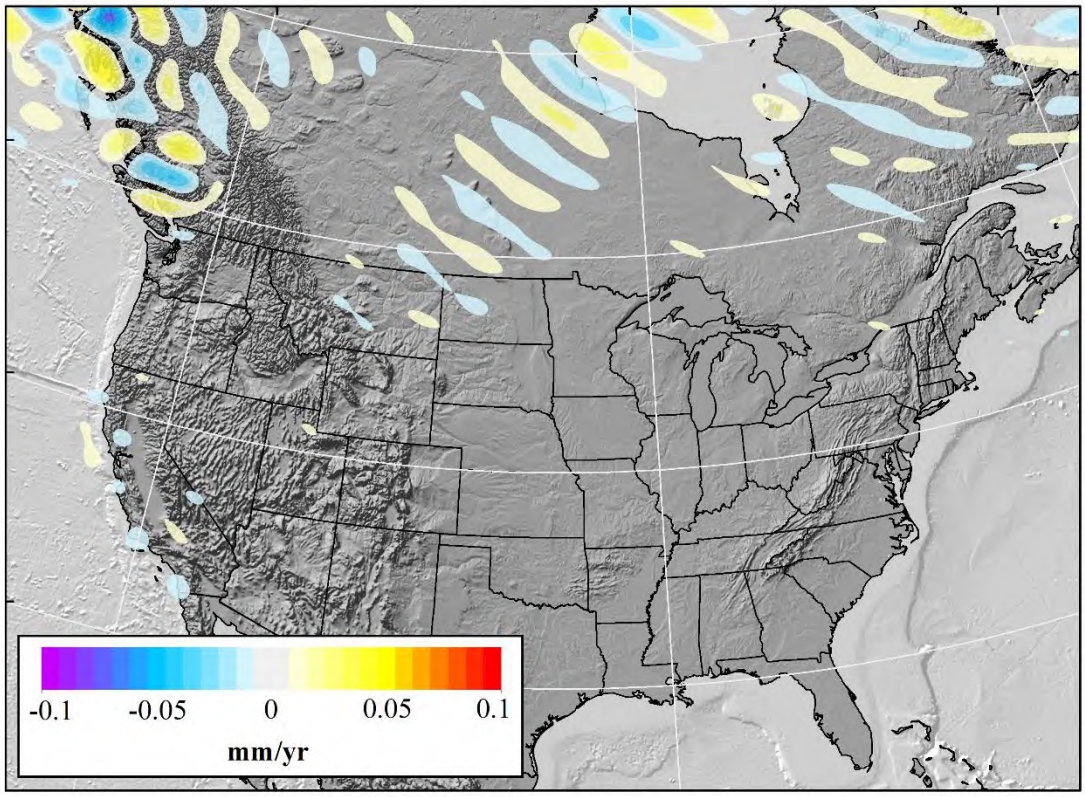

Figure 39: Omission Error in UTCSR spherical harmonic model [mm/yr]. Difference between GSFC mascon model (n_{max} = 180) and UTCSR spherical harmonic model (n_{max} = 96)

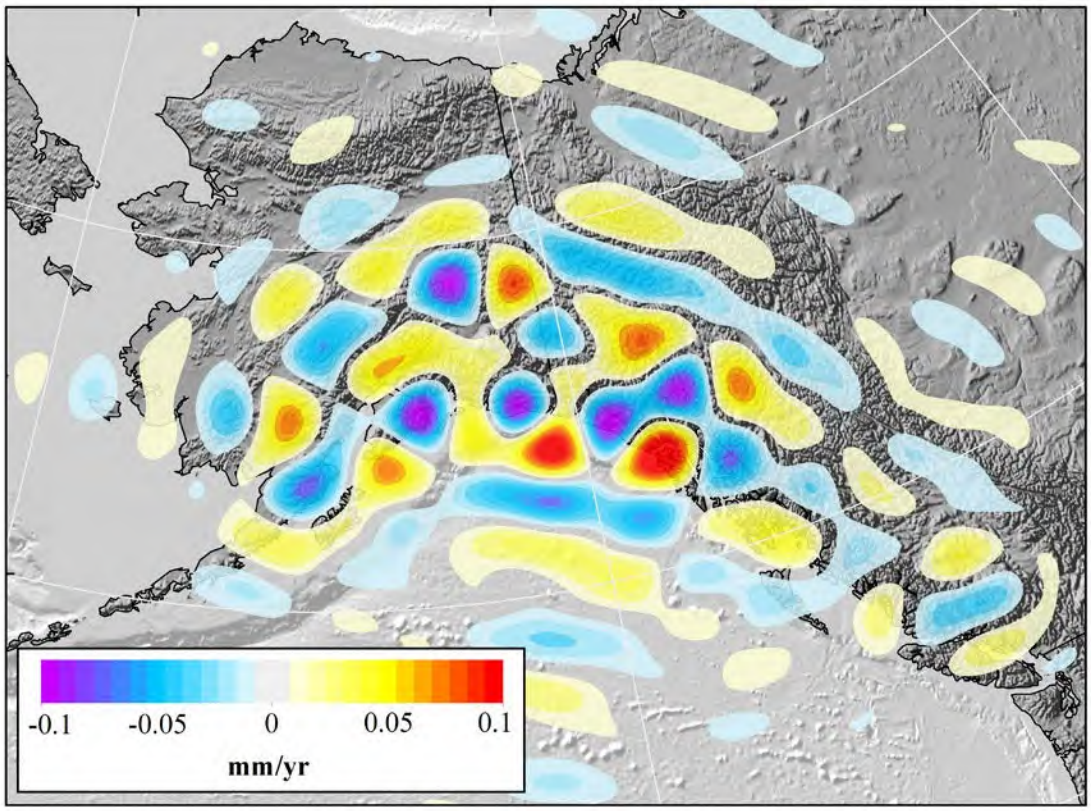

Figure 40: Alaska Omission Error in UTCSR spherical harmonic model [mm/yr]. Difference between GSFC mascon model (n_{max} = 180) and UTCSR spherical harmonic model (n_{max} = 96)

Table 8: GRACE Model Differences

	Model Differences	Model Differences	Omission
	Difference between GSFC & UTCSR at n = 60	Difference between GSFC & UTCSR at n = 96 [mm/yr]	Difference between GSFC at n = 180 and UTCSR at n = 96
Min.	-0.36998	-0.941	-0.311
Max.	0.217106	0.588	0.350
Mean	-0.00903	-0.011	0.000
StdDev.	0.06441	0.118	0.028

3.2 Satellite InSAR

Interferometric synthetic aperture radar (InSAR) is a radar remote sensing technique capable of measuring small-scale (mm to cm) changes in the Earth's surface topography (Bürgmann, *et al.*, 2000). This technique requires repeat acquisitions of the same ground swath to determine surface displacements in the radar line of sight (LOS) during the intervening period. Satellite InSAR provides more spatially dense measurements when compared to GNSS and other ground-based geodetic techniques, yet at lower temporal resolution (typically days to weeks between observations). As a result, InSAR is capable of capturing a detailed view of deformation sources which may impact the geoid such as instantaneous events (earthquakes, volcanic eruptions) and ongoing sources of deformation (e.g. GIA,

coastal subsidence, ice-mass changes) using InSAR time series analysis techniques. As a result of the imaging geometry of satellite SAR sensors, InSAR is most sensitive to vertical deformation which is particularly advantageous to a geoid monitoring service since this has the greatest impact on the geoid. Due to the side looking geometry of the radar, however, multiple viewing geometries (ascending and descending orbital configurations) are needed to infer the horizontal and vertical components of a deformation signal.

Table 9 shows a list of past, current, and future SAR missions. These sensors utilize different wavelengths (X-band, C-band, and L-band), imaging modes, and acquisition strategies making each more or less suitable for different applications.

Table 9: Past, Current, and Future SAR Missions

Mission	Wavelength	Agency	Time Span
ERS-1	C band	ESA	1991-2000
JERS	L band	JAXA	1992-1998
ERS-2	C band	ESA	1995-2011
Radarsat-1	C band	CSA	1995-2008
Envisat	C band	ESA	2002-2012
ALOS	L band	JAXA	2006-2011
Cosmo-SkyMed	X band	ASI	2007-
TerraSAR-X	X band	DLR	2007-
UAVSAR	L band	NASA	2008-
TanDEM-X	X band	DLR	2010-
Radarsat-2	C band	CSA	2007-
Sentinel-1	C band	ESA	2014-
ALOS-2	L band	JAXA	2014-
Cosmo-SkyMed SG	X band	ASI	2018-
Radarsat Contellation	C band	CSA	2018-
NISAR	L band	NASA/ISRO	2020-

InSAR is subject to various error sources such as atmospheric or ionospheric delays, orbit errors, and DEM errors. The performance of SAR interferometry is also affected by the landscape which dictates the scattering properties of the Earth's surface. Decorrelation occurs as a result of changes in the scattering properties of a resolution cell or differences in imaging geometry between acquisitions. At shorter wavelengths (e.g., X-band), InSAR is sensitive to shorter wavelength deformation signals but experiences decorrelation over shorter temporal baselines. In contrast, L-band sensors such as the upcoming NASA-ISRO NISAR mission remain coherent for considerably longer. SAR mission acquisition strategies also provide limitations to the observations available for analysis. Figure 41 shows the global Sentinel-1 acquisition strategy. In some instances, only ascending or descending imagery is collected over a particular region. When only a single viewing geometry is available, a priori information regarding the deformation source may be used to project the LOS observations into the appropriate dimension.

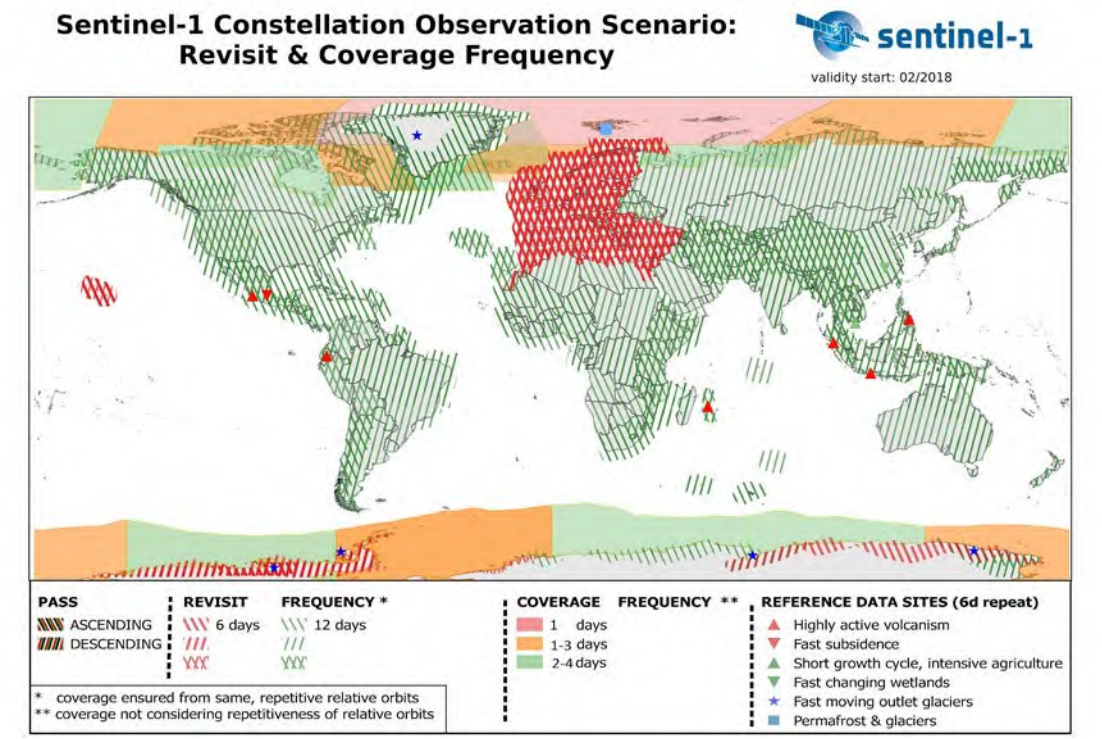

Figure 41: Sentinel-1 Orbit Design.

For example, in an investigation of subsidence in the Hampton Roads region of Virginia (see Figure 42), Bekaert, *et al.,* (2017) make the assumption that all deformation in their study area is in the vertical direction and project the InSAR LOS displacements into the vertical. Additionally, they use nearby GNSS observations to provide control for the InSAR observations. This study used an InSAR time series analysis approach to construct a longer time history of subsidence than is achievable with single interferograms and produce location specific time rates of change of the surface ($\dot{h}$) Time series methods such as small baseline subset (SBAS) and persistent scatterer approaches provide avenues to combat temporal decorrelation and additional sources of error while constraining long period sources of deformation (Berardino, *et al.*, 2002, Hooper, *et al.*, 2007).

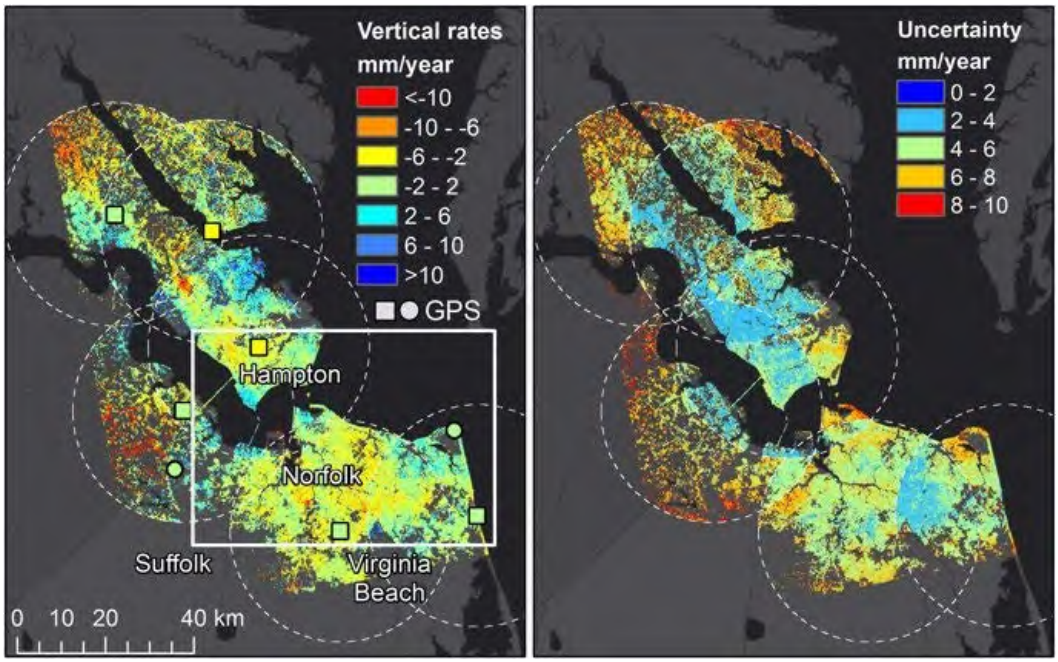

Figure 42: Vertical rates derived using InSAR from Bekaert, et al., (2017). Used with permission under Creative Commons License (http://creativecommons.org/licenses/by/4.0/)

3.3 Geophysical Models and their Combinations

The following section is a very ambitious undertaking as geophysical models are hypersensitive to the specific quantity of interest. Only a limited number of examples that are thought to have the most direct and largest impact on the geoid are presented in the following section.

3.3.1 Glacial Isostatic Adjustment Models for North America and Greenland

For approximately 2.5 million years, the earth has undergone repeated cycles of growth and collapse of continental ice sheets. These cycles, believed to be attributed to the Milankovitch cycles, have had a period of ~100,000 years for the last ~800,000 years. The last glacial period started ~115,000 years before present (BP) and lasted until 11,700 BP, with the last glacial maximum (LGM) occurring ~21,000 years ago. During the LGM, the Laurentide Ice Sheet covered large areas of North America with ice up to several km in thickness (see Figure 43).

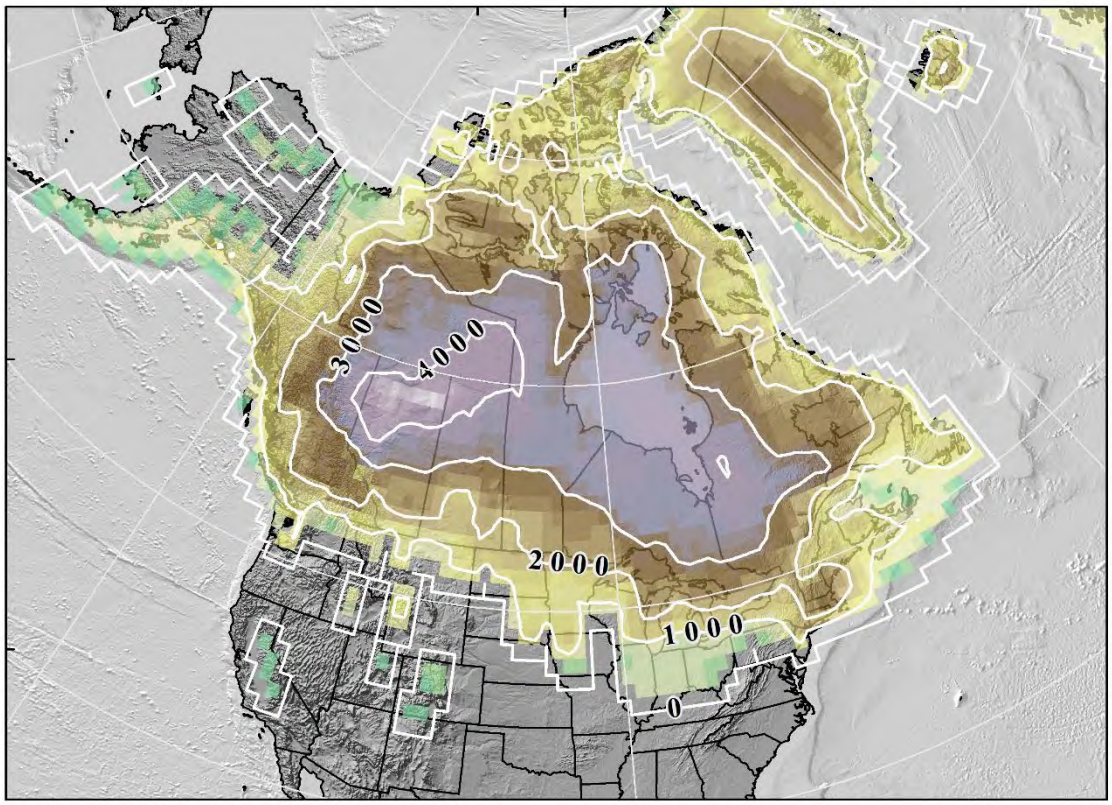

Figure 43: Glacial depths at Last Glacial Maximum from ICE-6G GIA model (Peltier, et al., 2015)

The massive weight of the ice sheet depressed the underlying lithosphere and upper mantle, deforming the local density structure of the earth (see Figure 44). Since the melting of the Laurentide Ice Sheet, the Earth's surface and the geoid have been adjusting to a new state of equilibrium as illustrated in Figure 45 with the largest vertical changes for both surfaces centered on the Hudson Bay region of Canada.

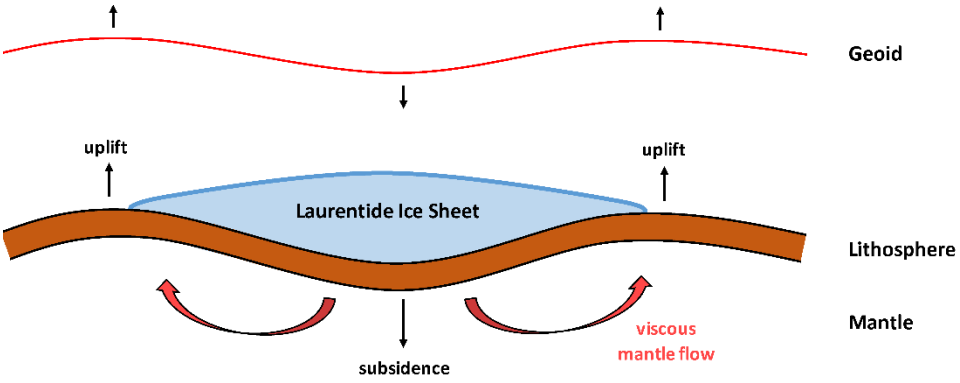

Figure 44: Effect on the geoid due to a surface load (Laurentide ice sheet in this case but any loading could be considered)

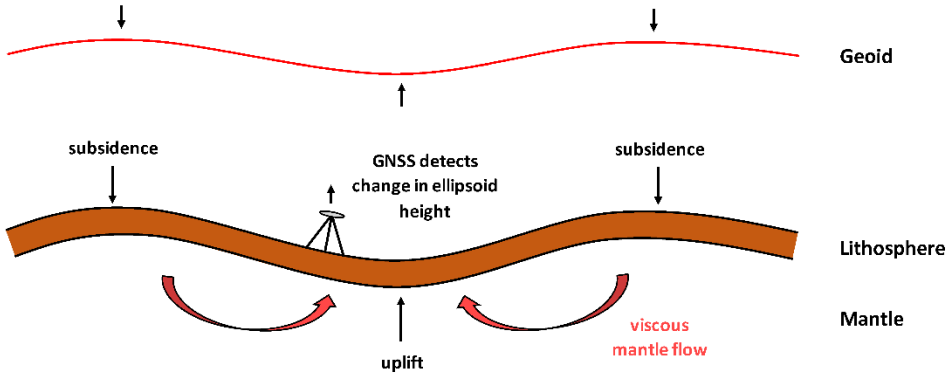

Figure 45: Effect on the geoid due to removal of a surface load (e.g. GIA)

When considering geoid monitoring efforts, the greatest change to the geoid from GIA processes is centered in northern Canada, but there is still a significant geoid height trend in the Northern Plains, Great Lakes, and Northeast regions of CONUS (see Figure 46). If GIA processes are not considered, a 10 mm error in the geoid undulation would occur within 18 years.

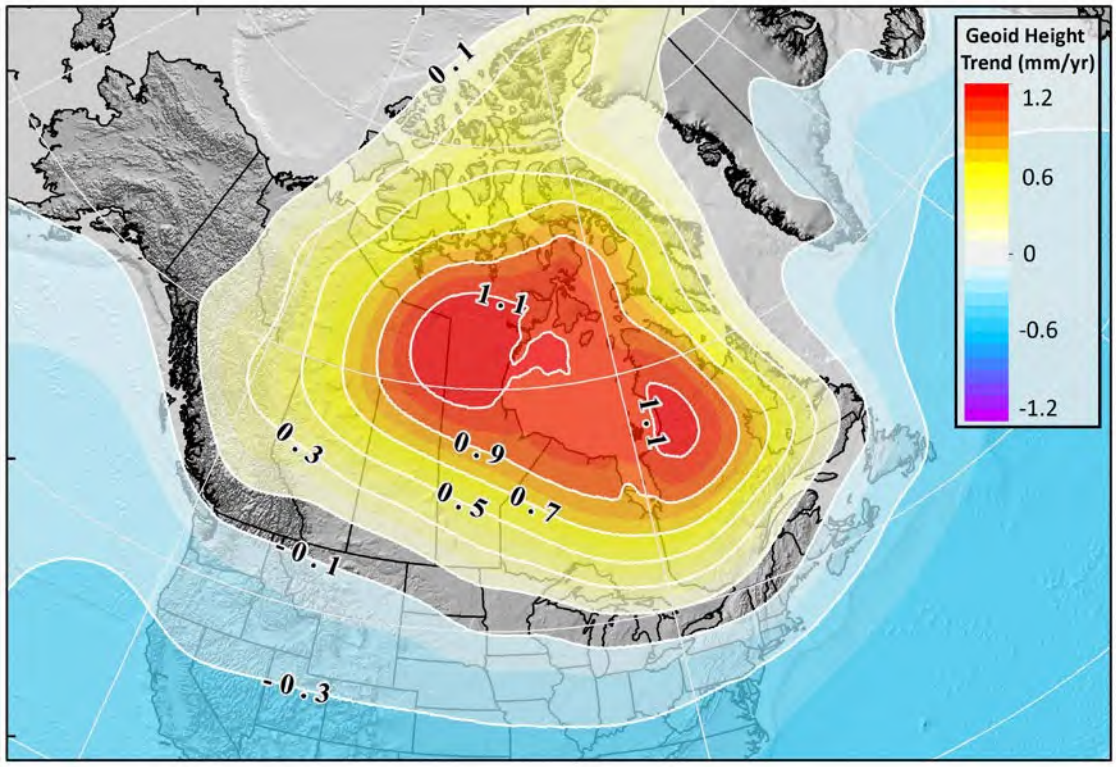

Figure 46: ICE-6G Geoid Trend [mm/yr] based on spherical harmonic model to degree and order = 256 (Peltier, et al., 2015)

Multiple international groups have produced models for the glacial isostatic adjustment (GIA) process. Some of the most widely used GIA models include Peltier, *et al.*, 2015; Caron *et al.*, 2018; and A, *et al.*, 2013. We use the ICE-6G model from Peltier, *et al.*, 2015 as a general GIA model example to illustrate how it could support GeMS.

The ICE-6G model (Peltier, *et al.*, 2015) was developed by iterating solutions of the sea level equation to obtain a best fit to relative sea level records at near and far-field sites, as well as sea level change derived from coral records near the island of Barbados. The model was further refined by including Global Positioning System (GPS) measurements of rates of vertical motion of the crust to constrain local variations in ice thickness and the timing of melting. Most importantly for GeMS, this model includes a set of coefficients to degree and order 256 that describe the geoid height trend. As this is provided in spherical harmonic coefficients, it is easy to incorporate into potential GeMS products.

3.3.2 Ice Mass Models for Alaska, Northwest Canada, and Greenland

There are ice sheets in North America that are currently undergoing significant enough change in their mass to impact the geoid. "If these computed geoid trends remain more or less constant into the future, one might expect **a geoid change of 10 mm every 3.5–6.5 years** immediately over the glaciated regions of North America." (Jacob, *et al*., 2012; emph. added). As seen in the GRACE results (see Figure 30 and Figure 33), there is considerable geoid change caused by the ice mass changes in Alaska, Northwest Canada, and Greenland.

There are groups throughout the world inventorying, surveying, and modeling the glaciated areas of North America to quantify this change using common observational techniques include LiDAR, GNSS, and airborne and satellite altimetry. As can be seen from the GRACE results (see Figure 30 and Figure 33), there is considerable geoid change being caused by the ice mass changes in Alaska, Northwest Canada, and Greenland.

For example, Larsen, *et al.*, (2015) estimate ice mass balances to be -75 ± 11 Gt/yr from 1994 to 2013 for the most glaciated region of Alaska determined by repeat airborne LiDAR surveys in support of NASA's Operation IceBridge on an individual glacier level. This type of modeling of the cryosphere provides a high-resolution window to the more local and regional changes in ice that will have an impact on the geoid over time. Taking their estimates and extrapolating them over the entire glacial area results in the mass balance shown in Figure 47. The mass change can then be spherically analyzed and converted into geoid change in a similar method as described in Section 3.1, which results in the geoid rate shown in Figure 48. The geoid rates derived from the ice mass balance have peak magnitudes of approximately -3 mm/yr compared to the GSFC mascon peak magnitudes of -1.5 mm/yr with peaks confined to the glacier basins. This 100% increase in geoid rates and reflects at least a 1.5 cm (omission) error over a decade. This reveals two critical implications for GeMS. First, GeMS needs to augment any GRACE-based model with additional ice-mass change information to provide the most accurate geoid change in these regions.

Second, there is a significant lack of information available to validate various models in the glaciated regions of North America. NGS will need to collect this crucial geodetic information, or work closely with partners, to get a sense of how accurate any GeMS model performs on the ground for users of the NSRS. This is reflected in the estimated 1.5 mm/yr omission error that is present in the GSFC mascon model when an ice-mass model is included into GeMS.

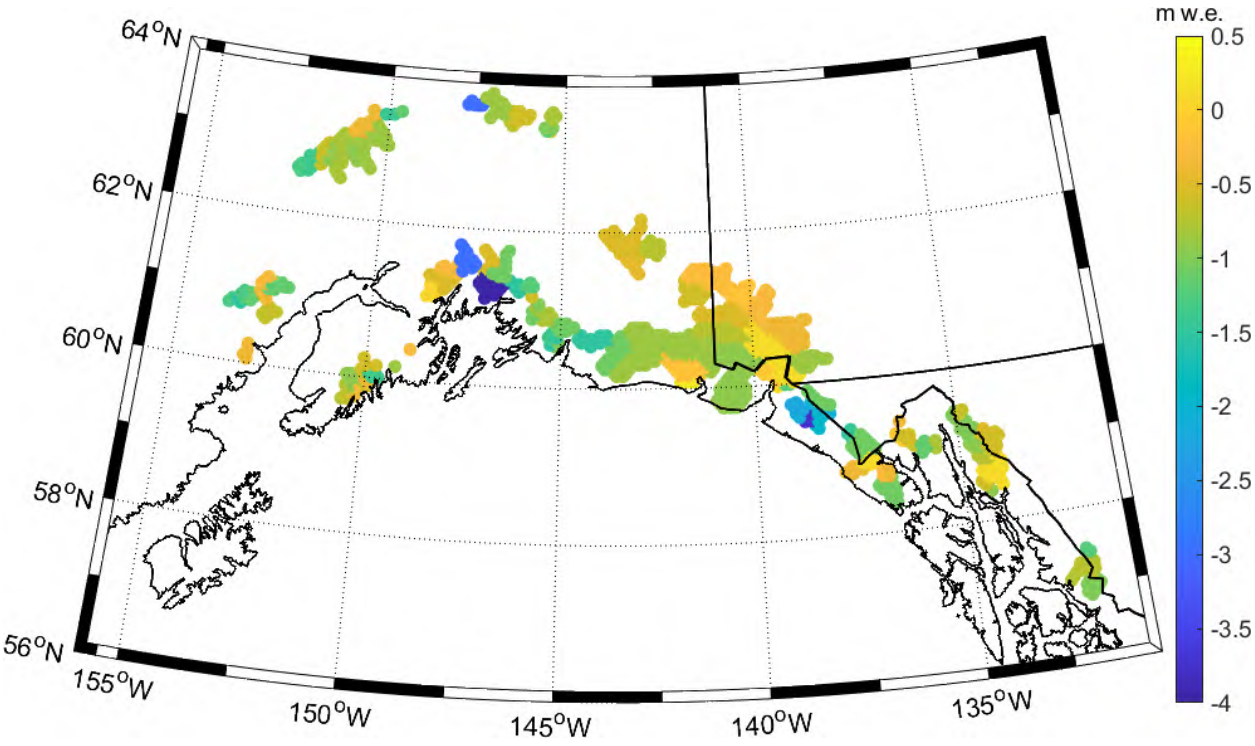

Figure 47: Ice Mass Balance Rate from Larsen, et al., (2015) [meters of water equivalent mass/yr].

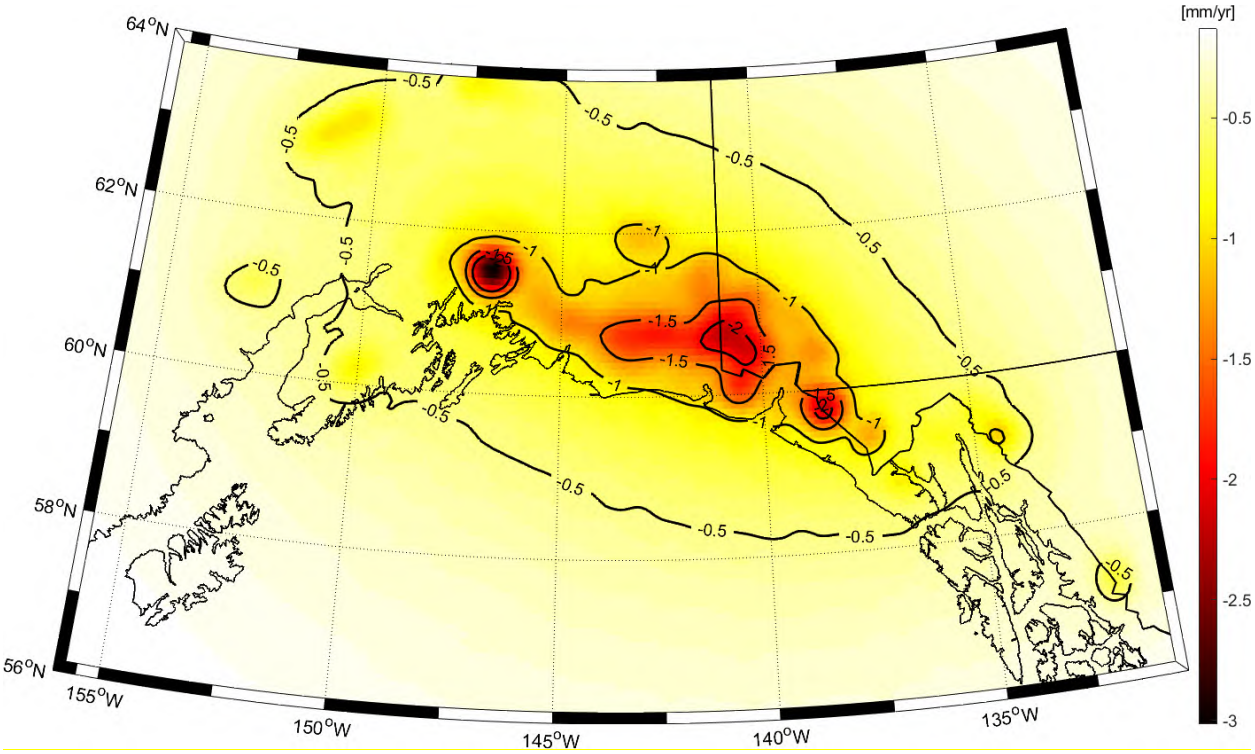

Figure 48: Geoid Rate due to Ice Mass Balance [mm/yr]

3.3.3 Earthquakes

Earthquakes occur when a sudden release of energy causes fractures in the lithosphere to rapidly propagate along major principal stress directions. Earthquakes deform the mass structure within the Earth, thereby altering the local gravity field and the geoid surface. The gravity field is primarily affected by the radial displacement of density contrast interfaces within the interior of the Earth, and the change in density caused by the tensile stress field of the earthquake (Jacob, *et al.*, 2012). Since the gravity field is most sensitive to changes in the radial density structure, only earthquakes with a large radial component need to be considered for geoid monitoring.

Earthquake strength (or size) is often reported in the moment magnitude scale (Mw), a logarithmic scale that is based on the seismic moment of the earthquake. Since the scale is logarithmic, a Mw 8.0 earthquake is 10 times larger than a Mw 7.0 earthquake. However, the Mw scale does not directly measure the amount of energy released by the earthquake, and an increase in one step of the Mw scale corresponds to 32 times as much energy being released.

Coseismic geoid change can be modelled as shown in Figure 49 using a normal mode summation scheme (such as the one employed in Gross and Chao, 2006) in combination with an earthquake source model (Jacob, *et al*., 2012). Looking at the relationship between earthquake magnitude, fault type, and the expected magnitude of geoid change, the general consensus is that only the very largest earthquakes (Mw 8+) that occur along a subduction zone will cause geoid impacts at the 5 mm level. The Mw 9.2 Alaska 1964 earthquake altered the geoid at 8-12 mm levels (see Figure 49a). The Mw 7.3 Landers 1992 earthquake produced only 0.15 mm level changes to the geoid (Figure 49b).

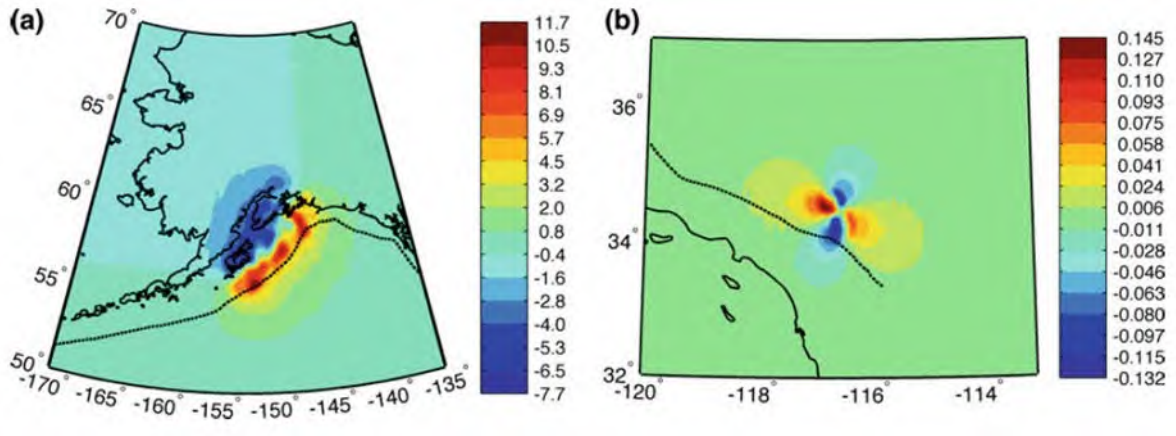

Figure 49: Modeled coseismic geoid change in mm for (a) the 1964 Prince William Sound megathrust earthquake and (b) the 1992 Landers strike-slip earthquake. Dotted lines represent major tectonic boundaries: the subduction zone in (a) and the San Andreas fault in (b). (from Jacob, et al., 2012 – reproduced with permission)

In an operational sense, a large event like the 1964 Alaska earthquake would warrant some sort of geodetic response, which would require resources and take time. This is exactly what was done by USGS and Coast and Geodetic Survey at the time as new gravity and leveling surveys were performed in Alaska after this event. The takeaway for GeMS moving forward is to have as much data as possible before and after a large event. This also was done after the Mw 7.8 Kaikoura 2016 earthquake in New

Zealand where the area was resurveyed using GNSS and relative gravity. This information was used to forward model an earthquake model and estimate the change to the geoid shape (J. McCubbine, personal communication, October 15, 2018). Over the entire Kaikoura region, most of the area experienced very little geoid change (0.5 mm std. dev.) but areas with large vertical surface deformation (approximately 5-10 m of uplift) experienced 4-5 mm of instantaneous geoid change.

For geoid monitoring efforts, and because the gravitational field is most sensitive to changes in the radial density structure of the Earth, only the largest megathrust earthquakes (Mw ~9.0 or greater) need to be addressed within GeMS products. These earthquakes produce sufficient displacements that lead to significant changes to the shape of the geoid. Since 1900, only 12 earthquakes have had a magnitude greater than 8.0 in North America (see Figure 50), all of them occurring at subduction zones off the coast of Alaska or Mexico. The only earthquake to have a magnitude above 9.0 is the 1964 Alaska earthquake, and the resulting geoid change is believed to be as much as ~1cm (see Figure 49 from Jacob, *et al.*, 2012).

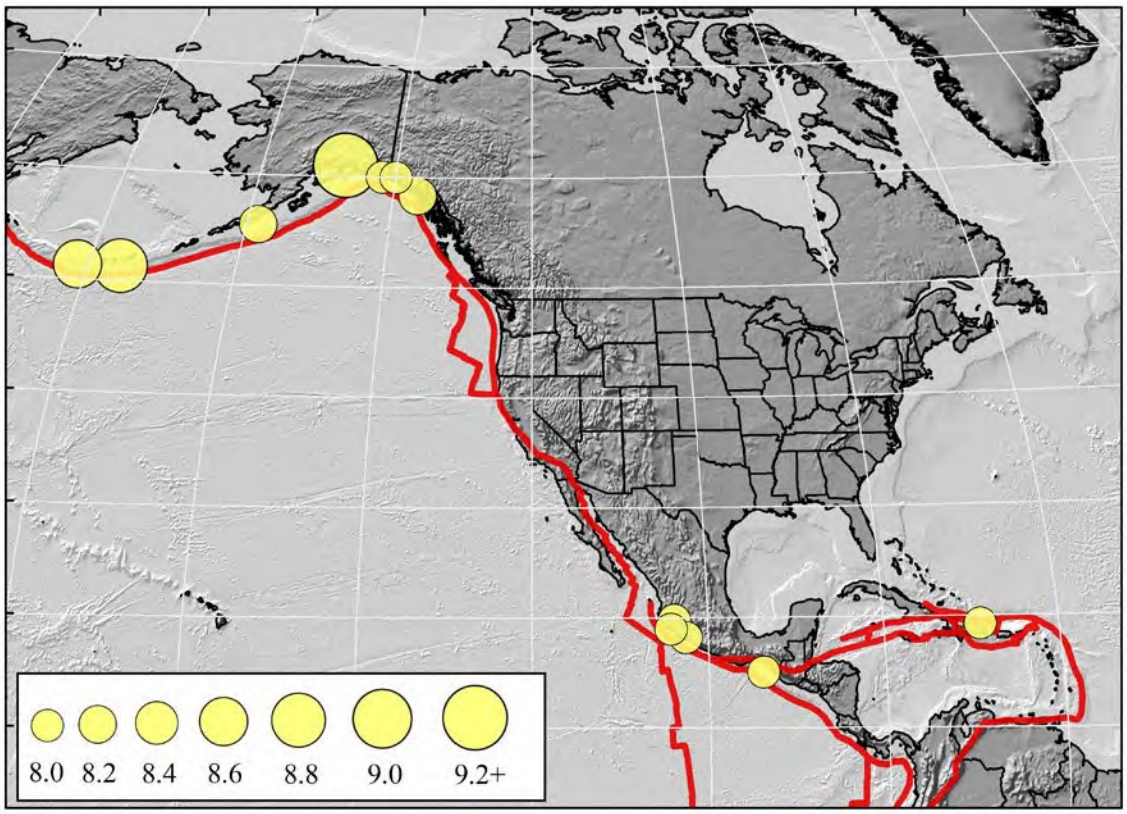

Figure 50: All recorded magnitude 8 and greater earthquakes in the last 118 years over North America.

3.3.4 Volcanic Events

Explosive principal eruptions occur at volcanoes along plate boundaries, when gas (often water vapor) gets trapped in the magma and decompresses as the magma rises. Like earthquake magnitudes, there is a scale for measuring the explosiveness of a volcanic eruption (Volcanic Explosivity Index or VEI). It runs from zero to 8, with eruptions increasing in material ejected by 100 times for each numerical increase. Eruptions at Novarupta and Krakatoa were a 6 on this scale, while Mt. St. Helens and Vesuvius (Pompeii)

were a 5. The last Yellowstone eruption 640,000 years ago was an 8. Two different situations within the volcanic system are considered in this section for impacts on the geoid shape: 1) intra-eruption periods and 2) eruptive periods and their immediate aftermath.

For the intra-eruption periods, the mass redistribution within a volcanic plumbing system can lead to a localized change in gravity on the order of 0.5 to 0.15 mGals/yr. These mass changes can occur with very minimal deformation at the surface, and are often associated with pre-eruptive and eruptive phases (Bagnardi, *et al.*, 2014). When considering the effect of mass redistribution on geoid height, even redistribution in large volcanic systems such as the Yellowstone caldera only leads to a height change of ~0.4 mm over a period of several years.

The volcanic eruption and its immediate aftermath can cause much greater impact on the geoid shape; however, only for the largest volcanic events. "Volcanic activity significantly affects the geoid only when cataclysmic events occur, such as the 1980 Mt. St Helens eruption and consequent flank collapse." (Jacob, *et al*., 2012). Two effects are critical to geoid change: First, an estimated volume of 2.7 km^3 of material was removed from the volcano's flank leading to geoid change. Secondly, the geoid also is impacted by the redistribution of this material over an estimated 62 km^2 region. Jacob, *et al.*, (2012) estimates that the removal of material due to the flank collapse creates a -100 mm change in the geoid shape in the immediate vicinity of the volcano while the redistribution of material creates a 22 mm geoid change over the larger region. In the event of a future eruption like Mt. St. Helens, Both of these effects are large enough for GeMS to be concerned with and new geodetic information would likely need to be collected to confirm how the geoid changes. This type of response would be event-specific and exact survey instructions would be determined in the immediate aftermath of an event.

3.3.5 Uplift and Subsidence of the Pacific and Caribbean Islands

Islands away from the continental shelves generally have a volcanic origin. Contributions to surface topography are volcanic effects (lava flows, ash fall deposits, lahars, calderas, fissures, resurgent domes, etc.), landslides, weathering and erosion, beaches and sandbars, coastal erosion, coral reefs, groundwater effects and processes that redistribute mass. Except for very large lava flows and landslides, these effects are rarely large enough (mass-wise) to cause island geoid change on human time scales.

3.3.6 Global Hydrology Models

The variability of the mass of water within the hydrology cycle can also create changes to the shape of the geoid. These water mass anomalies provide a meaningful contribution to geoid monitoring and can be estimated from global hydrology models. These models typically use a very heterogeneous slate of input datasets like surface data, satellite data, precipitation data, and other parameters such as soil types, elevation, and vegetation to produce a grids of precipitation, soil moisture, and other hydrologic outputs in space-time. One of the most commonly used hydrology models for geodetic applications is the Global Land Data Assimilation System (GLDAS) produced by NASA and NOAA (Rodell, *et al.*, 2004). This dataset is available globally at 0.25 degree grids at 3-hr. time intervals.

GeMS could make use of a global hydrology model in two possible ways: 1) as an input dataset to construct the model or 2) to support a GRACE determined model by removing unwanted hydrology effects from the model.

Geoid trends and annual amplitudes vary considerably between different hydrology models. Jacob, *et al.*, (2012) includes a comparison between the GLDAS/NOAH model and the Community Land Model v4 (CLM) (Oleson, *et al.,* 2010) as illustrated in Figure 51 and Figure 52. They found consistency in the annual amplitudes in the 5-7 mm range for both models (see subfigure (a) in both figures), but values for the geoid trend term differed, with CLM producing rates of up to 0.2 mm/yr while NOAH has maximum rates of 0.005 mm/yr (see subfigure (c) in both figures). These differences are attributed to the groundwater storage being present in the CLM model and not present in the NOAH model. Both of these models are based on a multi-decadal time series from the 1950s to early 2000s. This is a much different time span than any of the GRACE derived rates are using and care must be taken in heterogeneous data combination.

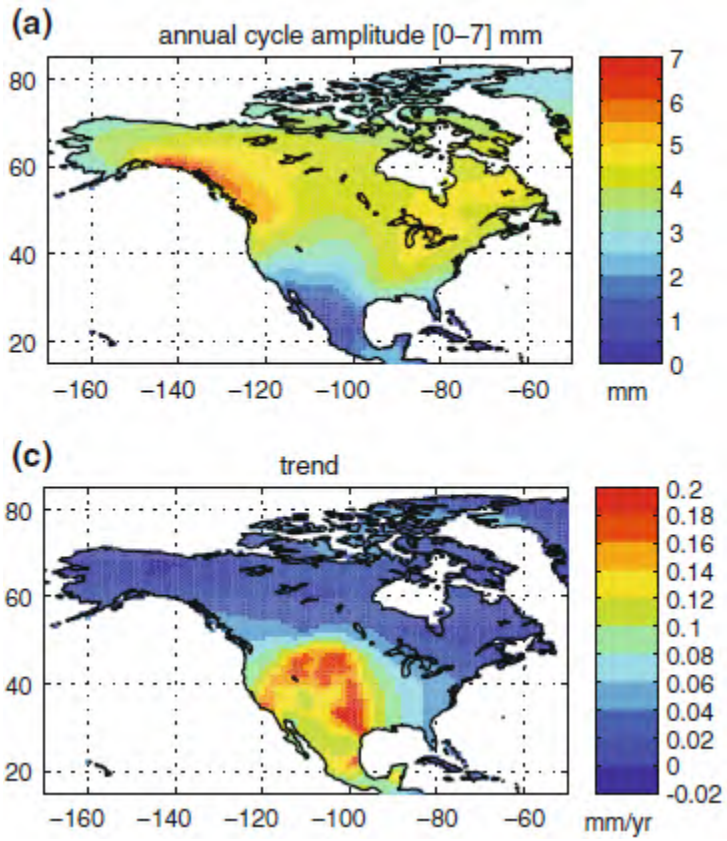

Figure 51: CLM 4.0 geoid undulation a) annual amplitude and c) trend in mm and mm/yr based on a time series from 1950s to 2000s. Figure 1 from Jacob et al., (2012). Used with permission.

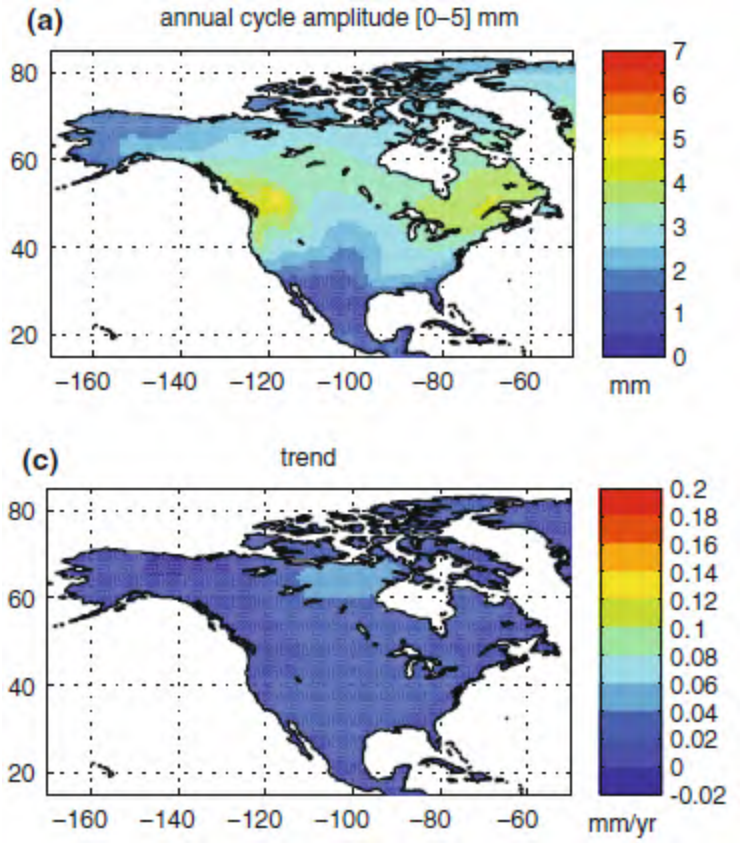

Figure 52: GLDAS/NOAH geoid undulation a) annual amplitude and c) trend in mm and mm/yr based on a time series from 1950s to 2000s. Figure 2 from Jacob, et al., (2012). Used with permission.

3.4 Other Terrestrial Gravity Programs in North America

3.4.1 NRCan Gravity Program

The NRCan Geodetic Survey operates a gravity program for similar purposes as NGS. NRCan maintains the Canadian Gravity Standardization Network (CGSN) that has a tiered approach ranging from Fundamental sites measured with a superconducting gravimeter, Core A and Core B sites measured with absolute gravimeters, additional scientifically important sites measured with absolute gravimeters, and a more dense network of sites observed with relative gravimeters. The Core A and Core B sites are in place to precisely monitor the changing gravity signal due to mass transport effects and each site is observed at least once every 10 years. There are approximately 65 of these sites distributed across Canada (see Figure 53). The Core A sites are colocated with continuously operating GNSS stations (part of the Canadian Active Control System, or CACS), while the Core B are colocated with a pillar monument that is episodically observed with GNSS (part of the Canadian Base Network, or CBN). At each core site, both $\dot{g}$ and $\dot{h}$ values can be estimated to monitor the change in the geoid surface.

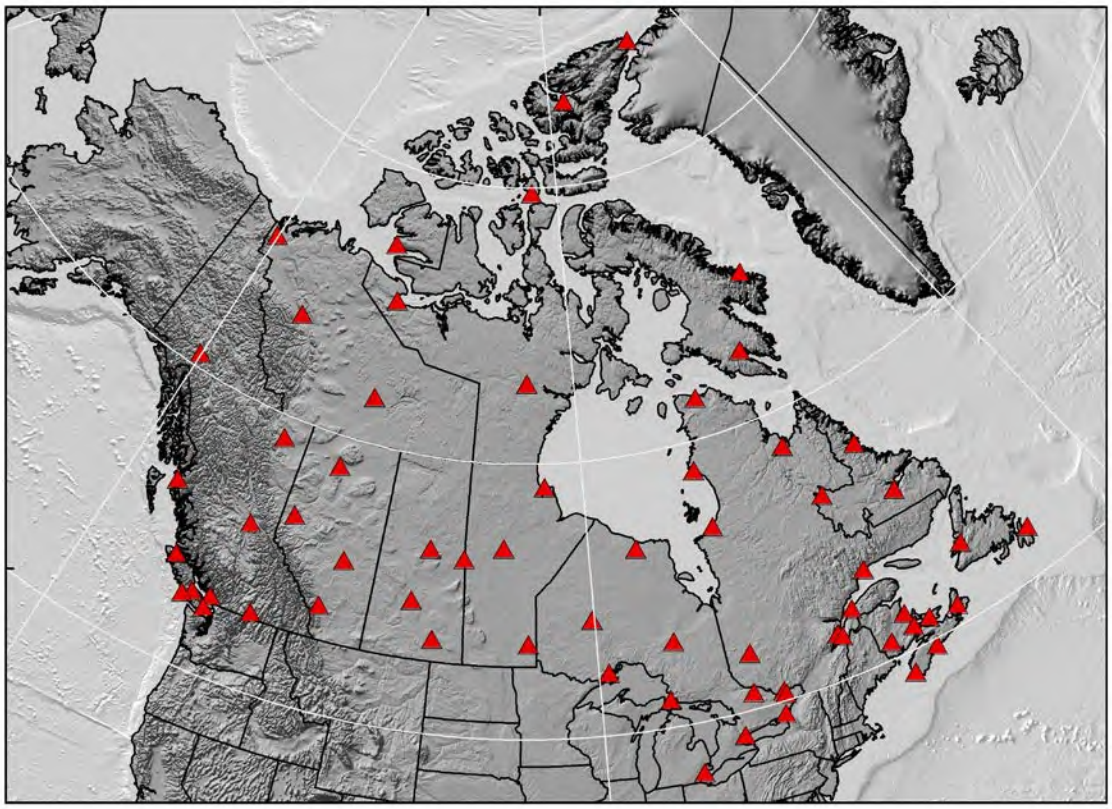

Figure 53: Canadian Gravity Standardization Network of Primary Stations (from NRCan Geodetic Survey)

3.4.2 Other Gravity Programs

The following section provides a non-comprehensive understanding of existing gravity programs doing work within North America that might be able to support GeMS in some form.

The US Geological Survey (USGS) has active relative gravimeter observation programs. These programs are primarily focused on regional Bouguer anomaly studies either for geologic or hydrologic mapping, and tend to rely on established or new Reference Base Station-equivalent stations. Most of these types of gravity surveys provide minimal support to geoid change efforts; however, there are a few situations that might aid and supplement the needs of GeMS. For example, the USGS offices in Arizona operate an A10 unit and relative gravimeters to study in-state hydrology in cooperation with the Arizona Department of Water Resources. This work has shown that surface elevations can change with changes in water-table (hydrostatic pore pressure and hydrophilic clays) without changing regional elevations or the geoid.

The National Geospatial-Intelligence Agency (NGA), based out of St. Louis, MO operates numerous absolute and relative gravimeters, and they conduct deployments around the world. However, NGA efforts have concentrated on specific site surveys of military interest or are in service to the establishment of foreign national geodetic networks. They have extensive holdings of relative gravity observations, both their own as well as contributions from around the world. Additionally, they maintain the Reference Base Station (RBS) system of gravity base stations descriptors for worldwide sites.

Louisiana State University, Center for Geoinformatics, actively operates an FG5 to study land subsidence in the Gulf Coast region, and has performed repeat gravity observations on 10-12 stations over the past few years. The University of California San Diego, Scripps Institute of Oceanography operated absolute gravimeters (land and ocean-bottom) in the 1980s and 1990s, largely in support of tectonics studies. The land data is incorporated into NGS data holdings. St. Louis University operates a cryogenic gravimeter at Sacramento Peak, NM.

The National Science Foundation in partnership with the University of Colorado owns and operates an FG5. This instrument is available to qualified operators for research purposes. To date, it has mostly been used for local geophysical studies and instrument testing. NGS holds most of the field data from this instrument collected prior to 1999.

The Canadian Geological Survey operates a number of absolute and relative gravimeters. They do observations in support of tectonics and hydrology, in addition to Bouguer anomaly studies.

In Mexico, the oil company (PEMEX), the Univ. Nacional Autonomous de México (UNAM) and the Instituto Nacional de Estadistíca y Geografía (INEGI) have extensive relative gravimeter holdings. The latter two have collaborated with NGS in surveys and comparisons of absolute gravimeters in 1996, 2016, and 2018.

There are numerous other companies, agencies and universities that have gravimeters and gravity holdings in the USA; these holdings are almost exclusively Bouguer anomalies used for exploration and mapping.

3.5 Other GNSS Networks (Non-NOAA CORS Networks)

Continuous GNSS stations and networks throughout the United States and its territories exist that are not part of the NOAA CORS Network that could support GeMS with $\dot{h}$ information. These networks and individual stations typically belong to and are operated by UNAVCO (Network of the Americas, formerly the Plate Boundary Observatory), individual universities, commercial RTN/RTK providers, private companies, and various state and local agencies. Some of these continuous stations could provide added spatial resolution to a geoid monitoring service. The Nevada Geodetic Laboratory at University of Nevada, Reno (UNR) stores and provides access to most public, continuous GNSS data that is known (Blewitt, *et al.*, 2018). This includes approximately 17,000+ continuous GNSS stations globally and 8000+ stations in the NAPGD2022 region (as of June 2018). The sites that are included in processing at UNR are shown in Figure 54 and Figure 55 below.

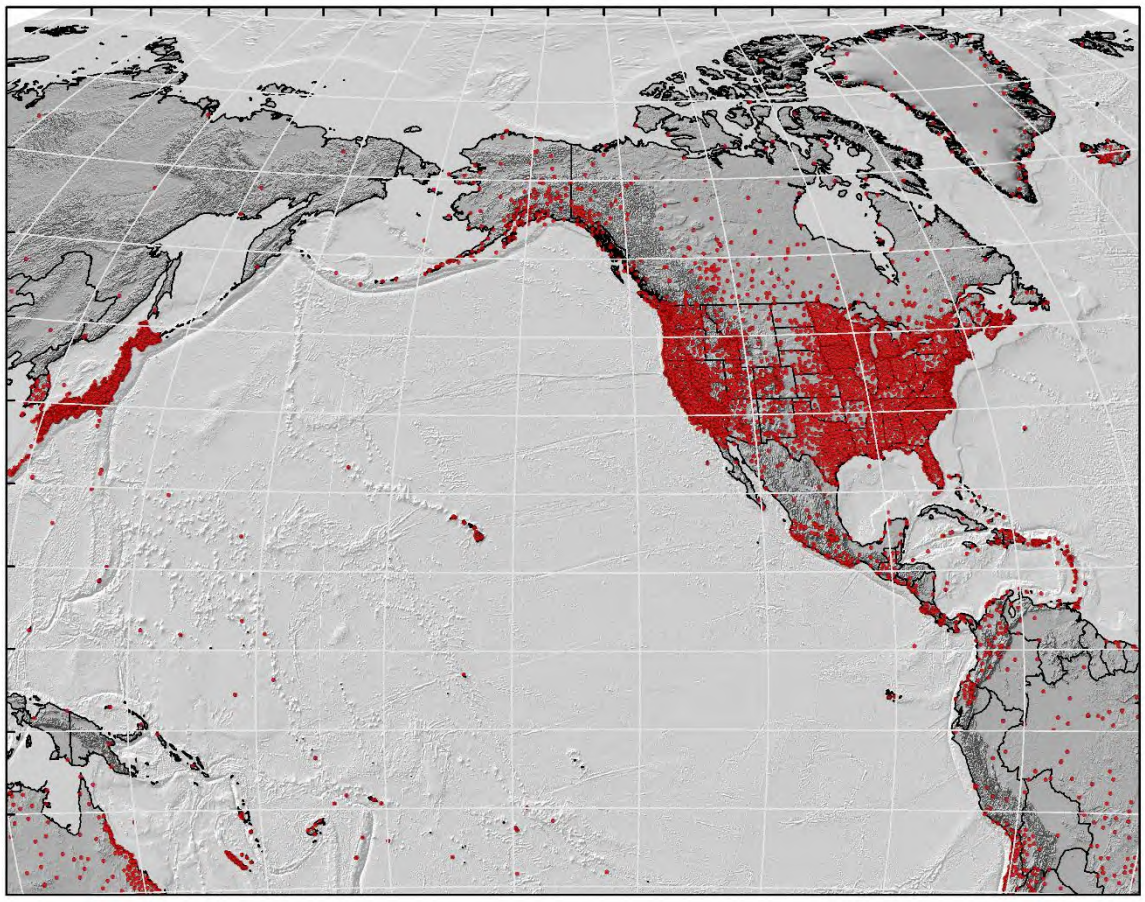

Figure 54: cGNSS Data Coverage available at UNR

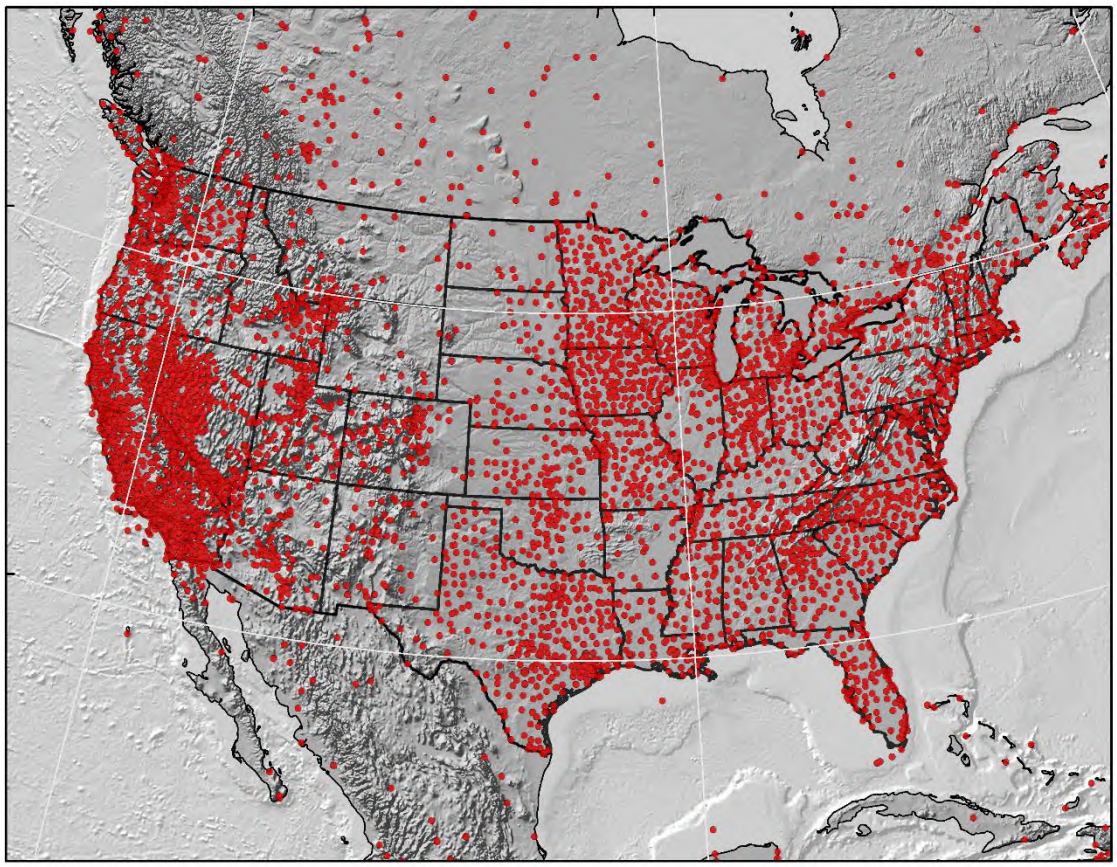

Figure 55: cGNSS Data Coverage in CONUS available at UNR

3.6 Deflection of the Vertical (DoV) Measurements

Astro-geodetic measurements determine the deflection of the local vertical (plumb line) from the normal to the ellipsoid at a particular location. These deflections, when integrated between observation sites, provide a direct measurement of the geoid undulation at the survey epoch (after correction for, or neglecting, local terrain effects). At a given time and location, the predicted star field along the ellipsoid normal is compared to what is observed along the local zenith after precisely leveling the instrument to the plumb line. Accuracies on the order of a tenth of an arcsecond are routinely achieved in about one hour of set up and observation (Hirt and Flury, 2007). There are restrictions to consider for DoV observations such as sky visibility and cloud conditions.

There are currently no commercial manufacturers of these instruments, but the CODIAC system (and its predecessor, DIADEM) from ETH Zurich, which was used extensively by NGS on the GSVS projects, and a new system from the University of Texas, Austin (developed in conjunction with NGA) are good examples of practical realizations of the method.

NGS has a network of historical DoV measurements (shown in Figure 56). In addition to this network, more modern DoV measurements are available in each of the GSVS project areas (Texas, Iowa, and Colorado).

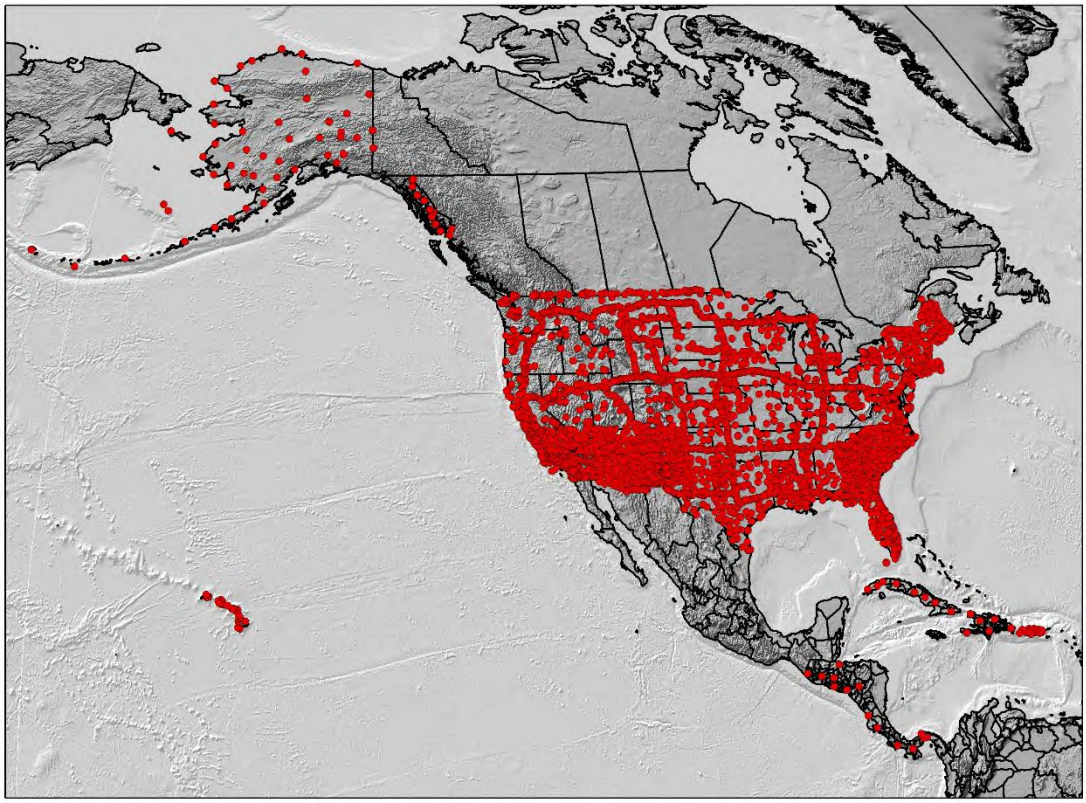

Figure 56: NGS's Historical DOV Observations

3.7 Tiltmeters

Tiltmeters have been used for monitoring crustal deformation for many decades. Originally, these tiltmeters were simply a horizontal water-tube (see Figure 57) that would track changes in the ground slope and deflection of the vertical over time. Currently, electronic borehole tiltmeters are available that can measure tilt changes to 1 milli-arcsecond. These instruments are placed a few meters (or more) below ground as they are extremely sensitive to wind, weather, and noise. These instruments typically are used in network configurations for volcano and earthquake monitoring.

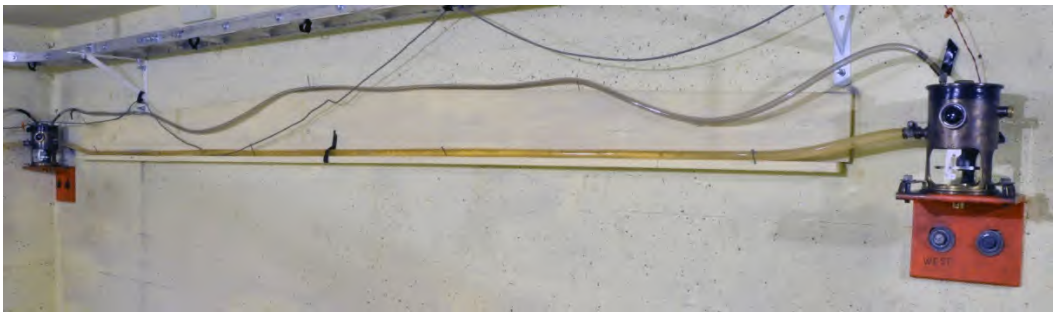

Figure 57: Water-tube Tiltmeter at Hawaiian Volcano Observatory installed in 1956. Image courtesy of USGS-M. Poland.

It is difficult to determine long-term drift characteristics of the electronic borehole tiltmeters, which will

interfere with estimating secular trends that GeMS would require. Using a long base water-tube tiltmeter, Boudin, *et al.*, (2008) found long-term stability to be 7.8 x 10^{-8} rad/year. However, the long-term drift characteristics of the electronic borehole tiltmeters are unknown and dependent on the instrument type (Furst, *et al.*, 2019). As such, they have very limited application for long-term crustal monitoring and GeMS until the long-term drift is resolved.

USGS currently operates a number of borehole tiltmeters in Hawaii, California, Washington, Wyoming, and Alaska. UNAVCO also has a database with a few dozen tiltmeters mainly for volcano monitoring.

3.8 Satellite and Airborne Altimetry

Satellite and airborne altimetry missions have supported numerous scientific objections in the last few decades, and both fundamentally measure the distance from the sensor to the surface of the Earth. Satellite altimeters rely on transmitting a microwave signal or laser pulse from the satellite that is reflected off the Earth's surface below (see Figure 58). The reflected signal is then received by the satellite, and the range can be determined based on the two-way travel time. Resolving the altitude of the satellite from GPS or other methods, the height of the Earth's surface can be determined with respect to a reference ellipsoid. The repeat ground track of a satellite orbit is ideally suited for GeMS as repeat observations are essential.

Airborne altimetry uses a fixed wing aircraft or helicopter as a platform and nowadays typically uses a sensor equipped with LiDAR to measure the Earth's surface. Airborne surveys would need to be repeated to be useful for GeMS in obtaining $\dot{h}$.

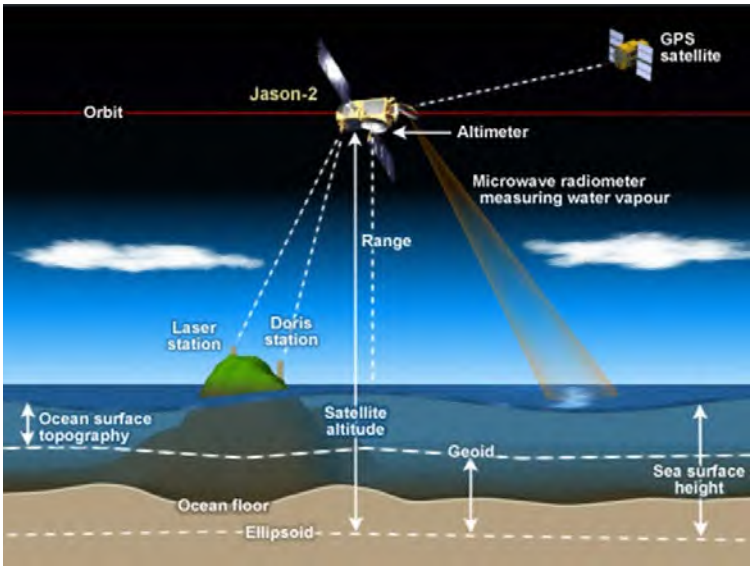

Figure 58: Satellite Altimetry (image from NOAA)

Early satellite altimeters, such as Seasat, Geosat, TOPEX/Poseidon, ERS-1, ERS-2, and JASON-1, were designed to return sea surface heights over the ocean. More recent altimetry missions have been designed to monitor the time-dependent location of the Earth's glaciers and ice-sheets (ICESat and CryoSat-2). While many altimeters collect echo returns from the solid Earth's topography, it is difficult to resolve this surface at high accuracy due to terrain, vegetation, and other surface effects.

Satellite altimetry can also be combined with ground-based sensors to resolve how the Earth's surface is deforming. For example, tide and other water-level gauges (such as those in the Great Lakes) quantify the height of water surfaces relative to fixed points on the shore, and in some places, to geodetic control. At tide gauges, 19-year observational records are used to define local mean sea level, which supported the selection of W_0 of NAPGD2022 and will be used in subsequent re-definition of the vertical datum as ocean levels change.

NOAA's Center for Operational Oceanographic Products and Services (CO-OPS) maintains the National Water Level Observation Network for the United States and its territories. In addition to the water-level information, CO-OPS has developed methodology for estimating the vertical land motion (VLM) at the tide gauge site (Zervas, *et al.,* 2013). By removing the oceanographic trend from a water-level gauge record, a 30–60 year VLM estimate is obtained. This provides a similar time rate of change of the Earth's surface as would be recorded at CORS location; however, the tide gauge record is typically much longer in duration (possibly by many decades).

Additionally, numerous studies (Nerem and Mitchum, 2001; Kuo, *et al.*, 2004; Jekeli and Dumrongchai, 2003) have shown that changes in the topographic surface ($\dot{h}$) can be observed by combining repeat satellite altimetry observations and water-gauge records. The water level with respect to a reference ellipsoid at a given time epoch is observed by the satellite altimeter. A lake surface has variability associated with it due to water storage levels, waves, tides, ocean currents, etc. However, the water-level gauge observes these features and can be used to remove them from the altimeter observations.

4 Anticipated Future Techniques for Geoid Monitoring

Many technologies with a potential to improve geoid monitoring are under-development or in research-only modes, however, several techniques and technologies appear promising for improving GeMS in the 10 to 20 year future (see Table 11). The metrics presented here are only predictions—most techniques are not yet operational—but they provide an outlook for how GeMS may be supported in the future.

Table 10: Summary and Performance Metrics for Future Geoid Monitoring Techniques

Type of Data:	Availability:	Operability:	Feasibility:	Affordability:	Accuracy:
Future Satellite Gravity	**Low**	**Low**	**Very High**	**Low**	**High**
Cold Atom Gravimeters	**Low**	**High**	**Very High**	**Medium**	**High**
Improved Airborne Gravimeters	**Low**	**High**	**Medium to High**	**Medium**	**Low to High**
Optical Atomic Clock Networks	**Low**	**High**	**Very High**	**Medium**	**Medium to Very High**

4.1 Future Satellite Gravity Missions

The GRACE Follow-On Mission was launched on 22 May 2018, so plans for a third generation GRACE-like mission are very premature. Mass change was identified as one of the eight priority observables and was specified as a 'Recommended NASA priority: Designated' in the 2017 Decadal Survey by The National Academies of Sciences, Engineering and Medicine (NASEM) Space Studies Board, Division on Engineering and Physical Sciences. It is likely that a continuity mission is developed with instrumentation and accuracy similar to the previous GRACE missions. More sophisticated missions including multiple pairs of satellites have been proposed, but these have not been successful in adoption by any space agency. An international group developed a thorough set of performance metrics and guidelines for improving the spatial resolution and signal captured by a future GRACE-like mission (Pail, *et al.*, 2015). In Table 11, the 'Threshold Scenario' (requiring only a minor investment in technological development) would provide a factor of 5 improvement over the resolution of the current GRACE and expected GRACE-FO satellites. Most importantly, this would provide geoid trends accurate to 1 mm/yr at 100 km resolutions. The 'Target Scenario' (if a major leap in technology were invested in) would be a factor of 10 better than GRACE and GRACE-FO (expected) performance (see Table 12). This would provide 0.1 mm/yr accurate geoid trends at 100 km resolutions.

Table 11: Threshold Scenario of a future satellite gravity mission (after Pail, et al., 2015)

Spatial resolution (km)	Equivalent water height		Geoid	
	Monthly field	Long-term trend	Monthly field	Long-term trend
400	5 mm	0.5 mm/yr	50 μm	5 μm/yr
200	10 cm	1 cm/yr	0.5 mm	0.05 mm/yr
150	50 cm	5 cm/yr	1 mm	0.1 mm/yr
100	5 m	0.5 m/yr	10 mm	1 mm/yr

Table 12: Target Scenario of a future satellite gravity mission (after Pail, et al., 2015)

Spatial resolution (km)	Equivalent water height		Geoid	
	Monthly field	Long-term trend	Monthly field	Long-term trend
400	0.5 mm	0.05 mm/yr	5 μm	0.5 μm/yr
200	1 cm	0.1 cm/yr	0.05 mm	5 μm/yr
150	5 cm	0.5 cm/yr	0.1 mm	0.01 mm/yr
100	0.5 m	0.05 m/yr	1 mm	0.1 mm/yr

4.2 Cold-Atom Gravimeters

Like the FG5(X) and A10 gravimeters described in previous sections, cold atom gravimeters (CAGs) are absolute instruments that determine the acceleration due to gravity, g, by monitoring the free fall of a test mass in a vacuum. In the case of CAGs, the test mass is a group of ultracold (microKelvin) atoms. The atoms are cooled using lasers and then allowed to freefall. During the freefall, they experience three laser pulses that split the atoms into two atomic states, swap the states, and then recombine the states. At the end of the sequence, the number of atoms in each state is proportional to the quantum mechanical phase difference between each state, which is in turn, proportional to g (Kasevich and Chu, 1992).

Many research groups around the world have created portable devices based on the above principle. However, as of publication, there is only one commercial manufacturer: MuQuans based in France. Their unit currently has an overall uncertainty of about 5 μGals, with a long term stability of about 1 μGal (Ménoret, *et al.*, 2018). While not yet as accurate as the FG5(X), the CAGs have advantages over a macroscopic freefall system:

- No moving parts mean that the system can run continuously (combining the advantages of an absolute gravimeter with a superconducting gravimeter or gPhone)
- Miniaturization. The magnetic-optical traps used to cool atoms are on 1 cm size chips, and the thought is that "shoebox" sized CAGs are possible in the next few years (Abend, *et al.*, 2016)

4.3 Improved Airborne Gravimeters and Platforms

Besides technical improvements to the existing gravimeters, there are two new gravimeter technologies that may be available for airborne gravity measurements in the future: gravity from an IMU and Cold-Atom. In addition to sensor development, new development in platforms such as Unmanned Aerial Systems (UAS) could make it possible to utilize a future shoebox gravity sensing device to observe gravity that would be cost-effective and meet the accuracy needs of GeMS. Because of the operational requirements of GRAV-D, NGS has not seriously explored these technologies at the time of this document's publication, but international groups have been conducting surveys or tests with these developmental sensors and platforms.

Gravity from an IMU is a long-term goal of the airborne gravity community. Benefits of this technology are that the sensor is very small, light, and has minimal moving parts. The challenges is that the varying drift must be accurately modeled and constrained to calculate gravity. Danish Technical University (DTU) and Columbia University, Lamont Earth Observatory, currently use an iMAR IMU (see Figure 59) to

supplement a traditional gravimeter. Both groups based their implementation on research conducted at the Technical University of Darmstadt in Germany (led by David Becker, supervised by Matthias Becker). At this point, there are no known groups that conduct IMU-only operations to measure gravity, but with DTU and Lamont's efforts it is not unlikely that this will be developed in the future.

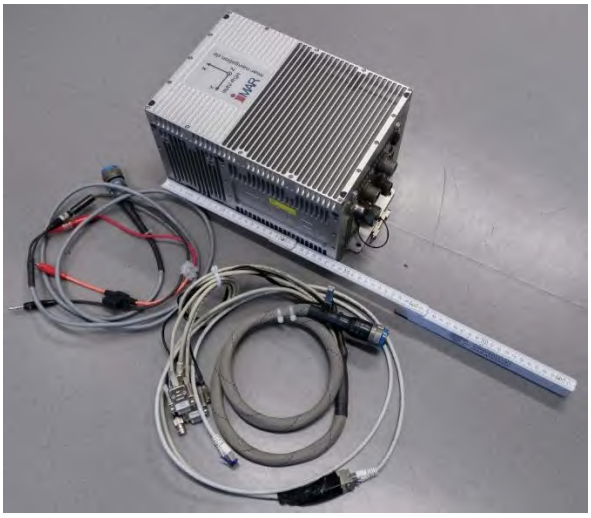

Figure 59: iMAR gravimeter which uses an IMU to observe the gravity field

NGS has collaborated with David Becker to include an iMAR on a Pilatus PC-12 (single engine turboprop) during GRAV-D data collection in New Mexico, Texas, and Oklahoma. Due to resource constraints and operational priorities, the iMAR data have not been analyzed as of publication.

With the advances in cold-atom gravimeter technology described above, airborne gravity with a cold atom gravimeter is a very new development. At publication, there has only been one test of a dynamic cold atom gravimeter, a ship-based test in a marine environment by ONERA, the French Aerospace Lab, in 2015–2016 (Bidel, *et al.,* 2018). Based on the success of this test, ONERA is planning to evaluate the gravimeter on an aircraft in the near future. The outstanding challenge with this technology is adapting the size and design to work on an airborne platform, and with an installation that would meet FAA certification requirements in the US. However, dynamic absolute gravity measurements would increase the accuracy and resolution of airborne gravity significantly, meaning airborne gravity measurements could become a more efficient method of monitoring of the geoid.

NGS has been on the forefront of using UAS-type platforms in airborne surveying. In 2016-2017, GRAV-D utilized an optionally-piloted aircraft, Aurora Flight Sciences' Centaur, for surveys. This plane was operated at GRAV-D's typical altitude and ground speed requirements. Smaller UAS platforms with the ability to hold a small gravimeter could also be evaluated for use in a GeMS-related project.

4.4 Chronometric Geodesy – Optical Atomic Clock Networks

Einstein's theory of general relativity indicates that when any clock is operated at a location "higher" than another ("up" is measured away from the mass that generates the local gravity field) it will be observed to run faster. That is, it will appear to "tick" at a higher frequency to those observers "below." So-called "optical" atomic clocks now have accuracies approaching a few parts in 10^{18} (Chou, *et al.,* 2010), and this precision is expected to improve by at least two orders of magnitude in the next few

years. At the 10^{18} level of precision, changes in a clock's height of approximately 1 centimeter (or equivalent change in geopotential) will cause a noticeable difference in the clock's output frequency (Bjerhammar, 1985). Looking forward, these clocks may one day be linked across continental or even global scales. Observed differences in the frequencies of separated clocks can then be used to infer geopotential differences directly using (17). This real-time "geo-potentiometer" would revolutionize the way vertical height datums are realized and accessed, and would significantly improve geoid monitoring.

$$\frac{\Delta f_{21}}{f_1} \approx \frac{\Delta W_{21}}{c^2} = \frac{-\Delta C_{21}}{c^2} = \frac{(C_1 - C_2)}{c^2} \tag{17}$$

where: f_i = frequency of clock at location i, W_i = gravity potential at location i, C_i = geopotential number at location i, and c = speed of light.

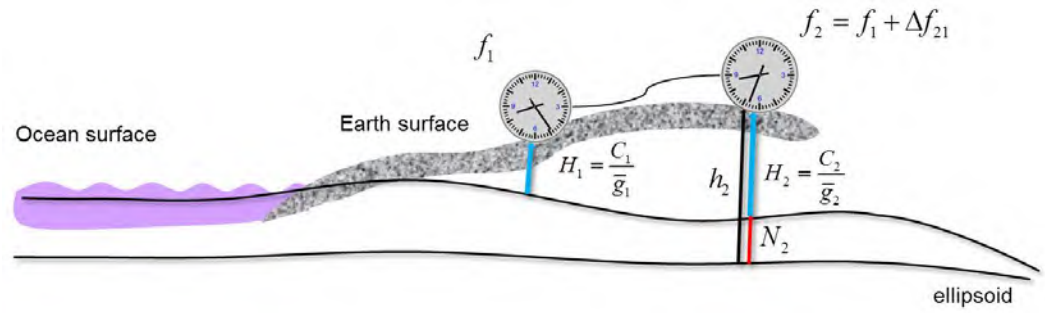

Figure 60: Optical clock network with various height systems (from Muller, et al., 2018). Used with permission.

Researchers have successfully demonstrated promising results on the scale of short distances (less than 100 km). Experiments between labs in France and Germany (Lisdat, *et al*., 2016) confirm the method, and a group in Germany has demonstrated a field-portable Strontium lattice clock (Grotti, *et al*., 2018). Over a 90 km line, this experimental clock network has produced results in geopotential that were within 2.1 m^2/s^2 (~20 cm) of the geodetic leveling results. However, the current limitation on the realization of this approach is the linking mechanism. The clocks are synchronized via a stabilized laser, and they must be linked either by line of sight or fiber optic cable; neither of which are practical over distances longer than a few 100 kilometers. A satellite-based linkage, something that could be feasible in the near future, would enable operational atomic clock networks.

5 Practical Considerations for Inclusion in the National Spatial Reference System

Any type of GeMS model needs to successfully function as part of the NSRS. Additionally, geopotential-related quantities obtained from complimentary techniques and used between products must be consistent with one another. This section describes the products that GeMS will provide, how they interact with other products in the NSRS, and how updates to NAPGD2022 will be informed by the GeMS contribution.

5.1 GeMS products and their connection to other NSRS Products

Most GeMS products directly correspond to static products within the NSRS. The GeMS products also interrelate to one another for consistency, and these relationships can be defined for certain products. For example, a spherical harmonic model for the Earth's external gravitational potential will be the basis for most of the elements in both the static and the dynamic case. All of the quantities have a static component, a dynamic component, and a combined model as specified below with their working acronym according to NGS, 2017b:

1) Spherical harmonic model (SHM) of the Earth's external gravitational potential (GM2022)
    a. Static Geopotential Model of 2022 (SGM2022)
    b. Dynamic Geopotential Model of 2022 (DGM2022)
2) Geoid Undulation (GEOID2022)
    a. Static Geoid Model of 2022 (SGEOID2022)
    b. Dynamic Geoid Model of 2022 (DGEOID2022)
3) Digital Elevation Model (DEM2022)
    a. Static DEM of 2022 (SDEM2022)
    b. Dynamic DEM of 2022 (DDEM2022)
4) Surface Gravity Model of 2022 (GRAV2022)
    a. Static Gravity model of 2022 (SGRAV2022)
    b. Dynamic Gravity model of 2022 (DGRAV2022)
5) (Surface) Deflection of the Vertical (DoV) model of 2022 (DEFLEC2022) for both North-South component (ξ (xi)) and East-West component (η (eta))
    a. Static Deflection of the Vertical model of 2022 (SDEFLEC2022)
    b. Dynamic Deflection of the Vertical model of 2022 (DDEFLEC2022)

The official combined products (GEOID2022, DEM2022, GRAV2022, and DEFLEC2022) are obtained by adding the static and dynamic model contributions at the desired or appropriate time epochs.

The SGM2022 and DGM2022 coefficients can also be combined spectrally at a desired time epoch to compute a user specified quantity that isn't directed computed from a grid (e.g. gravity at altitude, deflection at altitude). It is likely that NGS would use this combined GM2022 model internally and provide users the information and software to obtain coefficients at a desired epoch.

5.2 GeMS and NAPGD2022 Model Updates

The NGS Blueprint for 2022, Part 2 document (NGS, 2017b) outlines how NGS intends to deliver updates to the NAPGD2022 model. In particular, it specifies that updates to any of the components within

NAPGD2022 (GM2022, GEOID2022, DEFLEC2022, and GRAV2022) will trigger a new version for all of the components (i.e. NAPGD2022v05 contains SGEOID2022v05, DGEOID2022v05, etc.). Throughout these updates, the epoch of the static field will remain the same, but the dynamic components may be updated to reflect current global conditions. For example, updates could capture location-specific rate changes and episodic events incrementally and then incorporate these changes into the dynamic component models of subsequent versions of NAPGD2022.

The details of exactly how this process will operate is still TBD, but the implementation of this vision as a functional product will be the central mission of GeMS going forward. Therefore, a hypothetical example is provided for the purpose of facilitating thought experiments that can help advance this vision. In Figure 61, a hypothetical geoid undulation time series is shown for an unspecified example location. This time-dependent model spans three versions of NAPGD2022, all with the same static epoch of t_0 = 2020.0.

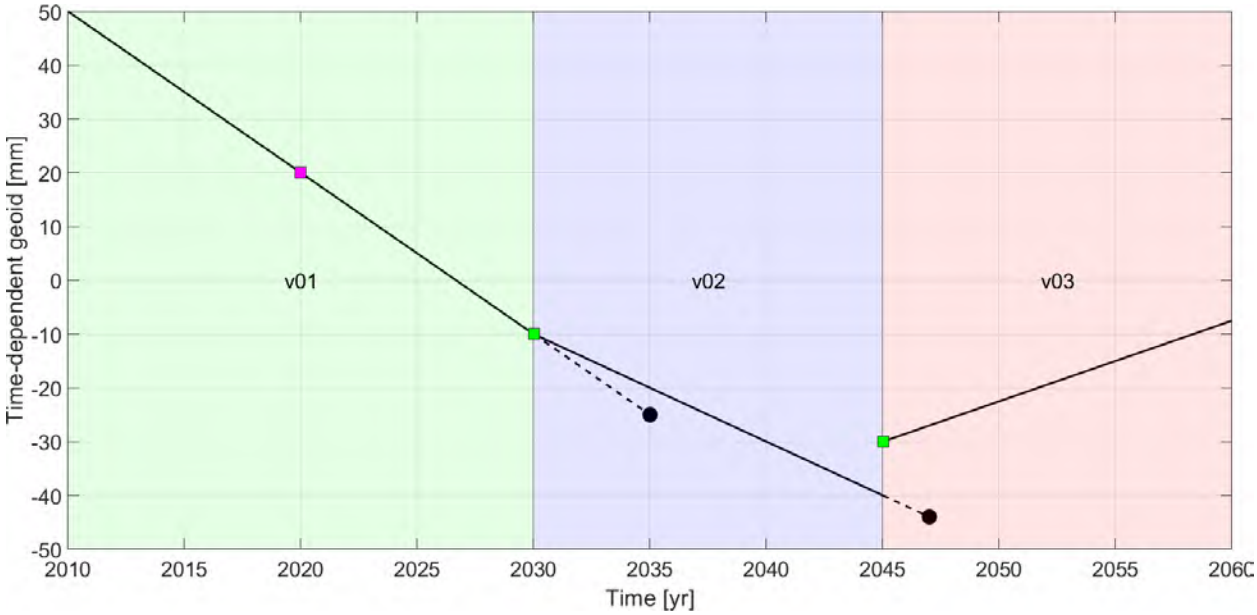

Figure 61: Time Series of Hypothetical GeMS Product at an unspecified example location. The magenta square represents the initial epoch of the geoid model (2020.0). Each shaded region represents a different version of NAPGD2022 (v01, v02, v03). The green squares represent breakpoints in the model versions where something necessitated an update to the model and a new trend was estimated.

In the hypothetical GeMS product illustrated above, the first linear trend in time ranges from 2010 to 2030 is incorporated into v01. At some point after 2030 (say 2035), v02 is created which still includes the 2010-2030 time range but now also includes the second linear trend from 2030 to 2045. At some time after 2045 (say 2047), v03 is created which includes all the linear trends from 2010 to 2060 as well as an offset in the geoid at 2045 due to an episodic event. In this way, all subsequent iterations are back-compatible with the initial static epoch. The model versions are also forward looking (in prediction-mode), until something significant warrants a change to that version's rates. NGS recognizes that blunders and mistakes could occur and how NGS updates NAPGD2022, time-dependent components, and models to fix these issues is TBD.

It is completely expected that 'patches' to the various dynamic models will be necessary to capture

changes in the future. These patches could be defined over a much smaller geographic region (maybe < 1^o x 1^o) and could be provided at higher spatial resolutions than the original models. In the versioning situation shown in Figure 61, the 'step' feature located at 2045.0 could be included in a locally defined patch where the episodic event is most prominent. The benefit of patches is that only a small geographic region has to be altered and can be delivered at higher resolutions than 1 arcminute (2 km). The difficulty with patches is in the implementation, software, and 'bookkeeping' that must be accomplished for a large geographic region like North America to keep pace with changes that occur at different locations, different scales, and different times.

6 Recommendations and Proposed Designs for NGS' Geoid Monitoring Service

In considering the design, implementation, and validation of a Geoid Monitoring Service, NGS has received and consolidated a spectrum of recommendations. Two sources of recommendations are most easily summarized in two groupings: the first group of recommendations are drawn from the NRC Geodetic Infrastructure document (NRC, 2010) and the second group was compiled by NGS staff from research and user feedback focused on successful GeMS implementation. These general recommendations are followed by proposed options for 1) designing the GeMS model and 2) validating the GeMS model. For each option, consideration of the design or validation scheme should be completed individually. For this reason, we use the term 'option' instead of 'recommendation'. Finally, present-day scenarios (i.e. Case Studies) are presented to illustrate how different models and validation schemes would work simply using the data NGS currently has available. These scenarios are very preliminary and could be enhanced with greater detail through additional investigation.

While the GRACE/GRACE-FO mission has allowed GeMS to be feasible, it should not be the lone contribution for GeMS. The reason for this is that GRACE observed geoid rates are at a very low resolution and compare very poorly with ground based observations in Southeast Alaska (see 6.3.5). This highlights the need and importance of including high resolution geoid changes in specific regions along with appropriate validation and testing where mass change is occurring below the GRACE resolution.

6.1 General Recommendations

The following general recommendations are presented in no particular order of importance.

6.1.1 NRC Geodetic Infrastructure Recommendations

The following are the GeMS-relevant recommendations provided by the National Research Council (NRC) in their Geodetic Infrastructure document (NRC, 2010). Many of the validation options discussed in Section 6.3 directly meet and support these recommendations.

1. Because absolute and cryogenic gravity observations, when combined with GNSS/GPS observations, offer unique insight into glacial rebound and subsurface mass movement, the United States should reinvigorate its once world-class gravity program.
2. The United States, to maintain leadership in industry and science, and as a matter of national security, should invest in maintaining and improving the geodetic infrastructure through upgrades in network design and construction, modernization of current observing systems, deployment of improved multi-technique observing capabilities, and funding opportunities for research, analysis, and education in global geodesy.
3. In the long term, the United States should deploy additional stations to complement and increase the density of the international geodetic network, in a cooperative effort with its international partners, with a goal of reaching a global geodetic network of at least 24 fundamental stations.

6.1.2 Other GeMS Recommendations

1. NGS should be prepared for and investigate the impact and magnitude of episodic events (e.g. earthquakes, volcanic eruptions, landslides) on the geoid. The most suitable method of determining changes to the geoid caused by these events should be evaluated by NGS for approval and implementation in modernized NSRS maintenance.
2. NGS should continue to work with NASA and other federal partners to ensure the continuity and adequacy of future GRACE-like satellite missions to measure the dynamic gravity field.
3. NGS should continue to collaborate with NIST and other state, federal, and international partners/agencies to develop optical clock technology to an operational status. While not ready for an operational GeMS at this time, the use of chronometric leveling with a network of optical clocks would revolutionize how NGS monitors the geoid.
4. NGS should re-evaluate decisions made regarding the GeMS approach as improvements and advancements occur in geodetic observations, techniques, and general knowledge. An initial re-evaluation of this type is recommended within five years of this document's publication.

6.2 Options for Operational Models and GeMS Design

In the following section, three general design options are presented for building an operational GeMS model. These options are presented and summarized in different levels of detail, but they all provide an initial starting point for NGS to consider and build upon (Table 14). The NGS Strategic Plan 2019-2023 specifically calls for time-dependency in "Objective 2-2: Define and provide access to a geocentric, time-dependent, geopotential datum by year 2022" (NGS, 2019).

Table 13: Summary of GeMS Design Options

Operational Model:	Scientific Complexity & Effort	Potential Impact[5]	Affordability	Risk[6]
Option 1: GRACE/GRACE-FO Model	Low	High	Very High	Medium
Option 2: GRACE/GRACE-FO + (Present day) Ice-Mass Model	Medium	Very High	Medium	Medium
Option 3: Geophysical Models and Geodetic Data (No GRACE). Top row requires NGS to acquire the data. Bottom row assumes data is publically available.	High	Very High	Low	High
	Medium	Very High	Medium	High

6.2.1 Option 1: GRACE/GRACE-FO (Satellite-Only) GeMS Model

The GRACE/GRACE-FO (satellite-only) GeMS model is the most straightforward model to produce in terms of scientific complexity. NGS has existing staff and resources to create an initial model with this approach and minimal additional resources would need to be devoted to maintaining the model going

[5] The estimated return on investment for how much added geoid change information will be added at what cost.
[6] Risk of relying on this particular Option for a GeMS operational model, NGS mission, etc.

forward. Based on current evidence, if this approach is used, the NASA GSFC v02.4 mascon model solution is more effective in meeting GeMS objectives than the spherical harmonic models (see Section 3.1 and Figure 28 - Figure 40). There are temporal frequencies (annual, semi-annual, and even higher terms as well as accelerations) that could be included in GeMS. For North America at the present time, it appears that only a linear time rate of change term is significant enough to include in the model. There are two primary reasons for this: 1) it is simplest to implement and minimizes confusion, and 2) the annual amplitudes (and additional higher-order terms) are too small (5 mm maximum) to be practically captured in the model. If adopted, this approach should be re-evaluated as geophysical processes contribute to eventual non-linear geoid change and in the context of expanded user comfort around additional complexity in time-dependent NSRS products.

This approach yields maximum consistency across all GeMS products as it is possible to incorporate the mascon models into a GM2022 coefficient model ($\dot{C}_{n,m}$, $\dot{S}_{n,m}$), which provides the basis for all the GeMS products. In terms of time and cost needed to implement and maintain this type of model, there is very little additional incurred cost for NGS (< 50% of 1 person's time to build the grids, coefficients, software, websites, and to monitor changes to the mascon solutions provided by NASA).

There are a couple of concerns with this type of model. First, there is considerable risk to be completely reliant on a satellite system. GRACE and GRACE-FO have a specified lifespan of about 5 years. After this timeframe, NGS can continue to propagate GeMS products into the future, but uncertainties increase with time and it is difficult to estimate how long projected geoid change trends in a post-GRACE era can be sustained before the quality is unacceptable. Additionally, as of publication, monthly GRACE-FO solutions have just been released and only very limited analysis has been performed. To minimize complete reliance on satellite data and for validation purposes, a rigorous ground-based validation system should be incorporated to ensure aspects observed at satellite altitude are consistent with what a NSRS user would experience on the ground. Lastly, best estimates of geoid change in areas undergoing deglaciation predict that this change would exceed vertical accuracy targets for the modernized NSRS in as few as 5 to 10 years for NSRS users.

6.2.2 Option 2: GRACE/GRACE-FO Model + (Present day) Ice-Mass Model

This option does everything in Option 1 but expands it slightly by combining a present day ice-mass model with the GRACE/GRACE-FO model. This geophysical process over Alaska, Canada, and Greenland is probably the only signal large enough to significantly impact the geoid on the secular time frame and not be adequately captured in GRACE/GRACE-FO models. The geographic area where this approach is used to maintain the model could be restricted to Alaska and Northwest Canada to limit the complexity and cost/resources while still providing high impact to geoid model improvement in those regions. The additional risk to this type of model is that NGS would have to rely on the exo-NGS scientific community for ice mass models or else devote significant resources and time into developing its own. This risk is mitigated, however, due to the number of international groups studying North America's ice sheets and the openness of the datasets. This option, as proposed, will therefore completely rely on external models for ice-mass changes.

The positive impact of this model on NSRS vertical accuracy is quite high as much of the ice-mass change occurs at resolutions (10-100s of km) not adequately captured by GRACE/GRACE-FO. Various ice-mass models provide geoid rates that are 2 to 3 times larger than model rates provided by GRACE/GRACE-FO.

This represents a considerable disagreement that could be alleviated with this type of model and appropriate validation. Additionally, it would provide NGS the opportunity to develop modeling workflows and capabilities in a limited and specific nature so as to be prepared for a scenario without GRACE/GRACE-FO.

Drawbacks to this type of model are that it is specific to a relatively small portion of North America (mainly Alaska within the US). Secondly, this approach injects added complexity compared to GRACE/GRACE-FO only models, and would therefore require some level of additional resources.

6.2.3 Option 3: Geophysical Models and Geodetic Data (No GRACE/GRACE-FO)

This option would completely remove GRACE/GRACE-FO from the modeling portion of GeMS and rely completely on a suite of geophysical models. This option is the most complex from a scientific perspective and it is costly to incorporate into NGS's operational capabilities. NGS does not have existing staff capacity nor resources to perform integrated modeling of this type and an expanded research plan would need to be developed and staffed to execute this approach. The benefit to this option is that, as an independently developed product, it would provide NGS added resilience by removing reliance on GRACE/GRACE-FO. There is no guarantee that a future satellite mission similar to GRACE/GRACE-FO, and NGS must be prepared for how this impacts the NSRS and GeMS. The minimum geophysical models that would need to be included in GeMS are a GIA model, hydrology models, and ice-mass models (for gravity change) in combination with some form of vertical surface deformation model from NGS's IFVM (NGS, 2017a), InSAR, and/or the NOAA CORS Network. These individual components would not need to be created from scratch by NGS; various models from the scientific community could be harvested as discussed in previous sections. As a secondary benefit of this type of model, external validation against a GRACE/GRACE-FO model is possible; alternative validation would be needed in a future where GRACE/GRACE-FO are non-operational.

6.3 Specific examples of Validation Options

To get a sense of how well or poorly the models perform with currently available external validation datasets, a few scenarios are presented in the following section. These results all utilize datasets currently held by NGS, or that are available from public sources. The purpose of this exercise is to provide a preview of how potential GeMS models agree with the proposed validation datasets. These examples are all very preliminary are intended to spur further investigation. Results are based on three components: repeat absolute gravity values, repeat GNSS observations, and a gravity model solely from GRACE (either SH or mascon approach). Each of these components has error, which has been estimated as well as possible. Additionally, many of the AG sites have very few observations (e.g. 2 to 3) so estimating a rate is not statistically appropriate. To a much lesser extent, the same can be said for the GNSS observations and estimating a vertical deformation rate.

6.3.1 GeMS-VS in Alaska

GeMS-Validation Surveys with repeated gravity and GNSS measurements are one survey design to independently assess how a GeMS product is performing. Unlike the examples shown in Section 6.3 that use actual measurements, this example uses only GRACE gravity data to assess the feasibility of a GeMS-VS. While there are practical logistical challenges, the most scientifically advantageous place to

perform such a survey is in Alaska where the geoid rates could likely be captured after only 4 to 5 years. Obviously, there are logistical challenges for performing a survey in Alaska due to short summer seasons, variable weather conditions, lack of roads, sparse infrastructure, and other practical factors.

For a sense of numerical rates over different time scales at a realistic location, we show rates from GRACE along a 220 km line running southwest from Tok, AK to Glennallen, AK along the Tok Highway as illustrated in Figure 62.

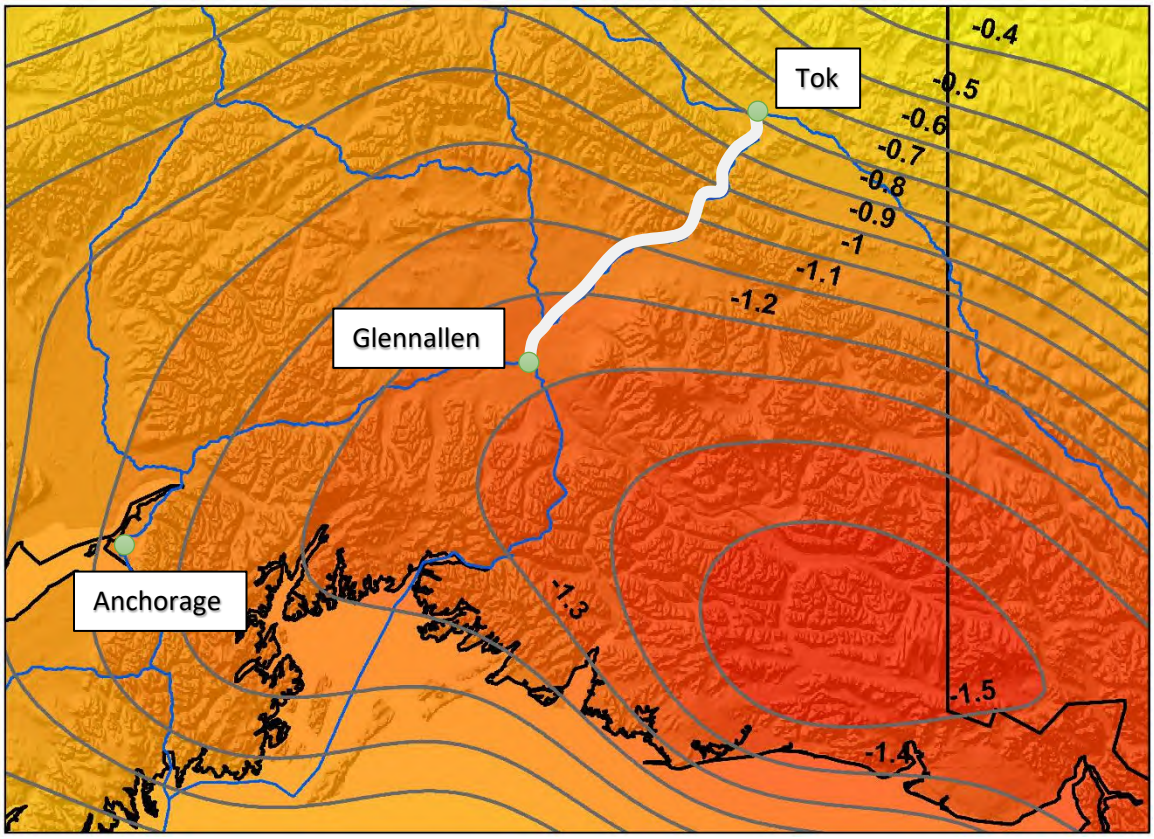

Figure 62: GeMS-VS Example in Alaska. Geoid rates shown as shaded contours in mm/yr from GRACE based UTCSR spherical harmonic model. Major roads in the area are highlighted in blue.

Tok has an estimated geoid rate of -0.68 mm/yr and Glennallen has an estimated geoid rate of -1.27 mm/yr, a difference of 0.59 mm/yr over approximately 214 km as shown in Figure 63. Additionally, Figure 63 shows the entire profile of geoid rates in the upper portion while the differential geoid change for the entire profile is shown for different time spans in the lower portion of the figure.

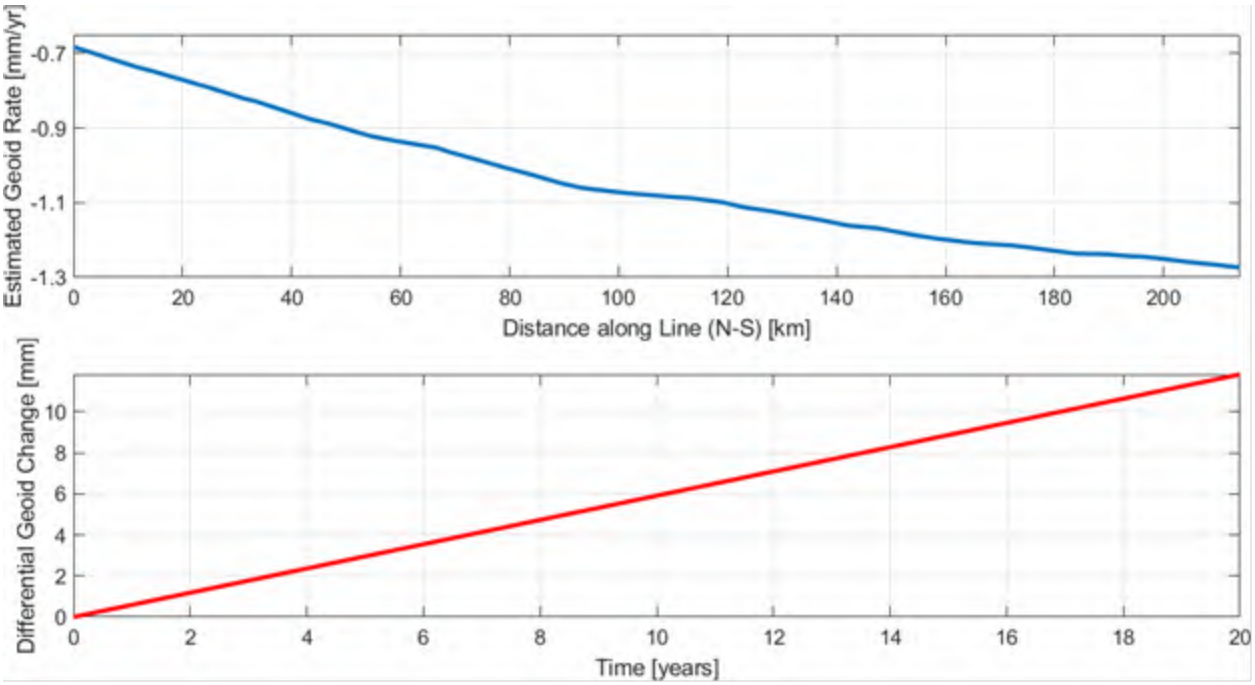

Figure 63: Geoid time rate of change for GeMS-VS from Tok, AK to Glennallen, AK

Based on the differential rate, an estimated 3 mm of geoid change would be present after 5 years, 6 mm at 10 years, and 10 mm after 17 years. These magnitudes would be difficult but not impossible to capture with repeated GPS and geodetic leveling surveys. The estimated geoid rates are very likely underestimating the true rates due to the nearby mountain glaciers; quantifying this difference would be the value of such as survey, however, the geoid rates determined by repeat GPS\Leveling would be very difficult to obtain even at 15-20 year time frames.

A much more promising experiment emerges if one examines the free-air gravity anomaly rates along this line from GRACE models. At Tok, gravity rates are +0.5 μgal/yr whereas they are estimated at -4.6 μGal/yr in Glennallen. Thus, this line would have a relative change of approximately 5 μgal/yr from Tok to Glennallen (see Figure 64). This is indeed measurable with even a CG-6 relative gravimeter.

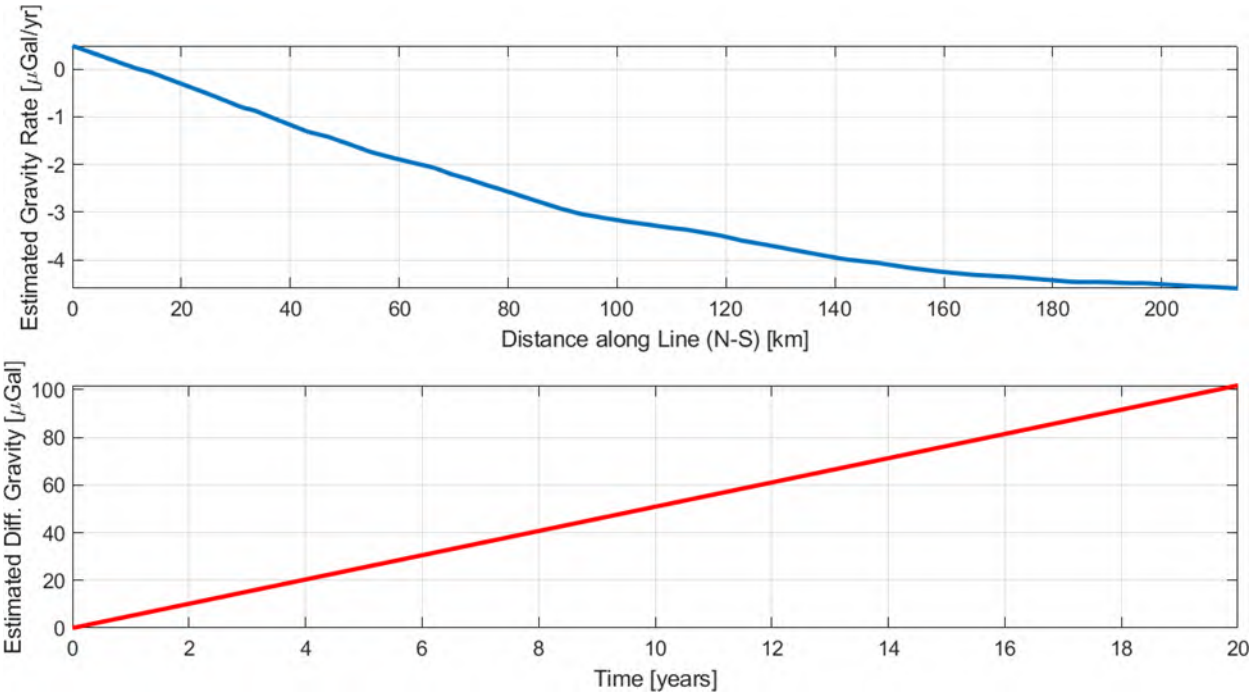

Figure 64: Gravity time rate of change for Alaska line from Tok, AK to Glennallen, AK

One consideration with surveying a line such as this in Alaska are the seasonal signals present in the gravity field. Taken from GRACE SH models, the annual amplitude in the free-air anomaly is on the order of 4 to 6 μgals (see Figure 29) so it is imperative that repeat surveys take place during the same time period each year. This is a bit more difficult in Alaska with limited field seasons, but surveys should occur in either April or October to limit the effect of any season signals. April and October are typically the times that mark the end of the snow and ice accumulation and melt seasons, respectively.

There are few places in CONUS that would be nearly as suitable for such a survey because the geoid rates are simply too small to recover with GPS/Leveling on experimental time frames. For example, a line running northeast from Duluth, MN along the North Shore of Lake Superior changes from 1 mm/year in Duluth to 1.2 mm/year in Grand Marais, MN or 0.1 mm/year over a 200 km line. However, again a gravity profile using high accuracy gravity (< 5 μgal) might still be a possibility.

6.3.2 Mid-Continental Glacial Isostatic Adjustment Line

This gravity line was specifically designed to monitor the rates due to GIA, so it is ideally suited to be used for GeMS validation. It is shown in this context to highlight the 'best case scenario' in validation data for GeMS due to the extended survey consistency. It shows a proof of concept over a rather small geographic area. The AG and GNSS rates are used from Mazzotti, *et al.,* (2011) so consistent processing is applied to all observations. The six sites along this line have all been observed roughly yearly beginning in the late 1980s/early 1990's and ending in 2009. As a result, there is a long time-span of approximately 15 years with 12–15 observations for each station that can be used to estimate the rate. This is reflected in the low standard errors for the gravity rate (approximately 0.1 μGal / yr at 1-sigma). Three gravity models (UTCSR n_{max} = 60, UTCSR n_{max} = 96, NASA GSFC mascon n_{max} = 180) are used for comparison against the observed AG and GNSS rates. The AG and GNSS rates are combined so that the

component due to vertical displacement is removed from the AG rates providing a way to compare the satellite-determined gravity rates.

Table 14: MCGL Results (from Mazzotti, et al., 2011)

Station	Latitude	Longitude	$\dot{g}\ [\mu Gal/yr]$	$\sigma\dot{g}\ [\mu Gal/yr]$	$\dot{h}\ [mm/yr]$	$\sigma\dot{h}\ [mm/yr]$
Churchill, MB	58.762	-94.086	-1.75	0.09	10.38	0.11
Flin Flon, MB	54.725	-101.978	-0.25	0.28	2.05	0.08
Pinawa, MB	50.259	-95.865	-0.07	0.18	-0.17	0.08
International Falls, MN	48.585	-93.162	-0.10	0.13	-0.12	0.12
Wausau, WI	44.920	-89.680	0.14	0.21	-0.99	0.13
Iowa City, IA	41.658	-91.543	0.51	0.18	-1.90	0.10

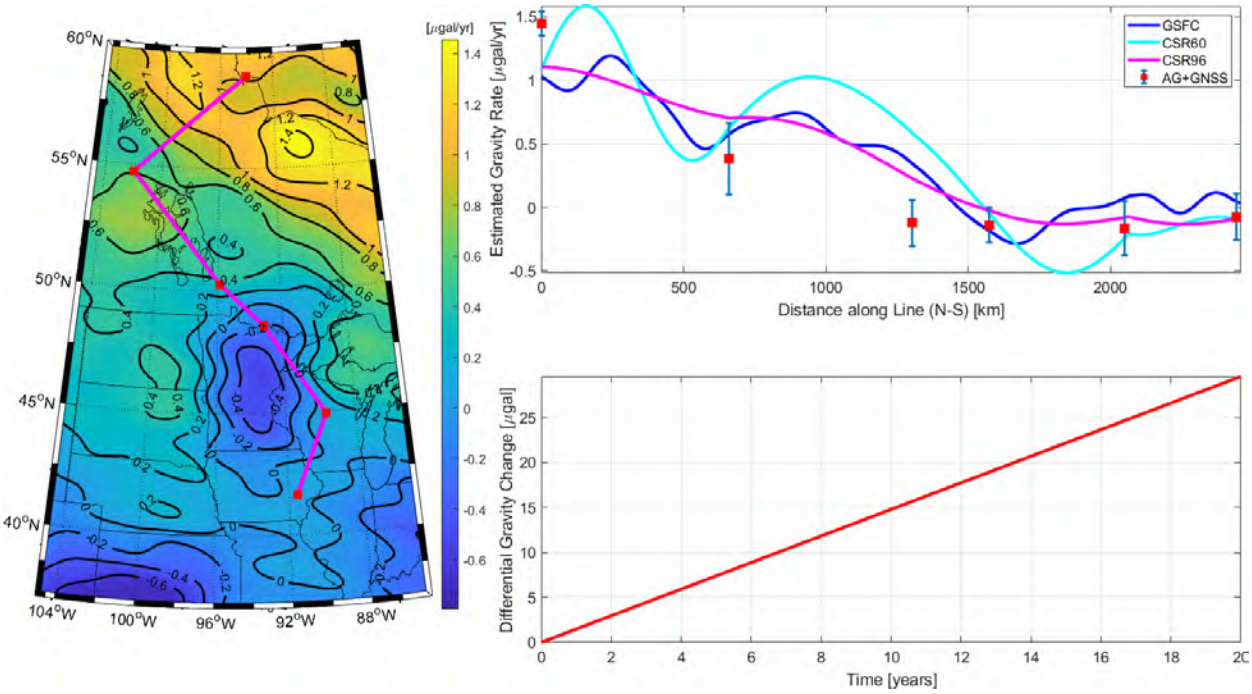

Figure 65: MCGL from Churchill Canada to Iowa City, Iowa. Left: GRACE derived gravity rates in μGal/yr with contour interval = 0.2 μGal/yr. Upper Right: Estimated Gravity Rate Profile from N to S with various GRACE model derived rates in μGal/yr. Blue curve = NASA GSFC mason model, Cyan curve = CSR SH model to n_{max} = 60. Magenta curve = UTCSR spherical harmonic model to n_{max} = 96. Observed AG rates shown in red with 1-sigma error bars. Lower Right: Amount of differential gravity change (μGal) that would build up from Churchill to Iowa City over various time spans.

The statistically small residuals along this line are notable. An improvement is observed if we substitute the published $\dot{h}$ values with rates from the University of Nevada-Reno network (see Section 3.5) (Blewitt, *et al.*, 2018) which is shown in Figure 66.

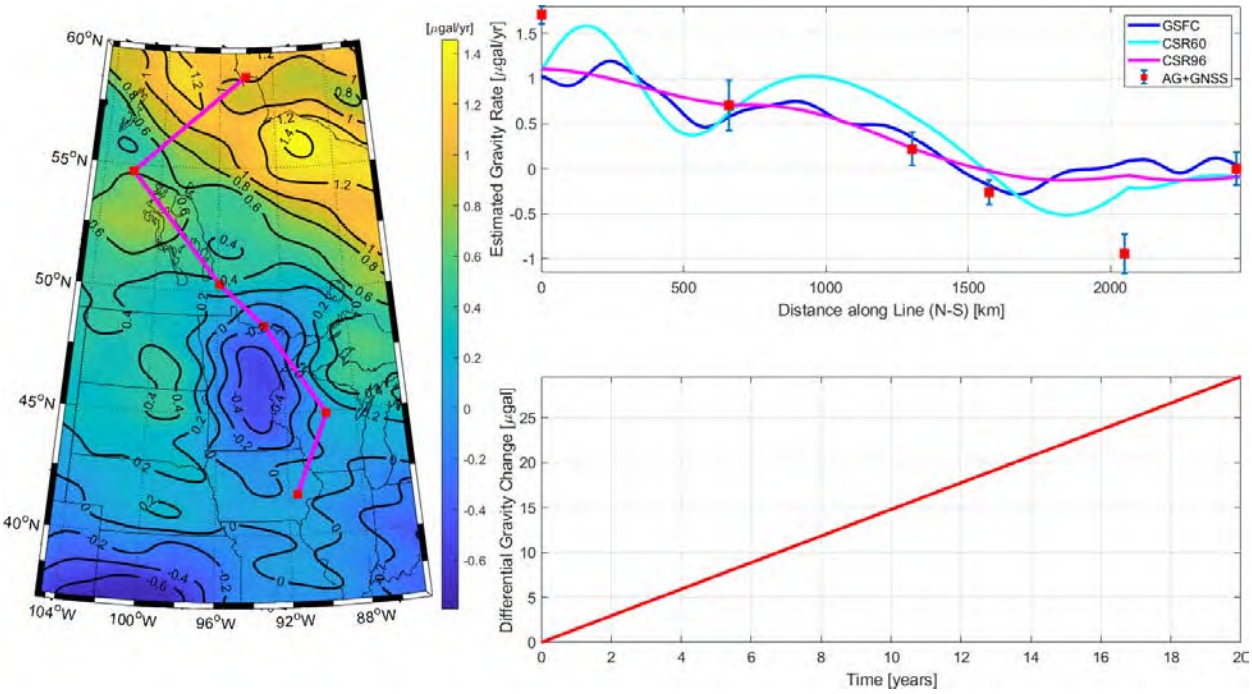

Figure 66: MCGL from Mazzotti, et al., (2011) and various GRACE models. Published GNSS rates are substituted with GNSS rates determined from UNR data. Left: GRACE derived gravity rates in μGal/yr with contour interval = 0.2 μGal/yr. Upper Right: Estimated Gravity Rate Profile from N to S with various GRACE model derived rates in μGal/yr. Blue curve = NASA GSFC mason model, Cyan curve = CSR SH model to n_{max} = 60. Magenta curve = CSR SH model to n_{max} = 96. Observed AG rates shown in red with 1-sigma error bars. Lower Right: Amount of differential gravity change (μGal) that would build up from Churchill to Waterloo over various time spans.

6.3.3 NRCan CGSN Stations

In this section, Canada's CGSN (see Figure 53) is investigated to provide an overall sense of how well the GRACE derived $\dot{g}$ models fit ground-based observations over a continental-scale geographic area. CGSN has much more recent observations on sites compared with sites across the US, and the observations are more evenly distributed (especially in southern Canada). The CGSN stations typically include a co-located GNSS site to determine the vertical deformation rate. For simplicity, we make use of UNR cGNSS station vertical rates (Blewitt, *et al.,* 2018), remove a small number of GNSS stations with short time spans (5 years) and/or high vertical rate uncertainties (5 mm/yr), and perform a simple gridding. This method could be refined to better resolve the free-air effect of the gravity change. There is not enough AG data for the entire CGSN network shown in Figure 53 to estimate a rate. We make use of a subnetwork of sites that have a minimum time span of 1 year, observations from either the JILA or FG5 meters, data collected from 1995 to the present, and NRCan's ABSGRAVPRO processing software. The CGSN sites (n = 35) that meet this criteria are shown in Figure 67 with their corresponding residuals compared to the GSFC mascon GRACE-derived $\dot{g}$ values. Residuals to the other GRACE spherical harmonic models are shown in Table 15 and Table 16. Additional information about the absolute gravity data can be found in

Appendix B. Only 19 of the 35 sites had rates that were determined to be statistically significant at the 90% level. The UTCSR (n_{max} = 96) and GSFC mascon model both perform roughly equivalently when compared against these 35 sites; all of these sites are primarily influenced by GIA and both of these GRACE models capture the long-wavelength GIA signal well. The overall results of this validation provide minimal support for this type of validation. The geoid change rates of interest in to this validation are 1-2 μGals/yr, so, a standard deviation of half that amount is inconclusive. However, this exercise demonstrates the need to observe ground AG measurements as accurately, consistently, and precisely as possible. Many of these 35 sites do not have desired consistency or compatible time series when compared with the 2002–2017 trend from GRACE. While beyond the scope of this document, this comparison between CGSN AG sites and the GRACE models could likely be further refined with consideration of instrument biases/differences, hydrologic modeling, and a better estimation of the vertical deformation to more adequately evaluate validation options.

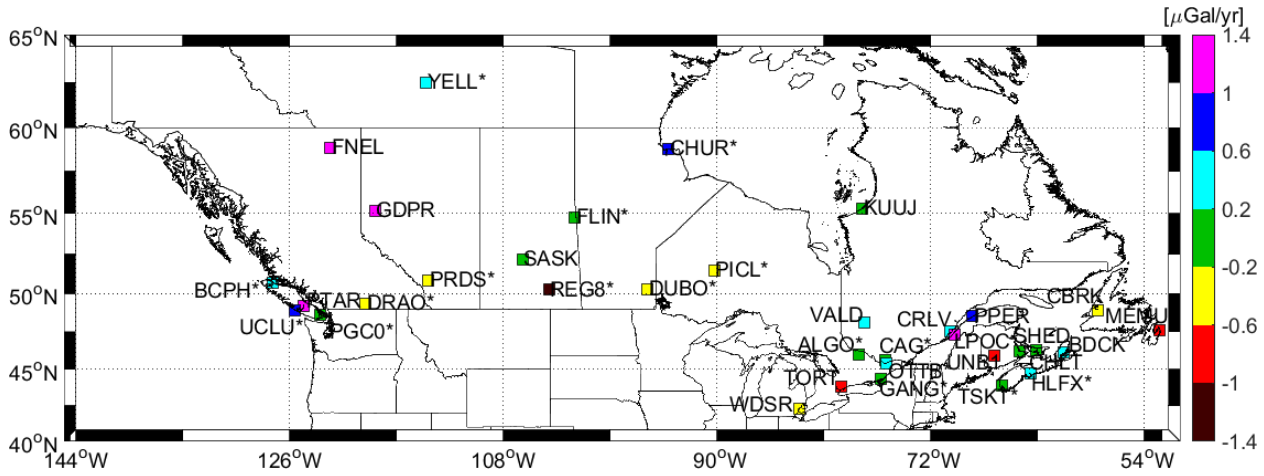

Figure 67: ġ residual at CGSN AG sites using GSFC mascon model (An asterisk next to the station signifies that the AG estimated rate is statistically significant)

Table 15: CGSN AG Site Residuals

GRACE Model - LS (n = 35)	Min	Max	Mean	Std. Dev.
UTCSR (n_{max} = 60)	-0.918	2.012	0.214	0.739
UTCSR (n_{max} = 96)	-1.160	1.737	0.164	0.670
GSFC (n_{max} = 180)	-1.124	1.569	0.129	0.666

Table 16: CGSN AG Site Residuals at statistically significant sites

GRACE Model Significant - LS (n = 19)	Min	Max	Mean	Std. Dev.
UTCSR (n_{max} = 60)	-0.800	1.351	0.090	0.573
UTCSR (n_{max} = 96)	-1.160	1.009	0.075	0.524
GSFC (n_{max} = 180)	-1.124	1.054	0.075	0.526

6.3.4 U.S. Absolute Gravity Stations with Repeat Observations

The U.S. has more sparsely sampled absolute gravity network covering CONUS and Alaska compared with the CGSN described in Section 6.3.3. The stations in this network are re-observed sporadically (in both space and time) making it difficult to predict a $\dot{g}$ value with any certainty. There are a total of 87 stations that have multiple observations that can be used to estimate a $\dot{g}$ value. Of these 87 stations, only 32 stations are statistically significant (at the 90% level). Due to the poor overall quality of this network, it is inadequate for comparison with a GRACE model, but for the purposes of illustrating the need for a US absolute gravity network to serve as a validation for GeMS the results of this comparison are shown in Figure 68 and Table 17.

The U.S. absolute gravity stations are approximately 1 order of magnitude less accurate than those from Canada's CGSN. The U.S. stations have overall residuals of approximately 9 μGals/yr (4 μGals/yr significant) compared with 0.6 μGals/yr (0.5 μGals/yr significant) from Canada's CGSN. This degraded data quality arises from a dearth of observations, both spatially and temporally. In certain areas where the sampling is more consistent, like Arizona and Louisiana, there is a general agreement with the AG values and the GRACE models, but continent-wide agreement is lacking.

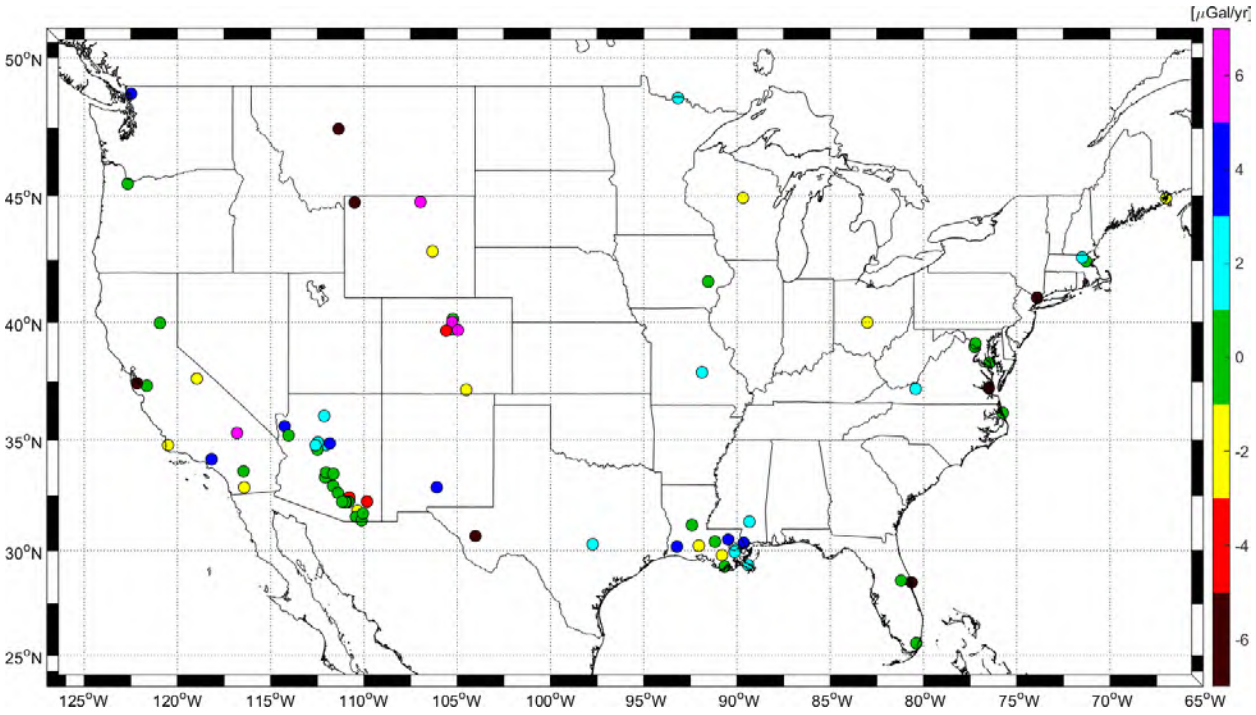

Figure 68: US Absolute Gravity Station Residuals between $\dot{g}$ observed at the station and NASA GSFC v02.4 GRACE mascon model.

Table 17: US Absolute Gravity Residual Statistics [μGals/yr]

	n	Min.	Max.	Mean	Std. Dev.
All AG stations	87	-74.3	20.5	-0.9	10.2
Significant at 90%	32	-10.9	9.6	0.7	3.6

While not shown in detail, a few of the absolute gravity time series are shown in Alaska in Figure 69 to further highlight the current state of these stations' time series and the difficulty in using them for GeMS validation. This AG network could be very useful for GeMS and an operational blueprint is proposed in Section 6.4.1 to ensure that this is built upon and maintained to support GeMS.

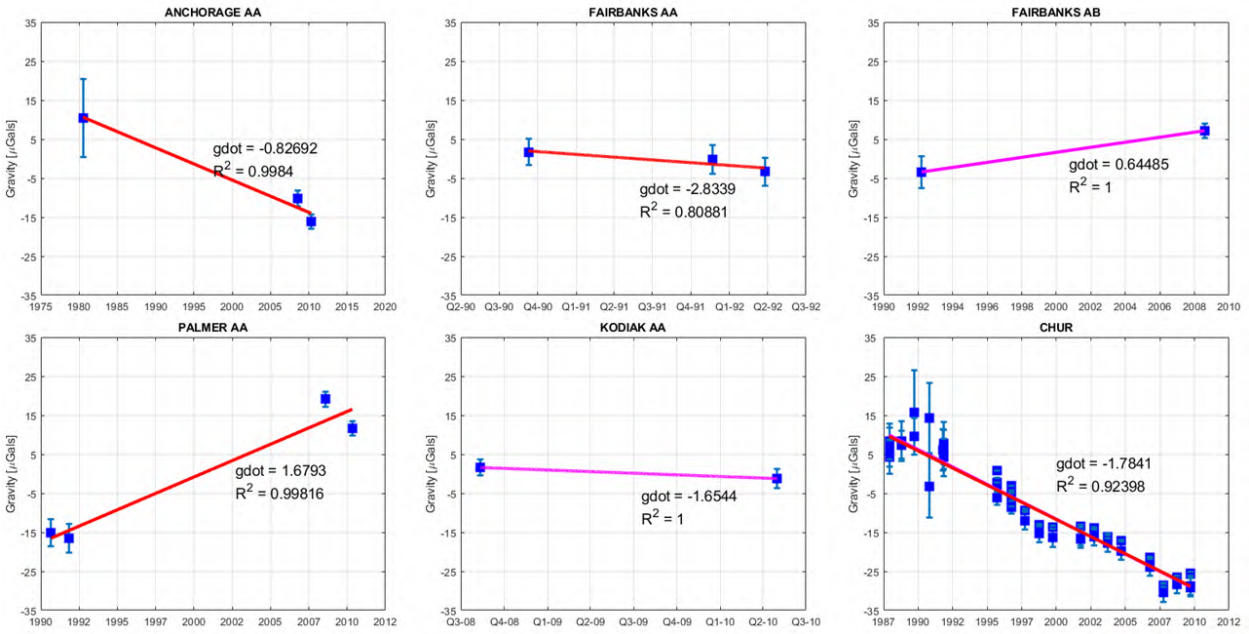

Figure 69: Time series for subset of NGS absolute gravity stations in Alaska. Lower right station (CHUR) is from NRCan's Churchill site. AG rates are shown as gdot on each sub-figure. Time spans are all variable depending on the observations.

6.3.5 Southeast Alaska with Ice-mass Model

This section discusses a small network in Southeast Alaska and neighboring Canada that was observed with an FG5 yearly from 2006 to 2008 by a Japanese team of researchers and colleagues (Sato, *et al.,* 2012). While this time series is too short to draw major conclusions with respect to GeMS, it does offer added insight into the extreme difficulty in using a GRACE-only GeMS model for areas with very localized mass change. Additionally, this comparison highlights the dire importance of augmenting GRACE-only models with some form of ice-mass model and maybe other geophysical models to capture the detailed high resolution changes impacting the geoid in specific areas. The AG time series is not of long enough duration, with a time span of only 3 years (from 2006-2008), to obtain conclusive results. This is reflected in the high sigma values (1.5 μGal/yr) published with the associated $\dot{g}$ values.

The GRACE-based models perform poorly in estimating the observed FG5 $\dot{g}$ value in this region. Notice how the labeled FG5 observed rates differ from the contours in Figure 70, as well as the misalignment of the observations and models shown in Figure 71. Even though none of the models (UTCSR n_{max} = 60, CSR n_{max} = 96, and GSFCv02.4) perform well, the general shape of the GSFC model does exhibit similarities with the FG5 observations; however, there is a significant bias of approximately 7 μgal/yr between them. The statistics from the survey results, when compared with multiple GRACE models, are shown in Table 18. If the GRACE model time series is restricted to a time span from 2005 – 2010 to coincide with the FG5 survey, the results are slightly better (see last column in Table 18) but the residual RMS is still

3.609 μGal/yr.

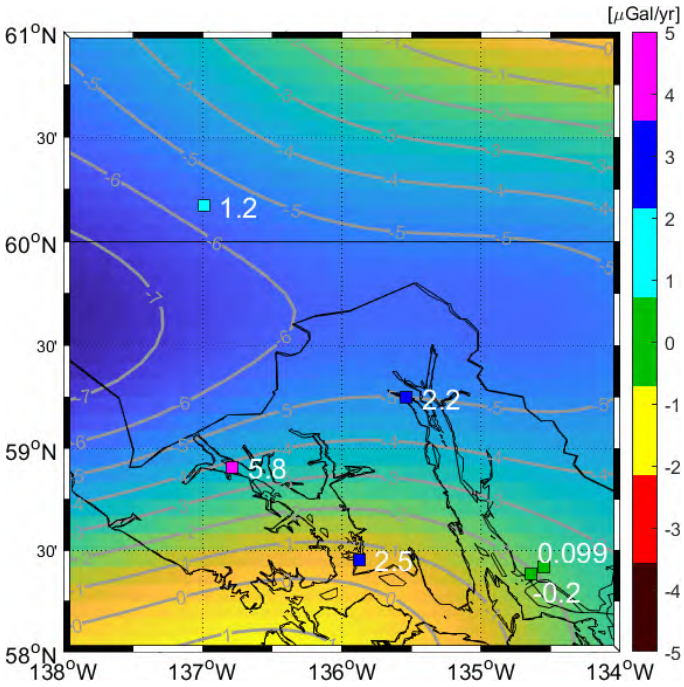

Figure 70: Southeast Alaska ġ [μGal/yr]. Marks are FG5 derived rates with labeled estimate. Contour lines and background show the GSFC v02.4 mascon GRACE derived ġ with contour interval = 1 μGal/yr.

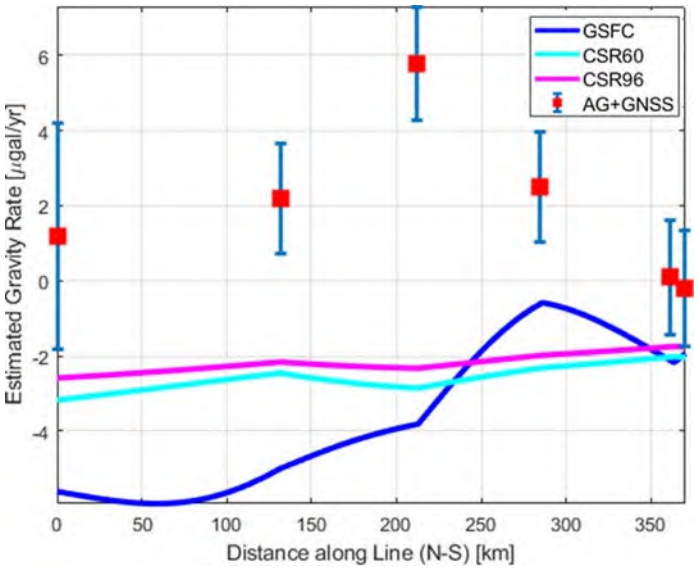

Figure 71: Simulated profile from N to S showing various GRACE model values and the AG observed model values. Blue = NASA GSFC v02.4 model. Cyan = UTCSR SH model to n_{max} = 60. Magenta = UTCSR SH model to n_{max} = 96. Error bars for AG sites are 1 sigma.

Table 18: Southeast Alaska Absolute Gravity Network Statistics

Station	GNSS $\dot{h}$ [mm/yr]	$\dot{g}$ from $\dot{h}$	$\dot{g}$ from AG	$\delta\dot{g}$ (AG - $\dot{h}$)	CSR60	Residual	CSR96	Residual	GSFC	Residual	CSR96 (2005-2010)	Residual
BRM	16.16	-4.98	-3.79	1.19	-3.18	4.37	-2.59	3.78	-5.61	6.80	-1.65	2.84
HNSG	23.05	-7.10	-4.92	2.18	-2.46	4.64	-2.16	4.35	-5.00	7.19	-1.00	3.19
RSLG	30.03	-9.26	-3.46	5.80	-2.86	8.65	-2.33	8.13	-3.81	9.61	-1.20	6.99
GBCL	26.09	-8.04	-5.54	2.50	-2.32	4.82	-1.98	4.49	-0.59	3.09	-0.77	3.27
MGVC	15.31	-4.72	-4.62	0.10	-2.02	2.12	-1.75	1.85	-2.18	2.28	-0.45	0.55
EGAN	14.49	-4.47	-4.67	-0.20	-2.04	1.83	-1.76	1.55	-1.94	1.74	-0.46	0.25

6.4 Options for Validation Schemes and Designs

Any eventual GeMS model will require independent validation to assess accuracy and quality of the resultant products. The following section describes options that provide this external validation to any individual model; each provides a slightly different validation of GeMS models arising from differences in either the spatial or temporal resolution of the validation dataset (see Table 19). A viable validation strategy may consist of some combination of these options.

Table 19: Summary of GeMS Validation Options

Validation Options:	Scientific Complexity & Effort	Potential Impact	Affordability	Risk[7]
Option 1: U.S. Network of $\dot{g}$ and $\dot{h}$	Low	High	High	Low
Option 2: Repeat GSVS (RGSVS) Lines with $\dot{g}$ and $\dot{h}$	Medium	Extremely High	High	Medium
Option 3: Continuous gPhone observations at high impact locations	Medium	Very High	Low (Acquisition) Very High (Operational)	Medium
Option 4: Optical Clock Network	Extremely High	Extremely High	Low	High

6.4.1 Validation Scheme 1: U.S. Network of $\dot{g}$ and $\dot{h}$

This option would develop, construct, and maintain a network of absolute gravity stations with appropriate FG5 (or similar instrument that meets repeatability and traceability requirements) space-time sampling. Additionally, this network should further leverage the existing NOAA CORS Network (NCN) and other cGNSS sites to measure changes to the topographic surface ($\dot{h}$). In geographic areas where the existing NOAA CORS Network doesn't provide necessary coverage, a new CORS could be

[7] Risk of relying on this particular validation option for a GeMS operational model and not getting satisfactory results.

established or additional geodetic techniques such as InSAR or NGS's IFVM could be used to determine the $\dot{h}$ values.

This option has Low scientific complexity, cost/resources, and risk. NGS currently oversees the NCN, which has spatial coverage that is better than what GeMS would require. However, any given location with high importance to GeMS may not be colocated with a CORS, requiring supplemental GNSS observations. The primary expense associated with this option is staff time and travel to gravity observation sites. Rough estimates of time and travel costs are provided at the end of this section to accomplish this validation option.

A drawback to this option is that only a very broad, long-wavelength validation would be achievable as the network has stations at 200 – 500 km spacings. In areas affected by localized geoid or gravity change, further high-resolution validation would be needed.

The specific recommendation is to leverage the existing NOAA Foundation CORS Network plus an additional subset of the NOAA CORS Network to build and maintain this $\dot{g}/\dot{h}$ network. The three geographic regions of focus would be Alaska, the Great Lakes, and rest of CONUS. The Alaska and Great Lakes regions will be prioritized as most of the geoid change is taking place in these two areas, and this change has a critical impact on marine transportation and commerce, flood mitigation, coastal resiliency, and tourism. The proposed validation networks, shown in Figure 72 and Figure 73are preliminary and provided primarily for illustrative purposes. Sites would be selected to achieve adequate spatial coverage/resolution with emphasis on location experiencing the most geoid change, while leveraging existing AG observations, the NOAA Foundation CORS Network, and the NOAA CORS Network.

In additional to the proposed networks shown, a summary table with a number of estimates for scope, time, and cost for each of these areas is presented in. Also included is an Outside CONUS entry, which would include Hawaii, Puerto Rico, U.S. Virgin Islands, Guam, Commonwealth of Northern Mariana Islands, and American Samoa. These remote sites are rarely visited by a gravimeter and will be re-observed as operations allow.

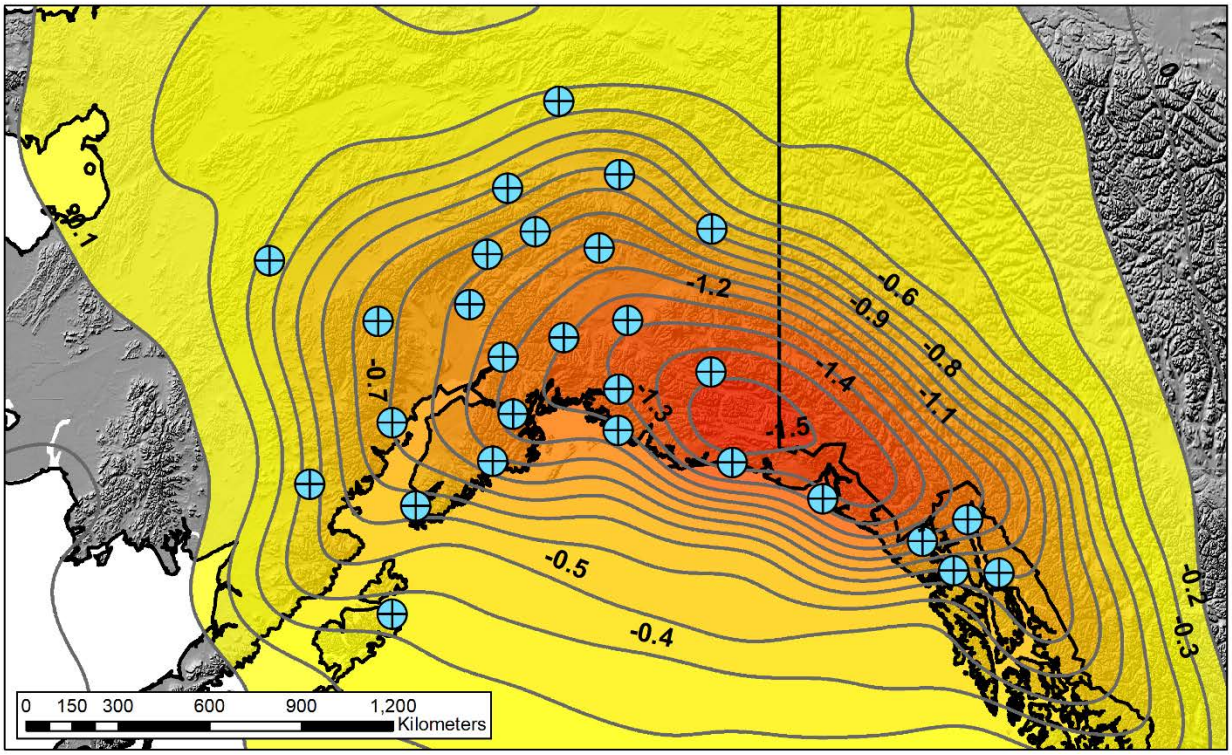

Figure 72: Preliminary Alaska Absolute Gravity Validation Network shown with geoid rates from GRACE in mm/yr (contour interval = 0.1 mm/yr)

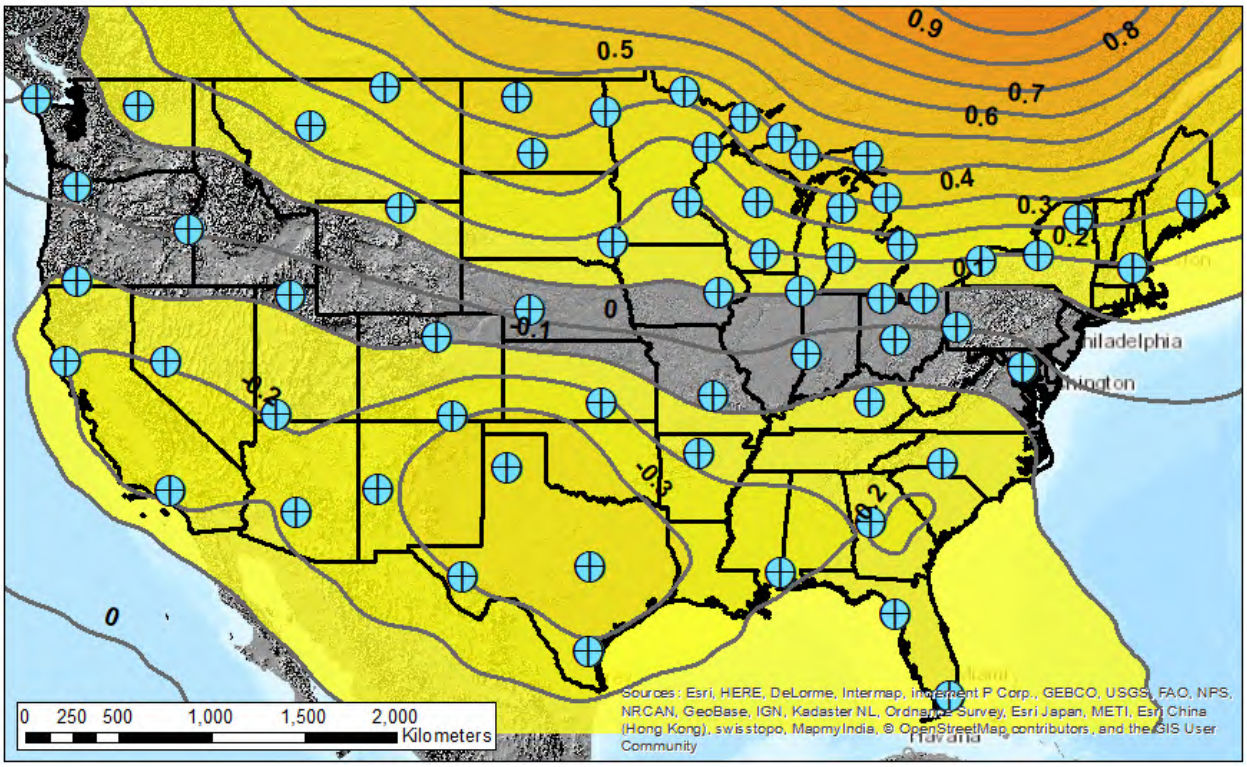

Figure 73: Preliminary CONUS Absolute Gravity Validation Network shown with geoid rates from GRACE in mm/yr (contour interval = 0.1 mm/yr)

Table 20: GeMS Validation Network

Region of Focus:	Total number of stations:	Approximate Geographic Spacing:	Repeat Frequency:	Number of stations per year:	Field time per year:	Cost per year:
Great Lakes	20	200 km	Annually	20	3 months	$40,000
Alaska	30	200 km (accessible areas)	Annually	30	3 months	$50,000
Rest of CONUS	42	500 km	3 years	14	2 months	$30,000
Outside CONUS	8	NA	TBD	TBD	TBD	TBD

6.4.2 Validation Scheme 2: GeMS Validation Surveys (GeMS-VS) with $\dot{g}$ and $\dot{h}$

Another option for validation relies on NGS's experience surveying the GSVS lines in Texas, Iowa, and Colorado. In order for the GSVS lines to be of use for GeMS, repeat GPS and leveling would need to be performed at set time intervals. Difficulties associated with this GPS/Leveling work include high costs, difficulty in obtaining the required accuracies of sub-cm for GNSS and leveling over 200+ km lines, and determination of only the relative $\dot{N}$ since a single leveling mark must be held fixed. However, we

propose a modified strategy for a GeMS-Validation Survey (GeMS-VS) where gravity and ellipsoid height are observed at yearly time intervals along a line resulting in $\dot{g}$ and $\dot{h}$ at high spatial scales (approximately 10 - 20 km) as illustrated in Figure 74. This methodology has a number of benefits and is relatively straightforward to perform. Additionally, this type of line would be ideal for repeat DoV observations to provide an independent and redundant assessment of geoid change. The DoV addition could be performed within the GeMS-VS with very minor additional costs. The DoV observations would be extremely useful for detecting past geoid change, because they would provide geoid profiles reflecting the geoid at the time of measurement rather than a reflection of 70+ years of terrestrial gravity surveys. Not only can DoV determine geoid change, it can be used to validate the static geoid in an extremely challenging place.

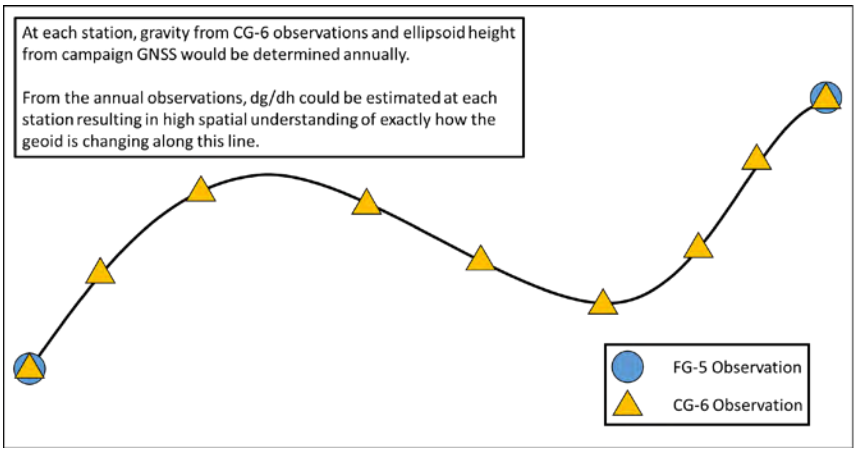

Figure 74: GeMS-VS design over a 200+ km line with relative gravity observations collected at high spatial scales (5-10 km).

The $\dot{g}$ component can be measured along the line with a relative CG6 gravimeter. This must be combined with a FG5 observation to provide the absolute tie on both ends of the line. NGS tests have shown that the CG-6 can meet the GeMS accuracy requirements (van Westrum and Kanney, 2017). The $\dot{h}$ component would be measured with 24 GPS, at a minimum. It would be possible to include any nearby NOAA CORSs so that the $\dot{h}$ term could be sampled more continuously in time. Additionally, an operational IFVM product and data could also be used to estimate the $\dot{h}$ term.

The scientific complexity and effort required for this type of survey is Medium, being only slightly more complex than Validation Option 1. The impact of this type of validation would be Extremely High for the surrounding area as higher spatial resolution sampling is captured. The affordability is Medium, with a modest amount of time and staff/resource expenses needed. Since we don't have to perform geodetic leveling, the time to perform the gravity work is only a few days (2-5 days) while the GPS survey could take up to 2-3 weeks (10 stations for 48 hours each). Finally, the risk to this option is Medium because this is a new type of survey design; known risks include interannual hydrologic variability that might overwhelm the secular signal when sampled at a coarse temporal scale.

The specific recommendation for this option is to perform this type of survey over three connected profiles in Alaska, which is laid out in additional detail in Section 6.3.1. The profiles are based out of Glennallen, AK with individual spokes to Tok, AK, Palmer, AK, and Valdez, AK. This GeMS-VS would deploy a FG5 and CG-6 every year for a duration of 5 years. The amount of field time needed is 1 month per year, with an estimated cost of $25K per year. Initial setup of the GeMS-VS would be a one-time cost of $20K (survey design, mark identification, limited mark setting, tree-trimming, and other reconnaissance). Total cost for 5 years is $135K USD not including salaries.

NGS would not have to wait years to obtain scientific value out of a GeMS-VS. With the first year of observations, we would leverage half a century of prior gravity and leveling observations on NSRS benchmarks along these routes. Such measurements would provide evidence of past geoid change, validate models, and fix the GNSS leveling dataset.

6.4.3 Validation Scheme 3: continuous gPhone occupations at high impact locations

This validation option provides a similar benefit to Validation Option 2 except higher temporal resolutions are obtained at a limited number of locations. The overall scheme would be to deploy a gPhone continuously at a high impact location to observe how changes in the gravity field affect the geoid at very short time spans (daily, weekly, and seasonally). This survey would require an FG5 observation at the beginning and end of the survey (and at regular intervals if of sufficient duration) to estimate long-term drift of the gPhone. Ideally, this type of survey could be deployed in conjunction with Validation Option 1 and/or 2, to yield information about how the gravity and geoid are changing in space (at 10s of km) and time (sub-annual).

The scientific complexity to this type of survey is Medium. The most difficult situation to overcome is determining sites colocated with the NOAA CORS Network. Additionally, some complexity exists to ensure that vertical motions measured at the receiver are consistent with the vertical motion of the gPhone platform. The impact of this type of survey is Very High due to the added information gained about how signals with a period of less than a year impact the geoid. The impact is lowered slightly due to extrapolating results to regional and continental scales without scaling the number of gPhones and/or sites. The cost for this is broken into acquisition cost and operational costs. Since NGS owns just a single gPhone, the acquisition cost is High to have enough sensors to make a regional impact on geoid change. The operational cost of a gPhone at a single site is Low. The only cost is a relatively modest amount of setup/closeout staff time and a very low day-to-day cost for electricity, security, etc. The risk for this type of survey are Medium. It is a new type of survey for NGS with various unknowns. Additionally, the gPhone would most likely be left unattended for long periods of time where a number of setbacks could occur including theft, vandalism, power failure, data logging failure, and internet issues.

If NGS would deploy a gPhone at each FCORS site (approximately 35), acquisition cost would be $100K per gPhone with $2K to install and maintain. Total cost to purchase and deploy at all FCORS sites is $3.6 million.

6.4.4 Validation Scheme 4: Optical Clock Network

This validation option relies on a network of optical clocks to continuously monitor the changes to the geoid surface ($\dot{W}$). It would provide the exact type of measurement NGS would need for geoid monitoring. In addition to the optical clock network, the $\dot{h}$ component from a CORS or other cGNSS site would be used at each clock location. It would also be possible to use InSAR to obtain the $\dot{h}$ component.

The scientific complexity is Extremely High. Currently, this technique is not operationally ready to deploy to remote sites. It is difficult to say when this might be operationally ready (5-10 years if technology continuous to progress at current pace maybe sooner). Additionally, it is not a technology that NGS can develop and build with reliance on existing staff expertise. The greatest possibility at the moment is to use two locations for testing purposes. For example, clock locations could be established between Anchorage and Fairbanks, Alaska, which has a gravity rate difference of 1.12 μGal/yr (-1.5 μGal/yr and -0.38 μGal/yr at Anchorage and Fairbanks, respectively). The cost of this technique is Very High. Numerous local, state, and federal partners would need to be brought into the project to successfully accomplish such a task. The potential impact of this technique is Extremely High because it would provide the exact quantity that NGS is trying to monitor (changes to the geopotential surface). The technique appears to be scalable to regional and continental levels much like the early days of global CORS networks. The risk is High though considering the technique is still in development.

7 Conclusions

This document serves as a deliberative summary of our state of knowledge surrounding two related considerations of great importance to NGS's launch and successful continuation of GeMS. The first consideration pertains to the basic science behind monitoring the geoid. A review of geoid monitoring techniques provides a foundation for understanding: where the geoid is changing, what's causing this change to happen, how much change occurs, and at what time-scales. GRACE and GRACE-FO are crucial observational missions that provide a basis for GeMS. However, GRACE-type observations do not provide the whole picture; many complementary localized geodetic data and models reveal geoid rates that are 2–3 times larger than the geoid change rate observed by GRACE in some locations (like Alaska). This systematic and quantified review has affirmed the requirement for GeMS in the modernized NSRS.

The second consideration is a practical question of how NGS will operationally support GeMS into the future. A series of recommendations and options are now available for NGS to consider and implement over the coming years, and these recommendations have shaped the development of three possible initial GeMS model approaches. Additionally, a number of presented validation options could function to assess the quality and accuracy of any implemented GeMS model. Many of these validation options support recommendations put forth by other national and international bodies including the International Association of Geodesy-Global Geodetic Observing System, United Nations-Global Geospatial Information Management Subcommittee on Geodesy, and the National Research Council.

8 References

A. Geruo, J. Wahr, and S. Zhong (2013), Computations of the viscoelastic response of a 3-D compressible Earth to surface loading: an application to Glacial Isostatic Adjustment in Antarctica and Canada, Geophys. J. Int., 192, 557-572,doi:10.1093/gji/ggs030.

Abend, S., Gebbe, M., Gersemann, M., Ahlers, H., Müntinga, H., Giese, E., ... & Schleich, W. P. (2016). Atom-chip fountain gravimeter. Physical review letters, 117(20), 203003.

Argus, D. F., Fu, Y., & Landerer, F. W. (2014). Seasonal variation in total water storage in California inferred from GPS observations of vertical land motion. Geophysical Research Letters, 41(6), 1971-1980.

Bagnardi, M., Poland, M. P., Carbone, D., Baker, S., Battaglia, M., & Amelung, F. (2014). Gravity changes and deformation at Kīlauea Volcano, Hawaii, associated with summit eruptive activity, 2009–2012. Journal of Geophysical Research: Solid Earth, 119(9), 7288-7305.

Bekaert, D. P. S., Hamlington, B. D., Buzzanga, B., & Jones, C. E. (2017). Spaceborne synthetic aperture radar survey of subsidence in Hampton Roads, Virginia (USA). Scientific reports, 7(1), 14752.

Berardino, P., Fornaro, G., Lanari, R., & Sansosti, E. (2002). A new algorithm for surface deformation monitoring based on small baseline differential SAR interferograms. IEEE transactions on geoscience and remote sensing, 40(11), 2375-2383.

Bevis, M., & Brown, A. (2014). Trajectory models and reference frames for crustal motion geodesy. Journal of Geodesy, 88(3), 283-311.

Bidel, Y., Zahzam, N., Blanchard, C., Bonnin, A., Cadoret, M., Bresson, A., ... & Lequentrec-Lalancette, M. F. (2018). Absolute marine gravimetry with matter-wave interferometry. Nature communications, 9(1), 627.

Bjerhammar, A. (1985). On a relativistic geodesy. Bulletin géodésique, 59(3), 207-220.

Blewitt, G., Hammond, W. C., & Kreemer, C. (2018). Harnessing the GPS data explosion for interdisciplinary science. Eos, 99.

Boudin, F., Bernard, P., Longuevergne, L., Florsch, N., Larmat, C., Courteille, C., ... & Kammentaler, M. (2008). A silica long base tiltmeter with high stability and resolution. Review of Scientific Instruments, 79(3), 034502.

Bürgmann, R., Rosen, P. A., & Fielding, E. J. (2000). Synthetic aperture radar interferometry to measure Earth's surface topography and its deformation. Annual review of earth and planetary sciences, 28(1), 169-209.

Caron, L., E.R. Ivins, E. Larour, S. Adhikari, J. Nilsson and G. Blewitt (2018), GIA model statistics for GRACE hydrology, cryosphere and ocean science, Geophys. Res. Lett., 45, doi:10.1002/2017GL076644.

Chou, C. W., Hume, D. B., Koelemeij, J. C. J., Wineland, D. J., & Rosenband, T. (2010). Frequency comparison of two high-accuracy Al+ optical clocks. Physical review letters, 104(7), 070802.

Farrell, W. E. (1972). Deformation of the Earth by surface loads. Reviews of Geophysics, 10(3), 761-797.

Fu, L. L., & Cheney, R. E. (1995). Application of satellite altimetry to ocean circulation studies: 1987–1994. Reviews of Geophysics, 33(S1), 213-223.

Furst, S., Chéry, J., Mohammadi, B., & Peyret, M. (2019). Joint estimation of tiltmeter drift and volume variation during reservoir monitoring. Journal of Geodesy, 1-10.

Gross, R. S., & Chao, B. F. (2006). The rotational and gravitational signature of the December 26, 2004 Sumatran earthquake. Surveys in Geophysics, 27(6), 615-632.

Grotti, J., Koller, S., Vogt, S., Häfner, S., Sterr, U., Lisdat, C., ... & Baynes, F. N. (2018). Geodesy and metrology with a transportable optical clock. Nature Physics, 1.

Heiskanen, W. A., & Moritz, H. (1967). Physical Geodesy. W.H. Freeman and Company. San Francisco.

Helmert, F. R. (1890). Die Schwerkraft im Hochgebirge, insbesondere in den Tyroler Alpen. Veröff.

Königl. Preuss. Geod. Inst, 1.
Hirt, C., & Flury, J. (2008). Astronomical-topographic levelling using high-precision astrogeodetic vertical deflections and digital terrain model data. Journal of Geodesy, 82(4-5), 231-248.
Hooper, A. (2008). A multi-temporal InSAR method incorporating both persistent scatterer and small baseline approaches. Geophysical Research Letters, 35(16).
Hotine, M. (1969). Mathematical geodesy. ESSA Monogram 2, Washington, D.C.
Jacob, T., Wahr, J., Gross, R., Swenson, S., & Geruo, A. (2012). Estimating geoid height change in North America: past, present and future. Journal of Geodesy, 86(5), 337-358.
Jekeli, C., & Dumrongchai, P. (2003). On monitoring a vertical datum with satellite altimetry and water-level gauge data on large lakes. Journal of Geodesy, 77(7-8), 447-453.
Kasevich, M., & Chu, S. (1992). Measurement of the gravitational acceleration of an atom with a light-pulse atom interferometer. Applied Physics B, 54(5), 321-332.
Kuo, C. Y., Shum, C. K., Braun, A., & Mitrovica, J. X. (2004). Vertical crustal motion determined by satellite altimetry and tide gauge data in Fennoscandia. Geophysical Research Letters, 31(1).
LaCoste Jr, L. J. (1934). A new type long period vertical seismograph. Physics, 5(7), 178-180.
Larsen, C. F., Burgess, E., Arendt, A. A., O'Neel, S., Johnson, A. J., & Kienholz, C. (2015). Surface melt dominates Alaska glacier mass balance. Geophysical Research Letters, 42(14), 5902-5908.
Lisdat, C., Grosche, G., Quintin, N., Shi, C., Raupach, S. M. F., Grebing, C., ... & Häfner, S. (2016). A clock network for geodesy and fundamental science. Nature communications, 7, 12443.
Luthcke, S.B., T.J. Sabaka, B.D. Loomis, *et al.,* (2013), Antarctica, Greenland and Gulf of Alaska land ice evolution from an iterated GRACE global mascon solution. J. Glac.; 59(216), 613-631, doi:10.3189/2013JoG12J147
Mainville, A., & Craymer, M. R. (2005). Present-day tilting of the Great Lakes region based on water level gauges. Geological Society of America Bulletin, 117(7-8), 1070-1080.
Mazzotti, S., A. Lambert, J. Henton, T.S. James, & N. Courtier. (2011). Absolute gravity calibration of GPS velocities and glacial isostatic adjustment in mid-continent North America. Geophysical Research Letters, 38(24).
Ménoret, V., Vermeulen, P., Le Moigne, N., Bonvalot, S., Bouyer, P., Landragin, A., & Desruelle, B. (2018). Gravity measurements below 10− 9 g with a transportable absolute quantum gravimeter. Scientific reports, 8(1), 12300.
Milbert, D. G. (1991). GEOID90: A high-resolution geoid for the United States. Eos, Transactions American Geophysical Union, 72(49), 545-554.
Moose, R.E. (1986), The National Geodetic Survey Gravity Network, NOAA Technical Report NOS 121 NGS 39, 32 p.
Morelli, C., Gantar, C., McConnell, R. K., Szabo, B., & Uotila, U. (1972). The international gravity standardization net 1971 (IGSN 71).
Müller, J., Dirkx, D., Kopeikin, S. M., Lion, G., Panet, I., Petit, G., & Visser, P. N. A. M. (2018). High performance clocks and gravity field determination. Space Science Reviews, 214(1), 5.
National Academies of Sciences, Engineering, and Medicine 2018. Thriving on Our Changing Planet: A Decadal Strategy for Earth Observation from Space. Washington, DC: The National Academies Press. https://doi.org/10.17226/24938.
National Geodetic Survey (2007). The GRAV-D Project: Gravity for the Redefinition of the American Vertical Datum. National Oceanic and Atmospheric Administration, National Geodetic Survey, Silver Spring, MD, http://www.ngs.noaa.gov/GRAV-D/pubs/GRAV-D_v2007_12_19.pdf, downloaded 2019 07 23.
National Geodetic Survey (2013). The National Geodetic Survey Ten Year Strategic Plan, 2013-2023: Positioning America for the Future. https://www.ngs.noaa.gov/web/news/Ten_Year_Plan_2013-2023.pdf.

National Geodetic Survey (2017a). Blueprint for 2022, Part 1: Geometric Coordinates. NOAA Technical Report NOS NGS 62. https://geodesy.noaa.gov/PUBS_LIB/NOAA_TR_NOS_NGS_0062.pdf

National Geodetic Survey (2017b). Blueprint for 2022, Part 2: Geopotential Coordinates. NOAA Technical Report NOS NGS 64. https://geodesy.noaa.gov/PUBS_LIB/NOAA_TR_NOS_NGS_0064.pdf

National Geodetic Survey (2019a). The National Geodetic Survey Strategic Plan 2019–2023 Positioning America for the Future. https://www.ngs.noaa.gov/web/about_ngs/info/documents/ngs-strategic-plan-2019-2023.pdf

National Geodetic Survey (2019b). Blueprint for 2022, Part 3: Working in the Modernized NSRS. NOAA Technical Report NOS NGS 67.

National Research Council. (2010). Precise geodetic infrastructure: national requirements for a shared resource.

Nerem, R. S., & Mitchum, G. T. (2002). Estimates of vertical crustal motion derived from differences of TOPEX/POSEIDON and tide gauge sea level measurements. Geophysical Research Letters, 29(19), 40-1.

Niebauer, T. M., Sasagawa, G. S., Faller, J. E., Hilt, R., & Klopping, F. (1995). A new generation of absolute gravimeters. Metrologia, 32(3), 159.

Oleson, K. W., Lawrence, D. M., Gordon, B., Flanner, M. G., Kluzek, E., Peter, J., ... & Heald, C. L. (2010). Technical description of version 4.0 of the Community Land Model (CLM).

Pail, R., Bingham, R., Braitenberg, C., Dobslaw, H., Eicker, A., Güntner, A., ... & Wouters, B. (2015). Science and user needs for observing global mass transport to understand global change and to benefit society. Surveys in Geophysics, 36(6), 743-772.

Peltier, W. R. (2004). Global glacial isostasy and the surface of the ice-age Earth: the ICE-5G (VM2) model and GRACE. Annu. Rev. Earth Planet. Sci., 32, 111-149.

Peltier, W. R., Argus, D. F., & Drummond, R. (2015). Space geodesy constrains ice age terminal deglaciation: The global ICE-6G_C (VM5a) model. Journal of Geophysical Research: Solid Earth, 120(1), 450-487.

Peter, G., Moose, R.E., & Wessells, C.W. (1989), The National Geodetic Survey Absolute Gravity Program, NOAA Technical Report NOS 130 NGS 43, 18 p.

Rangelova, E., & Sideris, M. G. (2008). Contributions of terrestrial and GRACE data to the study of the secular geoid changes in North America. Journal of Geodynamics, 46(3-5), 131-143.

Rangelova, E. (2009), PhD Dissertation. University of Calgary.

Rangelova, E., Fotopoulos, G., & Sideris, M. G. (2010). Implementing a dynamic geoid as a vertical datum for orthometric heights in Canada. Gravity, Geoid and Earth Observation, 295-302.

Rangelova, E., Van Der Wal, W., & Sideris, M. G. (2012). How significant is the dynamic component of the North American vertical datum?. Journal of Geodetic Science, 2(4), 281-289.

Rodell, M., Houser, P. R., Jambor, U. E. A., Gottschalck, J., Mitchell, K., Meng, C. J., ... & Entin, J. K. (2004). The global land data assimilation system. Bulletin of the American Meteorological Society, 85(3), 381-394.

Sato, T., Miura, S., Sun, W., Sugano, T., Freymueller, J. T., Larsen, C. F., ... & Motyka, R. J. (2012). Gravity and uplift rates observed in southeast Alaska and their comparison with GIA model predictions. Journal of Geophysical Research: Solid Earth, 117(B1).

Save, H. and the CSR Level-2 Team, "GRACE RL06 Reprocessing and Results from CSR," EGU2018-10697, EGU General Assembly 2018.

Smith, D. A., Holmes, S. A., Li, X., Guillaume, S., Wang, Y. M., Bürki, B., ... & Damiani, T. M. (2013). Confirming regional 1 cm differential geoid accuracy from airborne gravimetry: the Geoid Slope Validation Survey of 2011. Journal of Geodesy, 87(10-12), 885-907.

Stokes, G. G. (1849). On the variation of gravity on the surface of the Earth. Trans. Camb. Phil. Soc., 8, 672-695.

van Westrum, D., & Kanney, J. (2017). First Impressions of a Scintrex CG-6 Portable Gravimeter in an Extensive Field Campaign. In AGU Fall Meeting Abstracts.

Wahr, J., DaZhong, H., & Trupin, A. (1995). Predictions of vertical uplift caused by changing polar ice volumes on a viscoelastic Earth. Geophysical Research Letters, 22(8), 977-980.

Wahr, J., Molenaar, M., & Bryan, F. (1998). Time variability of the Earth's gravity field: Hydrological and oceanic effects and their possible detection using GRACE. Journal of Geophysical Research: Solid Earth, 103(B12), 30205-30229.

Wahr, J., Swenson, S., Zlotnicki, V., & Velicogna, I. (2004). Time-variable gravity from GRACE: First results. Geophysical Research Letters, 31(11).

Wahr, J., Swenson, S., & Velicogna, I. (2006). Accuracy of GRACE mass estimates. Geophysical Research Letters, 33(6).

Wang, Y. M., Becker, C., Mader, G., Martin, D., Li, X., Jiang, T., ... & Bürki, B. (2017). The Geoid Slope Validation Survey 2014 and GRAV-D airborne gravity enhanced geoid comparison results in Iowa. Journal of Geodesy, 91(10), 1261-1276.

Wessells, C. W. (1985). Blue Ridge gravimeter calibration base line, established 1985.

Zervas, C., Gill, S., & Sweet, W. (2013). Estimating Vertical Land Motion from Long-Term Tide Gauge Records.

9 Appendix A: Equations related to Time-Dependent Geopotential Coefficients

$$\dot{N}(\theta,\lambda) = R_E \sum_{n=0}^{N}\sum_{m=0}^{n}\left(\dot{\bar{C}}_{n,m}cos(m\lambda) + \dot{\bar{S}}_{n,m}sin(m\lambda)\right)\bar{P}_{n,m}(cos\theta) \tag{A.1}$$

$$\dot{\Delta g}(\theta,\lambda) = \frac{GM}{R_E^2}\sum_{n=0}^{N}\sum_{m=0}^{n}(n-1)\left(\frac{a}{R_E}\right)^n\left(\dot{\bar{C}}_{n,m}cos(m\lambda) + \dot{\bar{S}}_{n,m}sin(m\lambda)\right)\bar{P}_{n,m}(cos\theta) \tag{A.2}$$

$$\dot{\delta g}(\theta,\lambda) = \frac{GM}{R_E^2}\sum_{n=0}^{N}\sum_{m=0}^{n}(n+1)\left(\frac{a}{R_E}\right)^n\left(\dot{\bar{C}}_{n,m}cos(m\lambda) + \dot{\bar{S}}_{n,m}sin(m\lambda)\right)\bar{P}_{n,m}(cos\theta) \tag{A.3}$$

$$\dot{\eta}(\theta,\lambda) = \frac{GM}{\gamma R_E^2 \sin\theta}\sum_{n=0}^{N}\sum_{m=0}^{n}m\left(\frac{a}{R_E}\right)^n\left(\dot{\bar{C}}_{n,m}\sin(m\lambda) - \dot{\bar{S}}_{n,m}\cos(m\lambda)\right)\bar{P}_{n,m}(cos\theta) \tag{A.4}$$

$$\dot{\xi}(\theta,\lambda) = \frac{GM}{\gamma R_E^2}\sum_{n=0}^{N}\sum_{m=0}^{n}\left(\frac{a}{R_E}\right)^n\left(\dot{\bar{C}}_{n,m}\cos(m\lambda) + \dot{\bar{S}}_{n,m}\sin(m\lambda)\right)\frac{\partial\bar{P}_{n,m}(cos\theta)}{\partial\theta} \tag{A.5}$$

$$\frac{\partial\bar{P}_{n,m}(cos\theta)}{\partial\theta} = \frac{1}{\sin\theta}\left(n\cos\theta\,\bar{P}_{n,m}(\cos\theta) - f_{n,m}\bar{P}_{n-1,m}(\cos\theta)\right), (0 \le m \le n) \tag{A.6}$$

$$f_{n,m} = \sqrt{\frac{(n^2-m^2)(2n+1)}{(2n-1)}} \tag{A.7}$$

$$\dot{h}(\theta,\lambda) = R_E\sum_{n=0}^{N}\sum_{m=0}^{n}\left(\frac{h_n}{1+k_n}\right)\left(\dot{\bar{C}}_{n,m}cos(m\lambda) + \dot{\bar{S}}_{n,m}sin(m\lambda)\right)\bar{P}_{n,m}(cos\theta) \tag{A.8}$$

For areas where GIA is the sole driver of height change (A.9) and (A.10) can be used:

$$\begin{Bmatrix}\dot{\bar{U}}_{nm}\\ \dot{\bar{V}}_{nm}\end{Bmatrix} = \frac{2n+1}{2}a\begin{Bmatrix}\dot{\bar{C}}_{nm}\\ \dot{\bar{S}}_{nm}\end{Bmatrix} \tag{A.9}$$

$$\dot{h}(\theta,\lambda) = \sum_{n=0}^{N}\sum_{m=0}^{n}\left(\dot{\bar{U}}_{n,m}cos(m\lambda) + \dot{\bar{V}}_{n,m}sin(m\lambda)\right)\bar{P}_{n,m}(cos\theta) \tag{A.10}$$

10 Appendix B: NRCan Absolute Gravity Stations in CGSN

Table 21: CGSN and GRACE Model Statistics

	GNSS			AG Rates			AG - GNSS		GRACE Model Results			Significance Tests		
	Dist to GNSS [km]	h_dot [mm/yr]	g_dot from h_dot	Num. AG Obs.	AG g_dot	AG g_dot_robust	g_dot_masses	g_dot_robust_masses	csr_60	csr_96	gsfc_180	F value	P value	Significant
ALGO	0.1	2.203	-0.678	12	-0.494	-0.570	0.184	0.109	0.607	0.565	0.142	0.67	0.43	TRUE
BCPH	6.8	2.254	-0.694	21	-0.565	-0.490	0.129	0.204	-0.390	-0.180	-0.276	6.89	0.02	TRUE
BDCK	3.2	-1.623	0.500	2	1.064	NaN	0.565	NaN	-0.408	-0.171	0.252	NaN	NaN	FALSE
CAGB	0.0	2.861	-0.881	214	-0.576	-0.619	0.305	0.262	0.733	0.420	0.423	16.44	0.00	TRUE
CAGE	0.0	2.861	-0.881	177	-0.386	-0.465	0.495	0.416	0.733	0.420	0.423	14.68	0.00	TRUE
CBRK	0.0	0.606	-0.187	3	-0.072	-0.072	0.114	0.114	-0.243	0.030	0.415	0.10	0.80	FALSE
CHLT	94.5	-2.084	0.642	2	0.775	NaN	0.134	NaN	-0.145	-0.130	0.156	NaN	NaN	FALSE
CHUR	0.3	11.219	-3.458	16	-1.741	-1.727	1.716	1.731	1.082	1.106	1.030	174.42	0.00	TRUE
CRLV	0.4	1.934	-0.596	2	0.200	NaN	0.795	NaN	0.069	0.426	0.397	NaN	NaN	FALSE
DRAO	0.1	0.881	-0.271	23	-0.234	-0.211	0.037	0.061	0.123	-0.021	0.339	8.96	0.01	TRUE
DUBO	0.1	0.945	-0.291	31	-0.247	-0.245	0.044	0.046	0.576	0.223	0.336	6.17	0.02	TRUE
FLIN	0.0	3.091	-0.952	19	-0.410	-0.419	0.542	0.534	0.628	0.705	0.577	8.37	0.01	TRUE
FNEL	0.1	4.162	-1.283	2	0.850	NaN	2.133	NaN	0.333	0.396	0.604	NaN	NaN	FALSE
GANG	0.0	1.975	-0.608	4	-0.669	-0.662	-0.061	-0.054	0.369	0.236	0.117	0.66	0.50	TRUE
GDPR	31.9	2.370	-0.730	2	1.083	NaN	1.813	NaN	0.268	0.328	0.314	NaN	NaN	FALSE
HLFX	0.2	-1.333	0.410	5	1.035	1.032	0.625	0.622	-0.229	-0.151	0.169	2.96	0.18	TRUE
KUUJ	0.1	14.410	-4.440	2	-2.985	NaN	1.455	NaN	1.360	1.608	1.479	NaN	NaN	FALSE
LPOC	0.0	2.641	-0.813	4	0.561	0.561	1.374	1.374	0.024	0.365	0.320	1.53	0.34	TRUE
MEMU	1.9	-0.684	0.211	3	-0.121	-0.121	-0.332	-0.332	-0.026	0.054	0.570	0.01	0.95	FALSE
OTTB	8.2	0.884	-0.272	20	0.471	0.316	0.744	0.588	0.681	0.385	0.406	1.20	0.29	TRUE
PGC0	0.2	-0.105	0.032	206	-0.110	-0.120	-0.142	-0.152	-0.229	-0.092	-0.329	4.80	0.03	TRUE
PICL	7.3	5.482	-1.689	3	-1.667	-1.667	0.022	0.022	0.093	0.586	0.550	302.49	0.04	TRUE
PPER	0.1	3.374	-1.039	3	0.118	0.118	1.157	1.157	0.306	0.472	0.314	0.02	0.92	FALSE
PRDS	0.3	0.997	-0.307	19	-0.406	-0.394	-0.098	-0.087	0.136	0.203	0.304	6.64	0.02	TRUE
PTAR	6.9	2.781	-0.857	7	0.610	0.699	1.467	1.555	-0.545	-0.148	-0.103	0.17	0.69	FALSE
REG8	9.8	-1.703	0.524	3	-0.133	-0.133	-0.657	-0.657	0.143	0.503	0.467	4.96	0.27	TRUE
SASK	0.1	-0.113	0.035	13	0.147	0.147	0.113	0.112	0.819	0.587	0.312	0.32	0.58	FALSE
SHED	1.4	-0.177	0.054	2	0.274	NaN	0.219	NaN	0.068	-0.086	0.184	NaN	NaN	FALSE
TORT	12.6	-1.335	0.411	2	-0.373	NaN	-0.784	NaN	0.134	0.249	0.036	NaN	NaN	FALSE
TSKT	0.0	-1.281	0.394	3	0.568	0.568	0.174	0.174	0.188	-0.108	0.329	2.16	0.38	TRUE
UCLU	0.5	2.115	-0.651	77	-0.109	0.083	0.542	0.734	-0.372	-0.127	-0.399	1.83	0.18	TRUE
UNB1	0.0	-0.271	0.083	2	-0.375	NaN	-0.458	NaN	0.105	-0.012	0.312	NaN	NaN	FALSE
VALD	0.0	6.905	-2.126	7	-1.083	-0.772	1.043	1.354	1.021	0.931	0.645	0.12	0.74	FALSE

WDSR	4.8	-3.178	0.978	2	0.450	NaN	-0.528	NaN	-0.006	0.048	-0.093	NaN	NaN	FALSE
YELL	0.1	7.368	-2.272	6	-1.118	-1.038	1.154	1.233	0.528	0.662	0.778	2.71	0.18	TRUE

11 Appendix C: US Absolute Gravity Stations

Table 22: US Absolute Gravity Stations with estimated $\dot{g}$ and significance

Station	Latitude	Longitude	Elevation	Num Obs	First Date	Last Date	Time Span	$\dot{g}_{OLS}$	$\dot{g}_{robust}$	R^2	P value
ALAMOGORDO A	32.8948	-106.0977	1249.70	6	7/1/1977	3/8/1995	17.68	3.98	3.63	0.394	0.182
ALEXANDRIA LSUA	31.1792	-92.4123	24.41	2	6/21/2002	9/8/2006	4.22	-0.51	NaN	1.000	NaN
ANCHORAGE AA	61.1556	-149.7953	71.00	3	7/1/1980	4/20/2010	29.80	-0.83	-0.83	0.998	0.025
ANCHORAGE AD	61.1909	-149.8240	44.51	2	7/25/2008	4/28/2010	1.76	-1.76	NaN	1.000	NaN
AUSTIN AA	30.2891	-97.7365	162.83	3	2/28/1989	2/25/2002	12.99	1.21	1.21	1.000	0.011
BATON ROUGE AA	30.4075	-91.1794	7.81	2	2/14/2002	7/28/2006	4.45	1.45	NaN	1.000	NaN
BELLINGHAM AA	48.7333	-122.4853	94.60	2	11/1/1988	9/14/2007	18.87	2.72	NaN	1.000	NaN
BENSON AA	31.8378	-110.3507	1413.93	4	11/9/2005	6/1/2007	1.56	-1.85	-1.85	0.785	0.114
BERGEN PARK AA	39.6991	-105.3728	2330.13	6	10/7/1987	1/10/1994	6.26	-0.19	-0.14	0.644	0.055
BLACKSBURG AA	37.2112	-80.4208	624.88	4	7/16/1987	4/25/1989	1.78	2.27	2.27	0.057	0.761
BOOTHVILLE BVHS	29.3366	-89.4061	1.00	2	6/12/2002	8/24/2006	4.20	2.84	NaN	1.000	NaN
BOSTON A	42.4522	-71.2701	38.95	12	12/1/1968	8/14/1991	22.70	0.73	0.71	0.632	0.002
BOSTON AB	42.6130	-71.4938	97.43	6	11/2/1990	9/8/1999	8.85	1.18	1.21	0.620	0.063
BOULDER AG	40.1310	-105.2326	1683.31	9	3/17/1999	6/6/2009	10.22	-0.20	-0.19	0.007	0.828
BOULDER AH	40.1310	-105.2326	1683.31	54	3/26/2002	7/6/2018	16.28	0.13	0.12	0.099	0.020
BOULDER D	40.0077	-105.2684	1634.54	9	5/27/1980	4/15/1982	1.88	20.51	-8.16	0.252	0.168
CANYON VILLAGE AA	44.7404	-110.4986	2413.81	2	9/14/2000	10/6/2001	1.06	-7.88	NaN	1.000	NaN
CASA GRANDE AA	32.9586	-111.6539	452.71	7	5/26/2001	11/29/2007	6.51	0.12	0.09	0.008	0.848
CASPER AA	42.8499	-106.3235	1557.70	2	7/17/1979	11/1/1996	17.30	-0.46	NaN	1.000	NaN
CLARKDALE AA	34.7701	-112.0263	1043.51	15	5/13/2001	11/8/2007	6.49	1.19	1.15	0.392	0.013
COCODRIE LUMCON	29.2550	-90.6618	1.90	2	6/1/2002	8/10/2006	4.19	2.21	NaN	1.000	NaN
COLUMBUS AA	39.9983	-83.0110	227.48	2	7/1/2005	5/28/2010	4.91	-0.80	NaN	1.000	NaN
DENVER H	39.6744	-104.9631	1633.10	4	10/19/1977	3/1/1982	4.36	10.65	10.62	0.846	0.080
DOLAN SPRINGS AA	35.6027	-114.2556	1100.10	4	10/20/2005	5/10/2007	1.55	2.94	2.94	0.979	0.010
DUCK AA	36.1816	-75.7514	6.00	2	11/7/1993	9/24/1999	5.88	1.42	NaN	1.000	NaN
EASTPORT AA	44.9037	-66.9852	10.80	4	10/22/1993	9/10/1999	5.88	-1.71	-1.70	0.742	0.139
FAIRBANKS AA	64.8993	-147.7954	314.83	3	9/9/1990	3/25/1992	1.54	-2.83	-2.83	0.809	0.288
FAIRBANKS AB	64.9778	-147.4976	307.39	2	3/18/1992	8/1/2008	16.37	0.64	NaN	1.000	NaN
FT. HUACHUCA AA	31.5579	-110.4294	1618.85	16	3/23/2000	10/25/2007	7.59	0.00	0.44	0.000	0.999
GLOUCESTER POINT AA	37.2488	-76.4995	5.02	2	4/15/1998	9/28/1999	1.45	-7.20	NaN	1.000	NaN
GOLDSTONE AA	35.3017	-116.8056	985.40	2	4/9/1982	5/25/1990	8.13	5.29	NaN	1.000	NaN
GRAND CANYON AA	36.0500	-112.1319	2124.56	2	5/2/2006	6/13/2011	5.11	2.53	NaN	1.000	NaN

GREAT FALLS AA	47.4775	-111.3602	1121.10	4	7/22/1979	7/1/1982	2.94	-73.69	-73.98	0.547	0.261
GREAT FALLS PARK AA	38.9969	-77.2549	46.73	13	5/27/1987	10/5/1999	12.36	0.96	0.93	0.843	0.000
HAMMOND HAMM	30.5131	-90.4674	10.00	2	6/11/2002	7/20/2006	4.11	3.59	NaN	1.000	NaN
HATTIESBURG AA	31.3287	-89.3336	64.52	2	2/9/2002	7/18/2006	4.44	1.91	NaN	1.000	NaN
INTERNATIONAL FALLS AA	48.5846	-93.1612	341.40	13	11/10/1988	7/19/2005	16.69	1.97	1.86	0.245	0.085
IOWA CITY AA	41.6577	-91.5428	208.61	5	8/17/1995	7/9/2005	9.89	0.16	0.17	0.175	0.484
KAUAI AA	22.1231	-159.6653	1142.23	4	11/6/1987	3/3/1992	4.32	1.44	1.53	0.025	0.840
KINGMAN AA	35.1973	-114.0415	1153.21	4	10/18/2005	5/11/2007	1.56	-0.22	-0.20	0.015	0.878
KODIAK AA	57.7813	-152.3959	27.11	2	8/12/2008	5/1/2010	1.72	-1.65	NaN	1.000	NaN
KSC AB	28.5088	-80.6331	2.10	2	8/6/1987	2/1/2002	14.49	-8.14	NaN	1.000	NaN
LAFAYETTE KJUN	30.2211	-92.0448	12.60	2	6/14/2002	9/6/2006	4.23	-1.62	NaN	1.000	NaN
LAKE CHARLES AA	30.1793	-93.2177	4.91	3	2/16/2002	10/28/2008	6.70	4.05	4.05	0.995	0.044
LICK OBSERVATORY AA	37.3414	-121.6428	1284.00	2	6/8/1980	3/27/1982	1.80	0.00	NaN	NaN	NaN
MAMMOTH LAKES FSVC	37.6478	-118.9604	2374.29	14	6/29/1984	10/18/2000	16.30	-4.06	-4.06	0.908	0.000
MCDONALD AB	30.6718	-104.0219	2062.30	3	7/1/1980	9/16/1994	14.21	-11.45	-11.45	1.000	0.010
MENLO PARK C-14	37.4556	-122.1727	4.14	2	12/8/1986	12/13/1987	1.01	-44.12	NaN	1.000	NaN
MIAMI AB	25.6139	-80.3840	4.88	4	3/8/1990	1/20/2002	11.87	-0.10	-0.10	0.990	0.005
MONUMENT PEAK	32.8917	-116.4217	1872.09	11	9/6/1985	11/5/1999	14.16	-2.37	-2.40	0.926	0.000
MT. EVANS AA	39.6556	-105.5937	3248.30	2	7/13/1979	3/13/1993	13.67	-4.32	NaN	1.000	NaN
NEW ORLEANS AA	30.0253	-90.0688	-1.43	7	3/15/1989	11/2/2008	19.64	1.41	1.40	0.507	0.073
NEW ORLEANS NOL	29.9346	-90.1201	3.11	2	1/14/2002	8/20/2006	4.60	0.94	NaN	1.000	NaN
OAHU AB	21.2792	-157.8343	3.31	2	4/14/1993	5/8/1994	1.07	-0.75	NaN	1.000	NaN
ORLANDO AA	28.5994	-81.2002	22.42	2	4/6/1989	1/18/2002	12.79	0.16	NaN	1.000	NaN
PALISADES AA	41.0042	-73.9052	116.63	4	11/8/1990	9/12/1999	8.84	-5.23	-5.23	0.970	0.015
PALMER AA	61.5926	-149.1332	83.23	4	9/4/1990	5/5/2010	19.67	1.68	1.68	0.998	0.001
PALOMINAS AA	31.3883	-110.1221	1295.61	13	4/21/2001	10/26/2007	6.51	-0.24	-0.08	0.026	0.597
PASADENA	34.1485	-118.1713	296.09	14	8/14/1984	10/28/1999	15.20	2.39	2.40	0.592	0.001
PAULDEN AA	34.8957	-112.4679	1341.71	12	5/11/2001	11/13/2007	6.51	1.79	1.47	0.651	0.002
PHOENIX AA	33.3481	-112.0836	432.07	14	7/17/1998	11/28/2007	9.37	0.21	-0.11	0.072	0.354
PHOENIX AB	33.5636	-112.0292	430.91	5	4/10/2002	5/4/2007	5.07	0.39	0.42	0.029	0.784
PHOENIX AC	33.4947	-111.6407	774.91	7	5/24/2001	5/3/2007	5.94	0.63	0.65	0.289	0.213
PICACHO PEAK AA	32.6453	-111.3991	578.81	7	5/14/2004	5/25/2007	3.03	-0.05	-0.07	0.001	0.944
PINYON FLAT AA	33.6122	-116.4588	1288.48	31	4/7/1982	10/21/1999	17.54	-0.58	-0.54	0.419	0.000
PORTLAND AB	45.4512	-122.6675	113.61	2	10/13/1988	8/9/2007	18.82	1.54	NaN	1.000	NaN
PRESCOTT AA	34.5728	-112.4965	1702.31	15	10/4/2000	11/16/2007	7.12	0.66	0.68	0.373	0.016
PRESCOTT AB	34.7681	-112.5957	1472.91	13	5/9/2001	11/15/2007	6.52	1.84	1.82	0.396	0.021

QUINCY HELIPORT	39.9733	-120.9401	1085.55	6	8/26/1985	9/21/1996	11.07	-1.69	-1.67	0.881	0.006
ROLLA AA	37.9183	-91.8733	254.82	9	11/23/1988	7/7/2005	16.62	1.91	1.93	0.755	0.002
SEDONA AA	34.8466	-111.8292	1360.31	14	5/16/2001	11/9/2007	6.48	3.57	3.46	0.673	0.000
SHERIDAN AA	44.7607	-106.9696	1207.60	3	7/19/1979	4/16/1982	2.74	13.83	13.83	0.487	0.508
SOLOMONS AA	38.3182	-76.4536	4.36	4	8/31/1994	10/4/1999	5.09	0.63	0.62	0.118	0.656
SSC AA	30.3497	-89.6361	8.01	2	2/12/2002	7/13/2006	4.41	4.56	NaN	1.000	NaN
THIBODAUX NSUT	29.7907	-90.8045	3.60	2	6/4/2002	8/8/2006	4.18	-0.48	NaN	1.000	NaN
TOMBSTONE AA	31.7058	-110.0572	1410.32	16	3/24/2000	10/30/2007	7.60	0.66	0.72	0.207	0.077
TRINIDAD AA	37.1730	-104.5150	1850.57	3	7/11/1979	9/1/1995	16.14	-2.83	-2.83	0.783	0.309
TUCSON AA	32.3095	-110.7848	903.12	19	2/11/1989	11/3/2007	18.72	0.13	0.14	0.694	0.000
TUCSON AB	32.4414	-110.7910	2780.10	9	2/16/1989	3/31/2006	17.12	-4.53	-4.56	0.863	0.000
TUCSON AC	32.2376	-110.8312	784.71	7	7/21/1998	5/21/2004	5.83	-1.32	-1.31	0.321	0.185
TUCSON AD	32.2285	-110.9558	738.71	17	7/22/1998	11/2/2007	9.28	-0.08	-0.09	0.005	0.788
TUCSON AE	32.2193	-111.0033	820.61	18	7/29/1998	11/6/2007	9.27	0.07	0.08	0.005	0.783
TUCSON AF	32.2440	-111.1689	867.31	12	7/29/1998	10/31/2007	9.26	0.30	0.46	0.231	0.114
VANDENBERG AA	34.7707	-120.5051	246.00	3	6/4/1980	7/1/1996	16.07	-1.52	-1.52	0.218	0.691
WASHINGTON AA	39.1261	-77.2211	123.00	12	3/14/1980	2/11/2012	31.91	-0.50	-0.44	0.647	0.002
WAUSAU AA	44.9200	-89.6803	531.33	8	8/8/1990	7/12/2005	14.93	-1.23	-1.23	0.502	0.049
WILLCOX AA	32.2488	-109.8355	1272.15	3	11/11/2005	11/15/2006	1.01	-3.99	-3.99	0.356	0.593